

ABSTRACT

Title of Dissertation: THE DEVELOPMENT OF AN AIR-COOLED
ABSORPTION CHILLER CONCEPT AND ITS
INTEGRATION IN CHP SYSTEMS

Xiaohong Liao, Doctor of Philosophy, 2004

Dissertation Directed By: Professor Reinhard Radermacher, Ph.D.
Department of Mechanical Engineering

This dissertation focuses on the feasibility, crystallization issues, and the integration of LiBr-H₂O air-cooled absorption chillers into Cooling, Heating and Power (CHP) systems. The concept of an air-cooled system is attractive because the cooling tower and the associated installation and maintenance issues can be avoided. However, crystallization of the LiBr-H₂O solution then becomes the main issue in the operation of the unit, since the air-cooled absorber tends to operate hotter than the water-cooled absorber due to the relative heat transfer characteristics of the coolant leading to crystallization of the working fluid. Differently from the conventional approaches to air-cooled absorption chillers, novel temperature control strategies in conjunction with a specialized application is proposed. This prevents crystallization but presents unique system integration challenges and opportunities. A model to accurately reflect the thermodynamic characteristics of air-cooled absorption chillers and to facilitate control is developed as part of this research, and field experiments that simulate air-cooled conditions with a water-cooled absorption chiller, which was

driven by the waste heat of a microturbine, were conducted to validate the feasibility of the air-cooled concept and the accuracy of computer model.

While CHP provides a good opportunity for the application of air-cooled absorption chillers, system integration issues need to be investigated. The capital cost of CHP equipment and the load fluctuation of a commercial building restrict the advantage of designing a unit sized for peak load. Therefore, the conventional Heating Ventilation and Air Conditioning (HVAC) system is needed to pick up the residual loads. Thus, the result of an extensive system integration analysis is that CHP should be arranged in series with the HVAC system to ensure obtaining more operating hours at its full capacity, so that the cost savings achieved through the recovery of waste heat are fully realized to repay its higher initial capital cost. The primary energy savings are presented for all potential configurations.

As a part of this research a fully integrated CHP system has been installed and instrumented at the Chesapeake Building. It is a commercial office building on the University of Maryland campus. The experimental setup, data processing, and experience gained are detailed here. Based on the computer simulation, extensive experiments, first hand installation, operation and maintenance experience, valuable guidelines on the integration of an air-cooled absorption chiller in CHP are developed. All the guidelines are also applicable to water-cooled absorption chillers.

THE DEVELOPMENT OF AN AIR-COOLED ABSORPTION CHILLER
CONCEPT AND ITS INTEGRATION IN CHP SYSTEMS

By

Xiaohong Liao

Dissertation submitted to the Faculty of the Graduate School of the
University of Maryland, College Park, in partial fulfillment
of the requirements for the degree of
Doctor of Philosophy
2004

Advisory Committee:
Professor Reinhard Radermacher, Chair/Advisor
Professor Shapour Azarm
Professor Tien-Mo Shih
Professor Paul Smith
Professor Yunho Hwang

© Copyright by
Xiaohong Liao
2004

Acknowledgements

My thanks and sincere appreciation goes to Dr. Reinhard Radermacher for allowing me the opportunity to realize my goals. Without his wisdom, encouragement, and advice this work would not be complete. I am also very grateful for the guidance of Dr. Aris Marantan, who taught me the knowledge of CHP.

I sincerely thank Dan Pearson and Chaoqin Zhai for you assisting me a lot during your internship. Special thanks also goes to the CHP team members, both past and present – namely, Dieter Mannschott, Matt Cowie, Sandeep Nayak, Shenglan Xuan, Ji Bian and Dennis Moran. It was a pleasure working with every one of you.

Finally, I would like to express my gratitude to my family and friends for their encouragement and love.

Contents

ABSTRACT	i
Acknowledgements	ii
Contents	iii
List of Tables	vii
List of Figures	viii
Nomenclature	xiii
Chapter 1 - Introduction	1
CHP and Absorption Chillers	1
Absorption Chillers	1
Crystallization Nature of LiBr Solution	2
Pros and Cons of Air-cooled Absorption Chiller	3
Literature Review	4
Research Emphases of Current Absorption Technologies	4
Absorption Chiller Modeling and Simulation	5
Experimental Work about Air-cooled Absorption Chillers	6
Crystallization Prevention	7
Application Investigation	7
Standards of Efficiency Evaluation	11
Chapter 2 - Motivation and Research Objectives	12
Motivation	12
Objectives	12
Chapter 3 - Experimental Setup	14
CHP Integration Test Center on the Campus of UMD	14
Features of Test Facility	15
Microturbine-based CHP System	16
Microturbine	17
Water-cooled Single Effect LiBr Absorption Chiller	18
Solid Desiccant Unit	19
Data Acquisition System	21

DAS Architecture.....	21
Instrumentation Setup	25
Sensor Calibration in HP VEE	28
Need and Method	28
Determination of the Calibration Correlation	29
Calibration Samples	30
Chapter 4 – Performance Tests on Components and CHP System	31
Exhaust Temperature Profile	31
Microturbine Performance.....	32
Water-cooled Absorption Chiller Performance.....	37
Solid Desiccant Unit Performance	38
Chapter 5 - Air-cooled Absorption Chiller Modeling.....	42
Principles of Single Effect LiBr Air-cooled Absorption Chillers	42
Software Selection.....	44
UA-LMTD Method	45
Assumptions	45
Equations of Component	46
Generator / Desorber	46
Condenser.....	47
Evaporator	47
Absorber.....	47
Solution Heat Exchanger	48
Efficiency Evaluation	48
Sensitivity Analysis.....	49
Baseline at Design Conditions	49
Effect of Exhaust Temperature into Desorber	50
Effect of Exhaust Flow Rate into Desorber	52
Effect of Ambient Temperature	53
Effect of Chilled Water Temperature.....	55
Summary of Simulation Results.....	56
Chapter 6 – Crystallization Control Strategies	57

Crystallization Causes and Precautions.....	57
Control Strategies.....	60
Chilled Water Temperature Control.....	60
Exhaust Temperature Control.....	64
Chapter 7 – Absorption Chiller Validation.....	67
Rationale for the Test Method.....	67
Data Processing.....	68
Chiller Validation.....	70
Altering the Exhaust Temperature.....	70
Altering the Coolant Temperature.....	72
Altering the Chilled Water Temperature.....	74
Chapter 8 – Integration of Air-cooled Absorption Chillers in CHP Systems.....	76
Operating Hours of Mechanical Cooling Equipment.....	76
Conventional RTU Baseline.....	80
Best CHP Practice.....	83
Desiccant as an Energy Transformer.....	83
CHP Arrangements in Parallel or Series with HVAC.....	84
Parallel Configuration (CHP DOAS).....	86
Series Configuration.....	90
Proposed Application of Air-cooled Absorption Chiller in CHP Systems.....	95
Component Assumption.....	95
System without Enthalpy Wheel.....	96
System with Enthalpy Wheel.....	97
Energy Analysis.....	98
General.....	98
System with Temperature-based Economizer.....	99
System with Enthalpy-based Economizer.....	102
Summary of Energy Analysis.....	104
Chapter 9 - Guidelines.....	106
General.....	106
Crystallization.....	106

Application	107
Integration.....	108
Packaged Absorption Chiller	108
Exhaust Heat Management	111
Simplicity	113
Standardizations	114
Chapter 10 Conclusions	115
Summary of Accomplishments	115
Conclusions	116
Future Work.....	119
Appendix A – ASHRAE Minimum Ventilation Rate History.....	121
Appendix B – Weather in Three Locations	122
Appendix C – Sensors and Uncertainty Analysis	125
Appendix D – Solid Desiccant Unit Catalogue	127
Appendix E – A Damper-Actuator Assembly	128
Appendix F – BCTDE P&I Diagram.....	129
Appendix G – Test Logs for Summer of 2003	130
Appendix H – Field Data and EnergyPlus Simulation	134
EnergyPlus Overview.....	134
Specifications of the Chesapeake Building	135
Program Input.....	137
Simulation Examples.....	138
Low Voltage Power	138
High Voltage Power.....	138
Summary.....	139
Bibliography	142
Publications and Reports.....	154

List of Tables

Table 1: Test schedule on weekday	16
Table 2. Three generations of the microturbine-based CHP system	17
Table 3. Technical Data of the 21 ton Broad Exhaust Absorption Chiller	19
Table 4. Allocation of user-installed sensors in the CHP Integration Test Center	21
Table 5. Sensor installation for absorption chiller and its accessories	25
Table 6. Thermodynamic state point summary.....	45
Table 7. State points for the single effect air-cooled LiBr absorption chiller baseline at design condition.....	50
Table 8. Heat duty and UA of each component at design condition	50
Table 9. Parameter settings for condensers and absorbers	67
Table 10: Instrumentation and Sensor Error.....	125
Table 11: Uncertainty of Calculated Results	126

List of Figures

Fig. 1. The property chart of LiBr/ H ₂ O solution with crystallization curve.....	3
Fig. 2. Coolants entering condenser and absorber	4
Fig. 3. Research emphases of absorption technology	5
Fig. 4. The load profile in the Chesapeake Building	9
Fig. 5. General configuration of the DOAS.....	11
Fig. 6. 3D Characterization of the Chesapeake Building with four exterior air- conditioning zones and one interior zone.....	14
Fig. 7. Microturbine-based CHP system at UMD.....	17
Fig. 8. Microturbine power shaving effect on the Chesapeake Bldg.....	18
Fig. 9. Schematic drawing of solid desiccant unit	19
Fig. 10. Enthalpy wheel	20
Fig. 11. DAS architecture	21
Fig. 12. Condensate collection device	23
Fig. 13. Saving the operation of condensate pump w/o HP VEE logic.....	24
Fig. 14. Saving operation of condensate pump with HP VEE logic.....	24
Fig. 15. P&I Diagram for the second-generation microturbine-based system	27
Fig. 16. Exhaust heat management and safety control for the second-generation microturbine-based CHP system	27
Fig. 17. The flow rate of exhaust gas and make-up air.....	28
Fig. 18. A calibration sample of temperature sensor	30
Fig. 19. Temperature profile of CHP system at UMD on a typical day of cooling season	32
Fig. 20. Microturbine operating profiles for a typical day.....	33
Fig. 21. Microturbine engine speed vs. compressor inlet air temperature.....	33
Fig. 22. Microturbine output vs. compressor inlet air temperature	34
Fig. 23. Microturbine compressor inlet air temperature vs. ambient temperature.....	34
Fig. 24. Microturbine natural gas and exhaust heat vs. ambient temperature	35
Fig. 25. Microturbine efficiency (HHV) vs. ambient temperature	36
Fig. 26. The absorption chiller operating profiles for a typical day	37

Fig. 27. Solid desiccant unit operating profiles for a typical day	39
Fig. 28. Enthalpy wheel performance on a typical day.....	40
Fig. 29. Moisture removal capacity of SDU	41
Fig. 30. Diagram of single-effect air-cooled absorption chiller.....	43
Fig. 31. The Dühring P-T chart of absorption cycle	43
Fig. 32. System pressure vs. exhaust temperature into desorber	51
Fig. 33. LiBr concentration vs. exhaust temperature into desorber	51
Fig. 34. Solution mass flow rate vs. exhaust temperature into desorber	52
Fig. 35. Heat exchanger load and COP vs. exhaust temperature into desorber	52
Fig. 36. Solution mass flow rate vs. exhaust flow rate into desorber	53
Fig. 37. Heat exchanger load and COP vs. exhaust flow rate into desorber.....	53
Fig. 38. System pressure vs. ambient temperature.....	54
Fig. 39. LiBr concentration vs. ambient temperature	54
Fig. 40. Solution mass flow rate vs. ambient temperature.....	54
Fig. 41. Heat exchanger load and COP vs. ambient temperature	54
Fig. 42. System pressure vs. chilled water supply temperature	55
Fig. 43. LiBr concentration vs. chilled water supply temperature.....	55
Fig. 44. Solution mass flow rate vs. chilled water supply temperature	56
Fig. 45. Heat exchanger load and COP vs. chilled water supply temperature.....	56
Fig. 46. The Dühring P-T chart of absorption cycle (dashed line) @ ambient 25°C and cycle (solid line) @ ambient 35°C.....	58
Fig. 47. The Dühring P-T chart of absorption cycle (dashed line) @ exhaust 280°C and cycle (solid line) @ exhaust 320°C	59
Fig. 48. Minimum chilled water supply temperature (exhaust @ 280°C and with constant flow rate)	61
Fig. 49. Chiller cooling capacity map over the chilled water and ambient temperature combination (exhaust @ 280°C and with constant flow rate).....	62
Fig. 50. Chiller COP map over the chilled water and ambient temperature combination (exhaust @ 280°C and with constant flow rate).....	63
Fig. 51. Chiller performance over the exhaust and ambient temp. combination	66

Fig. 52. Detailed chilled water temperatures and parasitic power in steady state at 1 minute interval.....	69
Fig. 53. Cooling tower fan operation comparison	70
Fig. 54. The experimental validation by altering the exhaust temperature.....	71
Fig. 55. The experimental validation under 2 different conditions for the crystallization control strategies	73
Fig. 56. The experimental validation by altering the chilled water temperature	74
Fig. 57. Year-round weather in College Park, Maryland, USA.....	78
Fig. 58. The coincident weather when the mechanical cooling is required.....	80
Fig. 59. Roof top unit and the conditioned space	81
Fig. 60. The conventional vapor compression air conditioning used to remove moisture and control air temperature with reheat.....	82
Fig. 61. Latent load, sensible load and reheat load of a building zone	82
Fig. 62. Desiccant wheel delivers the required latent load at the design condition by dehumidifying the mixed air	84
Fig. 63. Configurations of CHP and HVAC in parallel or series connection.....	85
Fig. 64. Schematic drawing of the parallel configuration.....	86
Fig. 65. CHP DOAS illustration	87
Fig. 66. Desiccant wheel takes care of the latent load at the design condition by dehumidifying the outdoor air	88
Fig. 67. Total moisture removed by RTU on 2 similar workdays	89
Fig. 68. The moisture removal rate by RTU on 2 similar workdays	89
Fig. 69. Schematic drawing of the series configuration.....	91
Fig. 70. The coincident mixed air condition entering the CHP and HVAC series system in the cooling season	93
Fig. 71. The coincident mixed air condition entering the CHP and HVAC series system in the cooling season with enthalpy recovery	95
Fig. 72. Proposed CHP application without an enthalpy wheel in RTU	97
Fig. 73. Proposed CHP application with an enthalpy wheel in RTU	98
Fig. 74. Enthalpy wheel does not benefit under all weather conditions	100

Fig. 75. Summary of RTU loads in cooling season (with temperature-based economizer)	101
Fig. 76. Primary energy consumption for each concept producing the same supply air and net electricity in cooling season (systems with a temperature-based economizer)	102
Fig. 77. Summary of RTU loads in cooling season (with enthalpy-based economizer)	103
Fig. 78. Primary energy consumption for each concept producing the same supply air and net electricity in cooling season (systems with an enthalpy-based economizer)	104
Fig. 79. The complicated second-generation MT-based system.....	110
Fig. 80. The simplified third-generation MT-based system	110
Fig. 81. P&I Diagram for the third-generation microturbine-based system	111
Fig. 82. Two kinds of plenum box (with circle) installed on the top of MT	112
Fig. 83. AutoCAD 3D design of the third-generation MT-based system.....	113
Fig. 84. ASHRAE minimum ventilation rate history (1CFM = 0.47 l/s)	121
Fig. 85. Year-round dry-bulb temperature (°C) comparison (top: College Park, middle: Baltimore, bottom: Dulles).....	122
Fig. 86. Year-round dew point (°C) comparison (top: College Park, middle: Baltimore, bottom: Dulles).....	123
Fig. 87. Year-round relative humidity (%) comparison (top: College Park, middle: Baltimore, bottom: Dulles).....	124
Fig. 88. Performance chart of a commercial solid desiccant dehumidifier	127
Fig. 89. Comparison of sequence simulation and integrated simulation	134
Fig. 90. Floor Plan	135
Fig. 91. Weekday schedule of occupancy.....	136
Fig. 92. Weekday schedule of lighting and office equipment	136
Fig. 93. Weekend schedule of lighting and office equipment	136
Fig. 94. The Year-round low voltage power in the Chesapeake Building.....	140
Fig. 95. Weekly low voltage power in the Chesapeake Building.....	140
Fig. 96. Year-round high voltage power for the 1 st and 2 nd floors.....	141

Fig. 97. Weekly high voltage power for the 1st and 2nd floors..... 141

Nomenclature

Abbreviations:

ABSIM	Absorption SIMulation
AC	Absorption Chiller
ASHRAE	American Society of Heating, Refrigerating and Air-Conditioning Engineers
BCHP	Combined Cooling, Heating and Power for Buildings
CFC	Chlorofluorocarbon
CHP	Combined Cooling, Heating and Power
CHP DOAS	Combined Cooling Heating and Power Dedicated Outdoor Air System
COP	Coefficient of Performance
DAS	Data Acquisition System
DB	Dry Bulb
DOAS	Dedicated Outdoor Air System
DOE	U.S. Department of Energy
DX	Direct Expansion
EES	Engineering Equation Solver
GHG	Greenhouse Gas
HCFC	Hydrochlorofluorocarbon
HHV	Higher Heating Value
HP VEE	Hewlett-Packard Visual Engineering Environment
HVAC	Heating, Ventilation and Air-conditioning
HX	Heat Exchanger
IAQ	Indoor Air Quality
LHV	Lower Heating Value
LiBr	Lithium Bromide
LMTD	Log Mean Temperature Difference
MT	Microturbine
OA	Outdoor Air
PA	Process Air
PEC	Primary Energy Consumption

RA	Return Air
REFPROP	REference fluid PROPERTIES
RTU	Roof Top Unit
SA	Supply Air
SBS	Sick Building Syndrome
SDU	Solid Desiccant Unit
TAT	Thermally Activated Technology
UA	Overall heat transfer coefficient
UMD	University of Maryland
VAV	Variable Air Volume
VC	Vapor Compression
VFD	Variable Frequency Drive
WB	Wet Bulb

Parameters/Variables:

h	Enthalpy
m	Mass flow rate
P	Pressure
Q	Heat exchange capacity
T	Temperature
x	Concentration of LiBr

Subscripts

a	Absorber
c	Condenser
e	Evaporator
g	Generator / desorber
hx	Solution heat exchanger
amb	ambient

Chapter 1 - Introduction

CHP and Absorption Chillers

CHP is an acronym for Combined Heat and Power (Cogeneration, i.e. a process that converts the energy content of a fuel into both thermal and electrical energy) or combined Cooling, Heating, and Power (other equivalent names are: BCHP - Buildings, Cooling, Heating and Power and Integrated Energy Systems or Trigeneration.). CHP is the most efficient use of fossil fuels since it captures and utilizes the waste heat that is generated during the power production process and delivers it in the form of heating, cooling and/or dehumidification. Absorption chilling is a key technology in the BCHP portfolio because it offers significant opportunities to transform waste heat into cooling.

Absorption Chillers

Absorption cycles have been used for more than 150 years. Early equipment used a mixture of ammonia and water as an absorption working pair, i.e., the refrigerant and absorbent. This working pair is still in use today in a range of applications. However, because of the toxicity of ammonia, it is often restricted to applications in which the equipment is outdoors to allow natural dilution of any leaks. Another absorption working fluid came into widespread use after 1945 when aqueous Lithium Bromide (LiBr) was introduced for building air-conditioning applications. In this working pair, water is the refrigerant. LiBr absorption machines account for approximately 5% of the U.S. commercial cooling market and as much as 50% of the markets in Japan, Korea, and China (U.S. DOE, 2004 a).

The advantage of using absorption chillers (AC) over other types of refrigeration equipment is that absorption chillers can make use of heat that is available from other processes such as steam from a district heating system, engine jacket and/or exhaust gas heat from an engine-generator, or heat available from other industrial processes. Other advantages also include reduced environmental impact because no CFC or HCFC refrigerants are needed, and they produce less noise and vibration. In this investigation, a LiBr-H₂O single-effect absorption chiller is examined. It is distinguished by its two internal pressure levels.

Crystallization Nature of LiBr Solution

Solid LiBr salt is structurally crystalline in nature. When LiBr is dissolved in water, it becomes an aqueous solution. The nature of LiBr solutions is that the salt component precipitates when the mass fraction of salt exceeds the solubility limit. The solubility limit is a strong function of mass fraction and temperature and a weak function of pressure. Furthermore, crystal nucleation is a process sensitive to the presence of nucleation sites. If no suitable nucleation sites are present, supersaturation can occur where the salt content of the liquid is greater than the solubility limit. Once crystals begin to form, the crystals themselves provide favorable nucleation sites and the crystals grow on themselves (Herold et al, 1996 b). The crystallization curve of LiBr is shown in Fig. 1.

In absorption chillers, usually the crystallization line for lithium bromide and water is very close to the working concentrations needed for practical LiBr/H₂O absorption chillers, such as Point A in Fig. 1. If the solution concentration is too high or the solution temperature is reduced too low, crystallization may occur and interrupt machine operation, such as Point B. Crystallization must be avoided since the formation

of slush in the piping network over time could form a solid and block the flow. To recover absorber operation after crystallization occurs is very labor intensive and time consuming.

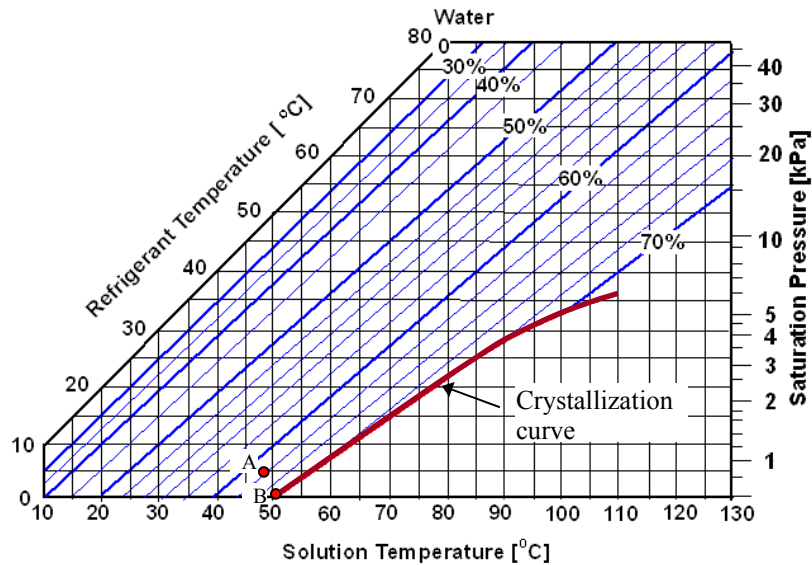


Fig. 1. The property chart of LiBr/ H₂O solution with crystallization curve

(Courtesy of Dr. Yunho Hwang)

Pros and Cons of Air-cooled Absorption Chiller

During the late 1980s and early 1990s, the development of LiBr/H₂O chillers with air-cooled condensers began (Sweetser et al., 2000). The motivation for an air-cooled option is to use air, a free coolant, to remove the heat of condensation and absorption processes. As a result, the cooling tower, water, and the associated maintenance, the winterizing procedure, and Legionella breeding are eliminated. Places in the world where water is a precious commodity can particularly benefit from this.

Since the water-cooled chiller has a cooling tower, it can maintain the entering condenser/absorber water temperature lower than the air-cooled condenser air inlet temperature when the weather is hot. Figure 2 shows the comparison of air temperature

and cooling water temperature. Therefore, water-cooled absorption machines generally can operate year-round with less crystallization issues.

But crystallization is the main obstacle to producing an air-cooled absorption machine based on LiBr, because the air-cooled absorbers tend to run hotter than water-cooled units due to the relative heat transfer characteristics of the coolants. Particularly in hot climates, this presents a difficult design problem (Sweetser et al., 2000).

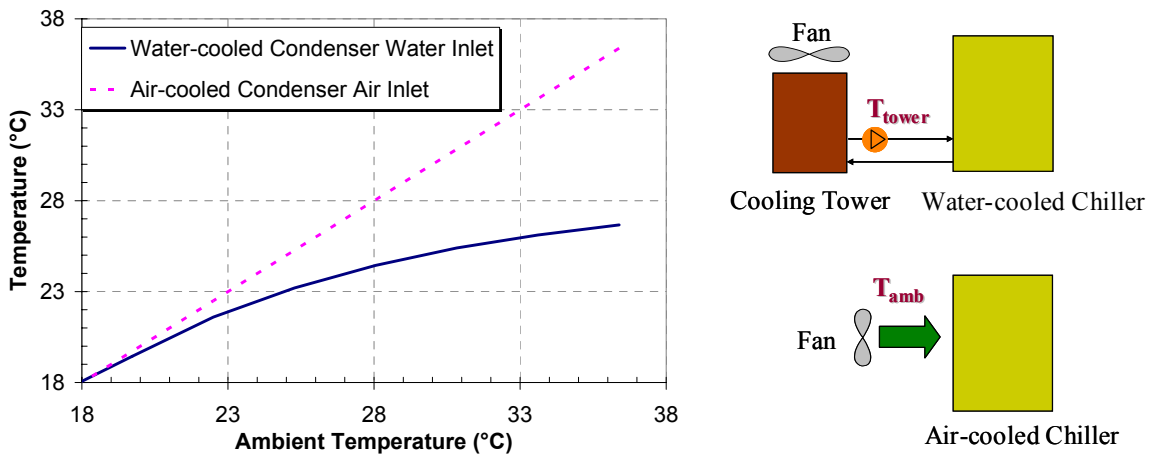


Fig. 2. Coolants entering condenser and absorber

Source: BinMaker[®] Weather Data for Engineering (GTI, 2004)

Literature Review

Research Emphases of Current Absorption Technologies

More than 100 papers associated with absorption technologies have been reviewed to classify the current research emphases. Figure 3 shows ten categories of research areas. A small percentage of the literature is about the integration of absorption machines into CHP (4%), and a very limited amount is about the air-cooled absorption machines alone (2%).

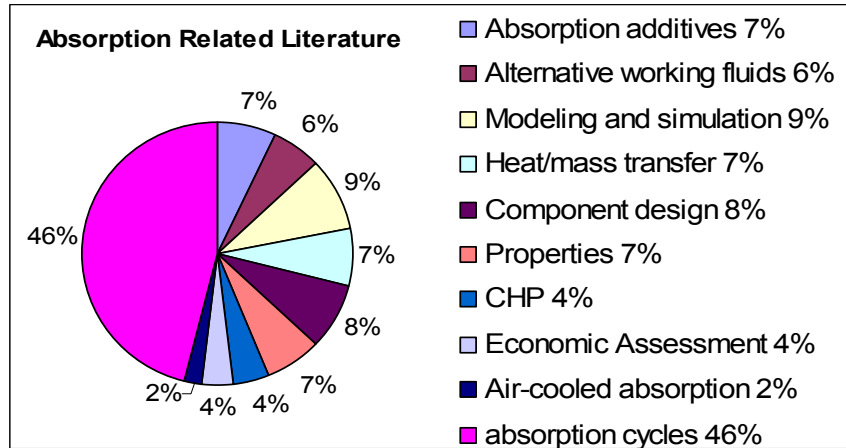


Fig. 3. Research emphases of absorption technology

Absorption Chiller Modeling and Simulation

There are many reports about the simulation of water-cooled absorption machines. For example on the water-cooled side: a single-effect lithium bromide absorption chiller computer model was validated with experimental data (Homma et al., 1994). The capacity of the absorption chiller is 30 ton (105.5 kW, 1 ton = 3.516 kW) and is driven by waste heat in the form of hot water from a gas engine. The absorption model consists of four main components (absorber, generator, evaporator, and condenser). The model of each component is based on a log mean temperature difference (LMTD), energy balance, mass balance, salt balance, and an overall heat transfer coefficient (UA). More detailed computer models have been developed by Koepfel, E.A. (1994) and Goodheart, K.A. (2000 a).

However, there is little literature on air-cooled absorption chillers, mainly due to the unavailability of a commercialized product, and most is restricted to purely theoretical simulation. Salim, M. (2001) simulated a 7kW cooling capacity automotive LiBr absorption air-conditioner by ABSIM (ABsorption SIMulation), but no

experimental validation is supplied. An interesting phenomenon is that most papers of this category are associated with solar applications. For example, Alva, L. (2002) simulated a proposed air-cooled solar-assisted absorption system with the cooling loads in the range of 10.5, 14 and 17.5 kW, and compared its performance to the performance of a water-cooled system. Again, no experimental validation is conducted.

Izquierdo, M. (2004) calculated the operating parameters of a single-effect and a double-effect LiBr air-cooled absorption system driven by solar energy with the objective of crystallization prevention. The cooling capacity of the systems is small, less than 7 kW. Some conclusions included: 1) The double-effect absorption cycle still might work without crystallization problems for the condensation temperature up to 53°C; for the single-effect the limit is 40~45°C. 2) For higher condensation temperature, the generation temperature required is very high and crystallization occurs.

Florides, G. (2003) mentioned several causes of crystallization occurring in a water-cooled LiBr absorption machine, which include: 1) Air leakage into the machine, which results in increased pressure in the evaporator; 2) Excessively cold condenser water, coupled with a high load condition; 3) electric power failure.

Experimental Work about Air-cooled Absorption Chillers

Little research has been reported on experimental work about air-cooled absorption chillers, and they are all restricted to small tonnage machines, such as a 3 kW air-cooled LiBr absorption prototype tested by Castro, J. (2002). He made several comparisons between theoretical and experimental results for capacity and performance were presented for different hot water temperature into the desorber, and the discrepancies were discussed.

Crystallization Prevention

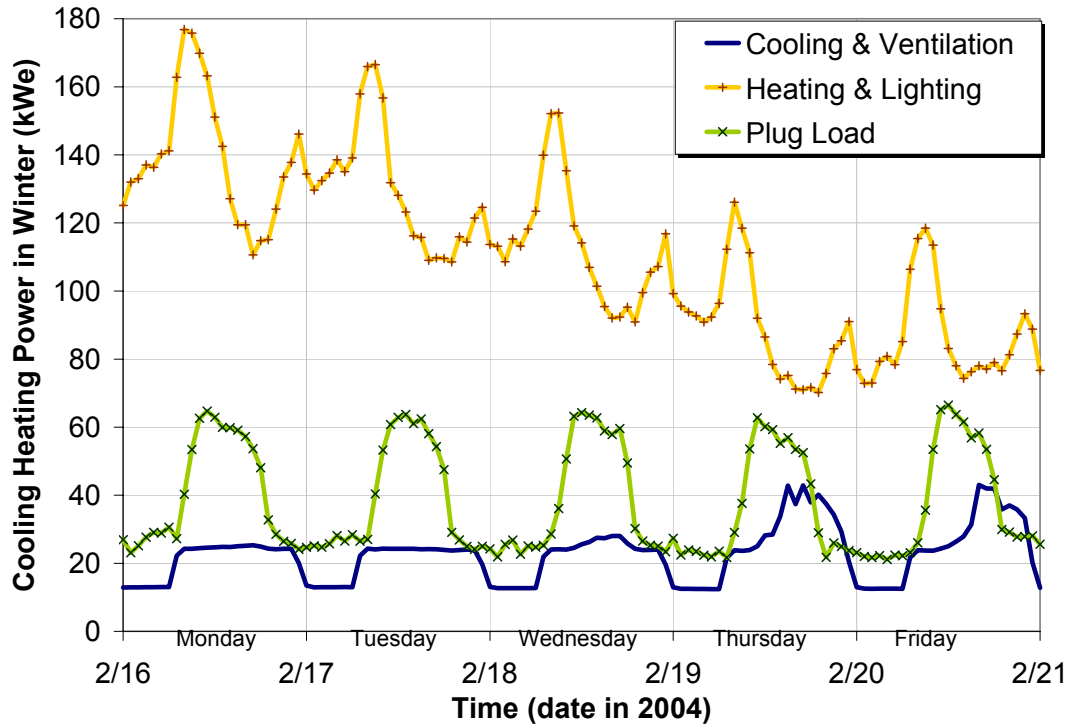
In the past, two principal technical approaches to LiBr absorption design have been used. They involve: (1) Mechanical design changes, such as very highly efficient heat exchangers, to bring the air-cooled operation within the existing LiBr/H₂O crystallization limits. This approach is significantly more expensive per ton of capacity than the conventional water-cooled LiBr/H₂O absorption chillers, and therefore it is not considered suitable in most applications (Sweetser et al., 2000). (2) The use of chemical additives, such as 2-Ethyl Hexanol, to shift the crystallization line to higher temperatures to allow air-cooled operation with commercially practical margins of safety from crystallization using conventional heat exchangers (Kulankara et al., 2001, Ghosh et al., 2002). However, all of the suitable chemicals exhibit negative characteristics that effectively limit their practical application. In this research, a third approach – implementing temperature control strategies – was proposed by the author in this research.

Application Investigation

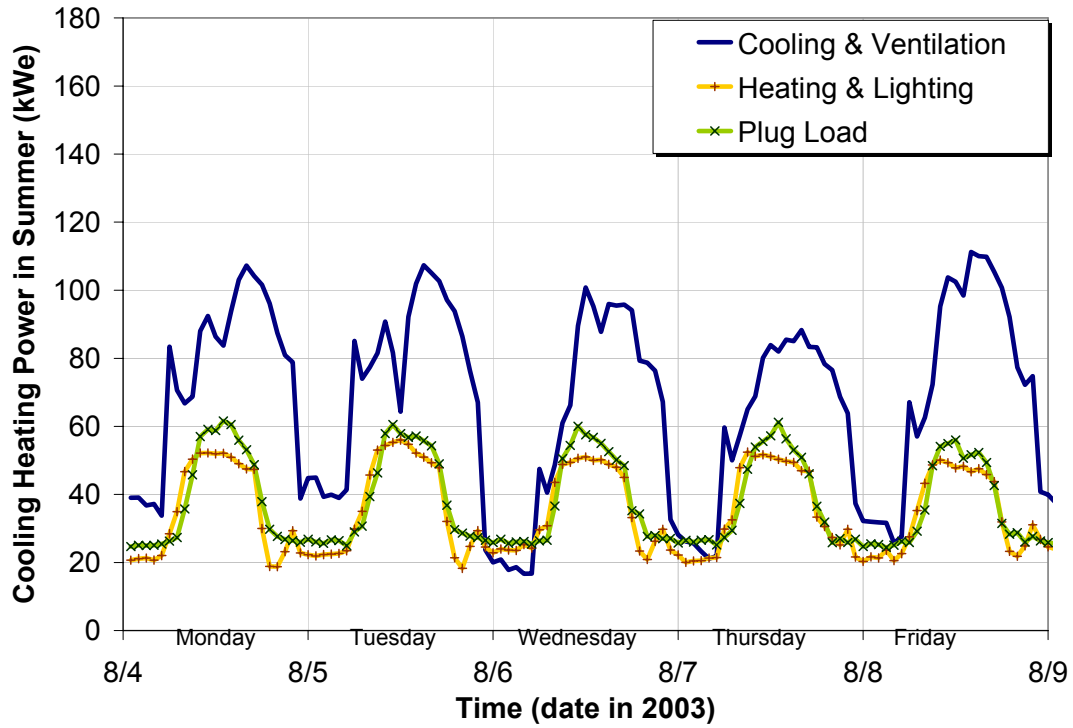
HVAC systems are typically operated at design conditions less than 1% of their running time (ARI, 1999). This situation is not unique for HVAC systems – if the CHP is sized to meet the peak load of the building, then it would have to operate at partial capacity for most of the time and dump the excess waste heat.

In a real commercial building with electric heating, the electricity is basically consumed and dominated by three categories: cooling and ventilation, heating and lighting, and plug load. However, Fig. 4 shows that the electricity load profile varies on a daily, weekly and seasonal timeframe, not only in magnitude, but also in shape as well.

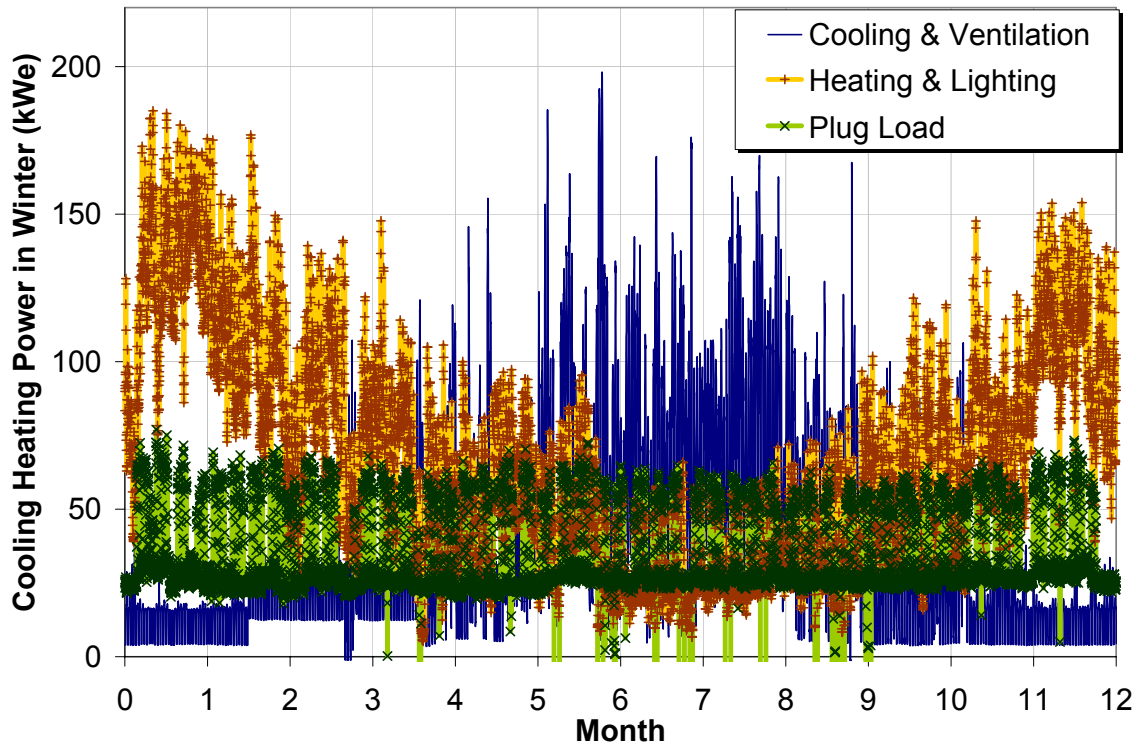
Although the building plug load used by the office and kitchen appliances is relatively constant, it is rather complicated to match simultaneous cooling, heating and power loads in this building.



(a) Heating season



(b) Cooling season



(c) Whole year

Fig. 4. The load profile in the Chesapeake Building

Source: Data acquired from the Chesapeake building at UMD

To speed the payback from the relatively more expensive CHP system, the operating hours at full electrical generating capacity should be maximized. Therefore a small capacity CHP system that runs with the conventional HVAC to provide the required capacity helps to ensure this.

A building always needs some outdoor air (OA) for ventilation. New standards for building ventilation (ASHRAE Standard 62-2001) require much greater quantities of minimum fresh air to provide acceptable indoor air quality (IAQ), assure the comfort of human occupants, and avoid adverse health effects. For more information, see Appendix A – ASHRAE Minimum Ventilation Rate History.

Mumma, S. (2001) introduced the Dedicated Outdoor Air System (DOAS), which conditions outdoor ventilation air separately from the conditioned space return air stream and eventually handles the entire building latent load. There are various configurations of DOAS (Trane Company, 2003), but the indispensable device in the proposed DOAS is a direct expansion (DX) coil as shown in Fig. 5, which cools and dehumidifies the outdoor air to 7°C dew-point temperature (note: usually the conventional system is set at 13°C). However, his publications do not mention the lower Coefficient of Performance (COP) due to lowering the dew-point to achieve higher moisture removal capacity. The DX coil is followed by a sensible wheel* intended to recover the building exhaust energy without introducing moisture from the more humid building exhaust air flow to the drier ventilation air flow. This approach is claimed to have superior humidity control when the primary source of humidity in most buildings - ambient humidity carried in from the outdoors - is dealt with directly at its source.

* The sensible wheel is not coated with desiccant and therefore transfers only sensible energy between two air streams as the mass of the material gains or loses heat to the opposite air stream.

Cowie, M. (2003 b) extended this concept to the CHP domain and named it CHP DOAS. However, more experiments and/or simulations are needed to validate and quantify the benefits.

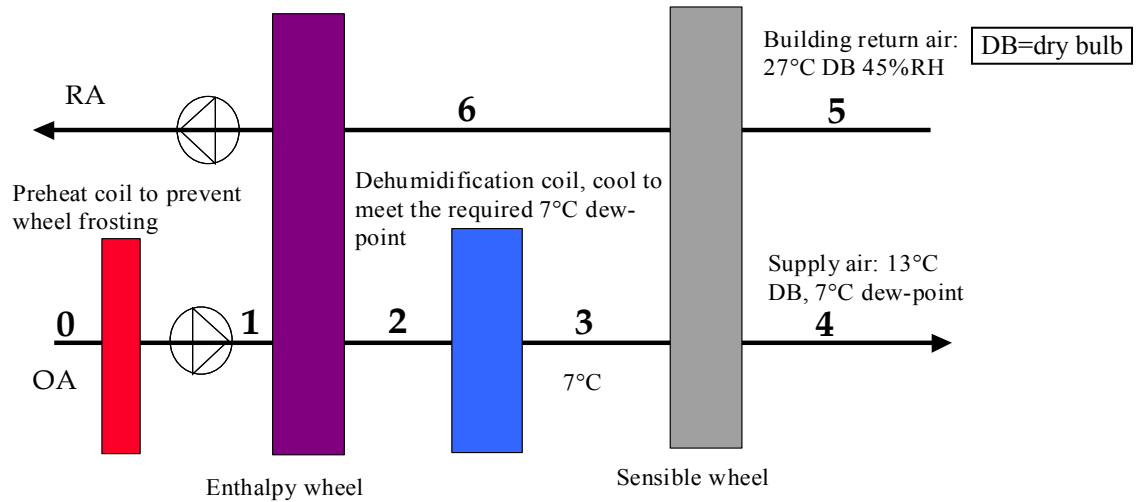


Fig. 5. General configuration of the DOAS

Standards of Efficiency Evaluation

The efficiency evaluation of CHP systems or energy conversion systems is more complicated than conventional vapor compression systems due to multiple energy outputs and inputs, and no standards are available so far, which is adverse to the system optimization because the objective of optimization is hard to define. Petrov, A. et al (2004 a) evaluated different efficiency concepts and suggested different equations. Cowie, M. (2002) also discussed the differences within several common efficiency terminologies.

Chapter 2 - Motivation and Research Objectives

Motivation

According to the literature review, there is no research being conducted in integration of an air-cooled absorption chiller into a CHP system, and no experiments or field experiments of integrated systems have been conducted to validate the feasibility of the air-cooled concept and computer modeling also. So this research fills in the gap and develops guidelines for reference in support of the future commercialization by facility owners, equipment operators or design engineers.

A representative commercial office building is located on the campus of the University of Maryland and is well suited to demonstrate the benefits of CHP technology (Marantan, 2002 a, Popovic et al., 2002). The building and its HVAC and CHP equipment were well instrumented, and the Data Acquisition System (DAS) has been running continuously for 4 years. All the existing conditions make it possible to validate and quantify the innovative concepts proposed here by experiments.

Objectives

The objectives of this research are:

(A) Experimentally,

- Demonstrate the feasibility of an air-cooled absorption chiller in CHP systems.
- Conduct a performance evaluation of the system, benchmark individual CHP equipment performance, and benchmark integrated equipment system performance in an occupied building.

(B) Theoretically,

- Create a computational air-cooled absorption chiller model, integrate it with the available microturbine model and other thermal equipment models to predict the performance of the integrated system, and verify it with experimental data.
- Propose the application of an air-cooled absorption chiller in CHP systems, and perform an energy efficiency evaluation of the integration options.
- Develop guidelines to assist designers, researchers and manufacturers in better understanding the characteristics and performance of air-cooled absorption chillers integrated in CHP systems.

Chapter 3 - Experimental Setup

CHP Integration Test Center on the Campus of UMD

The CHP Integration Test Center is located in the Chesapeake Building, a fully instrumented administrative office building at the University of Maryland, College Park (UMD). The building is 52,700 ft² (4896m²) and has four stories. It was constructed in 1991 and measures 128 ft in length, 96 ft in width and 50 ft in height (39m L×29m W×15m H). The physical size of the building puts it into a medium-sized office building category (10,000 to 100,000 ft² or 929 to 9290 m²). This category represents 23% of all buildings and comprises 46% of the total floor space in the U.S (Marantan, 2002 a, Popovic et al. 2002). There are approximately 200 employees in the building during normal operating hours (8AM-5PM, M-F) and the work is generally light duty office work. Figure 6 exhibits its three dimensional characterization. More specifications are listed in Appendix H – Field Data and EnergyPlus Simulation.

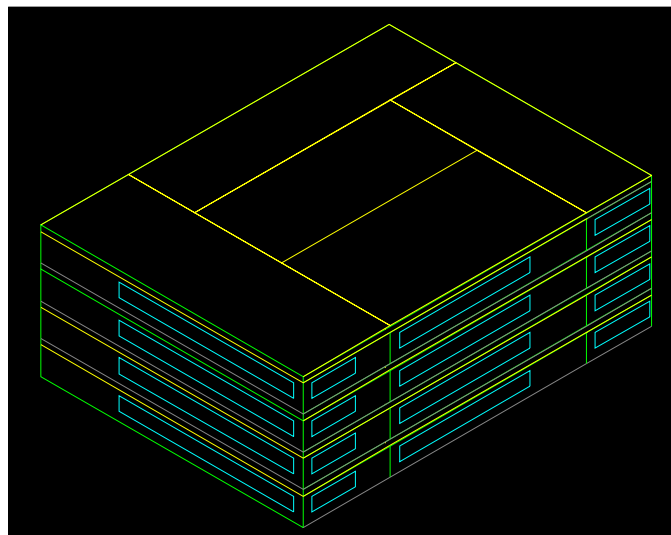


Fig. 6. 3D Characterization of the Chesapeake Building with four exterior air-conditioning zones and one interior zone

The original building entirely relied on grid electricity for power and roof top units (RTU) for cooling, and the electric heaters inside the variable air volume (VAV) units around the perimeter zone for heating or reheating. There are two CHP systems integrated with the existing building's RTU#1 and RTU#2 respectively.

Features of Test Facility

The unique feature of the Test Center is that the CHP system that comprises real commercial equipment is installed and operates in a real office building with comprehensive characterization. However, since the machines are installed outdoors, the operation conditions, such as the weather, cannot be controlled. Other factors, such as evacuating the chiller and the on/off switchover of the cooling tower fan, will also affect the performance. Besides, multiple test tasks on CHP components and systems also must be conducted simultaneously in the short summer. Therefore, extensive tests should be conducted to make full use of different weather conditions and compensate for the deficiency of real life building tests.

A weekly test schedule was developed and adopted. Each weekday had a different test task and some settings were altered according to Table 1, so that each test task could cover almost all the weather conditions. Use the air-cooled chiller test on Wednesday as an example: the microturbine is set at 60 kW power demand, and the SDU uses the residual heat from the absorption chiller, and the chiller runs on the default settings except that the cooling tower water is altered.

In addition, making a detailed test log is very important to the future data analysis, which should include the test date, time, purpose, operation condition settings, and weather range. See Appendix G – Test Logs for Summer of 2003.

Table 1: Test schedule on weekday

Weekday ¹	Microturbine	Absorption Chiller	Solid Desiccant Unit	Test Purpose
Monday	Run MT at 10-60kWe power output ²	Run chiller at default settings ³	Run SDU (burner is off)	Set up CHP baseline
Tuesday	Run MT at 60kWe	Run chiller at default settings	SDU runs on exhaust and burner (vary burner temperature)	ATS Integration test: SDU burner supplied the make-up heat
Wednesday	Run MT at 60kWe	Run chiller, and alter the cooling tower water supply temp. (up to 95°F)	Ran SDU on exhaust	Air-cooled chiller simulated test (1) – coolant temp ⁴ .
Thursday	Run MT at 60kWe	Run chiller at default settings	-	MT and chiller integration test: Investigate back pressure effect on MT
	-	-	Ran SDU independently on burner alone	SDU baseline and transient test to investigate the impact on RTU2
Friday	Run MT at 60kWe	Run chiller, and vary the chilled water temp. and exhaust temp. Cooling load is adjusted via the 3-way valve.	Ran SDU on exhaust	Air-cooled chiller simulated test (2) – chilled temp. and exhaust temp ⁴ .

Note:

1. On weekdays, microturbine, absorption chiller and solid desiccant should be turned on continuously from 9:00 am ~ 5:00 pm.
2. When altering the variables, the interval should be at least 2 hours to maintain stable operation.
3. Chiller default settings: chilled water outlet temp at 45°F±1.5°F, cooling water inlet at 85°F, and exhaust at 540°F. The 3-way valve on the water coil is set at 100% opening.
4. Air-cooled chiller simulated test: to simulate air-cooled conditions with a water-cooled absorption chiller.

Microturbine-based CHP System

As listed in Table 2, the microturbine-based CHP system has evolved through three generations so far. This investigation focuses mainly on the second-generation system, which includes a 60 kW microturbine, an 18 ton (63 kW) water-cooled absorption chiller and a 3000 CFM (5097 m³/hr, 1 CFM = 0.47 l/s) Solid Desiccant Unit (SDU). The CHP system integrates with the existing RTU#2 on the building. Figure 7

depicts the system components along with their energy flows and parasitic power consumption.

Table 2. Three generations of the microturbine-based CHP system

Generation	Microturbine	Absorption chiller	Solid desiccant Unit
1 st	75 kW Honeywell	Broad 18 ton	ATS 3000 CFM
2 nd	60 kW Capstone	Broad 18 ton	ATS 3000 CFM
3 rd	60 kW Capstone	Broad 21 ton with built-in cooling tower, pumps, power and control panel. See Appendix F – BCTDE P&I Diagram and Table 3	ATS 3000 CFM

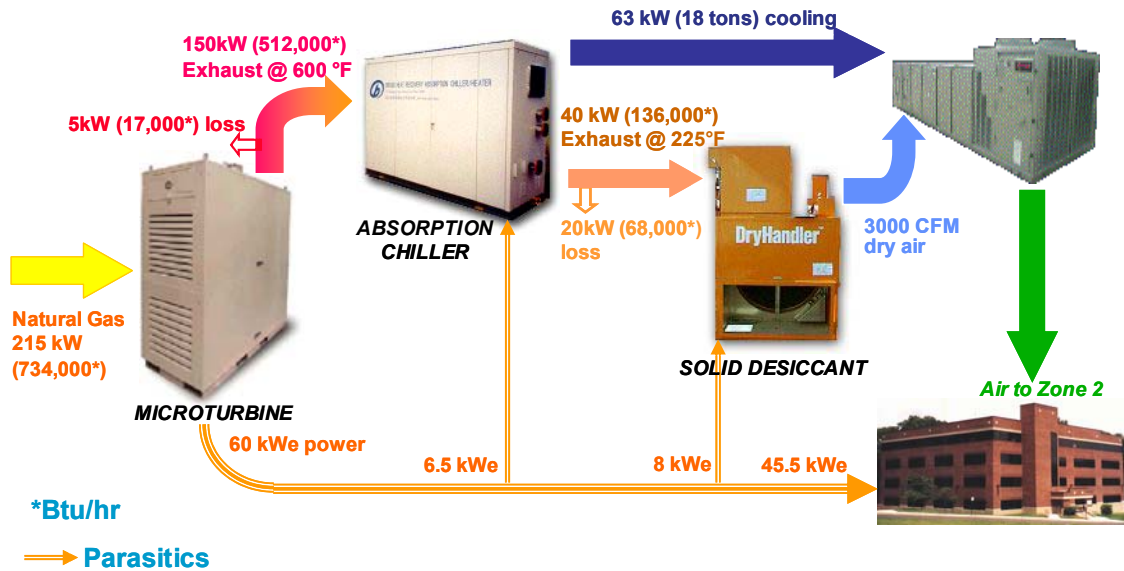


Fig. 7. Microturbine-based CHP system at UMD

Microturbine

The microturbine generates electricity onsite; its peak shaving effect is clearly illustrated in Fig. 8. The microturbine used as part of this investigation is a Capstone 60 kW high-pressure natural gas unit. It is grid-connected in parallel to the building's 480 volt 60 Hz grid service. The unit has an external fuel gas compressor that compresses the

natural gas from 5.5"W.C. up to 90 psig, which is then regulated down in a gas regulator to 75 psig for the microturbine to operate on natural gas.

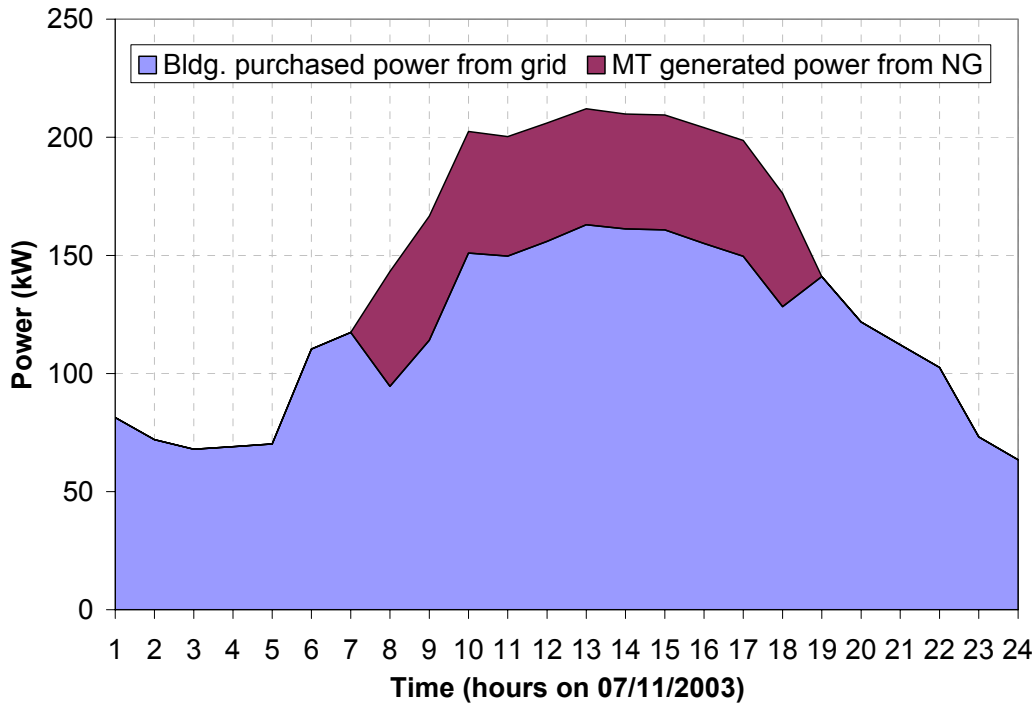


Fig. 8. Microturbine power shaving effect on the Chesapeake Bldg.

Water-cooled Single Effect LiBr Absorption Chiller

The absorption chiller is an 18 ton single-effect water-cooled LiBr absorption chiller that is designed to use the exhaust gas of the microturbine directly as its heat input source. The chilled water provided by the absorption chiller is delivered to the existing RTU#2 through a chilled water coil inserted in the air stream directly before the original direct expansion (DX) coil of RTU#2. The chilled water pump overcomes the pressure drop along the water loop to maintain the desired flow rate.

Table 3. Technical Data of the 21 ton Broad Exhaust Absorption Chiller

Model	Unit	BCTDE75-310-115
Cooling capacity	kW (RT)	75 (21)
Heating capacity	kW (MBH)	90 (307)
Chilled water outlet /inlet temp.	°C (°F)	7.2 (45) / 12.2 (54)
Heating water outlet /inlet temp.	°C (°F)	50 (122) / 43.9 (111)
Chilled water flowrate	m ³ /h (GPM)	12.7 (56)
Exhaust inlet temp.	°C (°F)	230/590
Exhaust flowrate	kg/s (lb/h)	0.49 (3885)
Parasitic power	kW	5.78
Weight	kg (lb)	1900 (4185)

Solid Desiccant Unit

The exhaust of the absorption chiller is used to regenerate the ATS solid desiccant unit (SDU), which provides dehumidification of 3000 CFM outdoor air for the 3rd and 4th floors of the building, i.e. Zone 2 as marked in Fig. 7. The dry air is delivered to RTU#2 directly and cooled there.

The SDU at the Chesapeake Building is a two-wheel system. Figure 9 depicts the configuration of both wheels inside the unit and the associated air flows.

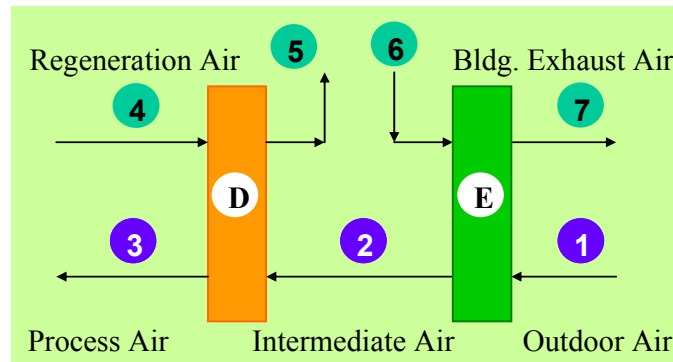


Fig. 9. Schematic drawing of solid desiccant unit

The enthalpy wheel is similar to the sensible wheel – a wheel or heat exchanger that is not coated with a desiccant and therefore transfers only sensible energy – except that a desiccant medium is added to the wheel’s surface. The warm/humid summer air is cooled and dried by the building exhaust air in summer. In winter, the building exhaust is

usually warmer and more humid than the outside air, and it preheats and humidifies the ventilation air. The enthalpy wheel reduces the load on the HVAC system and boosts the efficiency in either case.

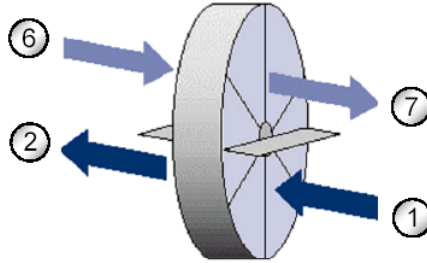


Fig. 10. Enthalpy wheel

Normally the enthalpy wheel is evaluated by effectiveness (ε). Using the numbers described in Fig. 10, ε is defined as follows:

$$\varepsilon = \frac{\dot{m}_1(x_2 - x_1)}{\dot{m}_{\min}(x_6 - x_1)} = \frac{\dot{m}_6(x_6 - x_7)}{\dot{m}_{\min}(x_6 - x_1)} \quad (1)$$

where:

x = humidity ratio, dry bulb temperature or enthalpy at the given location

\dot{m} = air mass flow rate

\dot{m}_{\min} = the smaller value of two streams.

The desiccant wheel is constructed by placing a thin layer of the desiccant material “Silica Gel” on a support structure, and it is used when low dew point conditions are required. A hot air stream is used to drive off moisture and regenerate $\frac{1}{4}$ of the wheel. The remaining $\frac{3}{4}$ of the wheel area is available for the process air. This process of dehumidification also heats the air as latent load is simply transformed into sensible load.

Normally the desiccant wheel is evaluated by latent COP - a measure of the desiccant dehumidification unit’s efficiency. It is calculated by the ratio of the latent load to the thermal energy input to the regeneration side.

Data Acquisition System

DAS Architecture

A Data Acquisition System (DAS) and 172 instruments were installed to determine the performance of the building and its HVAC and CHP equipment at baseline and other operating conditions. The allocation of user-installed sensors is listed in Table 4. The types of data include: temperature, humidity, gas/air/exhaust/liquid flow rate, electricity, current, building pressure, equipment status, and weather station data. The DAS is capable of providing high accuracy data and completely customized measurements by programming in the HP VEE (Hewlett-Packard Visual Engineering Environment) software, a visual programming language specifically designed for instrument control, monitoring and data acquisition.

Table 4. Allocation of user-installed sensors in the CHP Integration Test Center

Machine/facility	Sensor quantity
Microturbine	2
Absorption chiller	7
Solid desiccant unit	17
RTU units	33
Building environment	57
Building power	5
Weather station	6
VAV units	22
System 1	23
Total	172

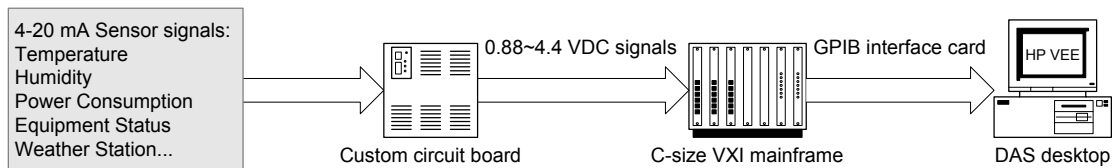


Fig. 11. DAS architecture

Figure 11 shows the DAS architecture. Most sensors can output 4~20mA signals. The advantage of using ampere analog signals is to avoid the signal attenuation over long wires. A custom electric board converts the amperage to 0.88~4.4VDC voltage. The HP VEE program converts the 0.88~4.4VDC signals picked up by the GPIB interface card to readings, then records at one-minute interval into text format log files in the DAS computer.

Correct programming in HP VEE can bring higher accuracy, convenience to the data acquisition, and even reduce some redundant hardware. Use the condensate collection device (Fig. 12) as an example, the condensate water condensed by the RTU is drained to a container, a water level switch triggers a pump to pump the water out of the container when the level reaches to the upper limit, and stop the pump when the level reaches to the lower limit. The DAS records the on/off status, which corresponds to high/low voltage signals (12Vdc/0V), once every minute to a log file. By knowing the frequency of pump operation and the water volume of each operation (a constant for the specific condensate collection device), the moisture removed by the RTU can be known. It is a direct way to show whether the CHP system can dehumidify all building latent load or not - when CHP cannot accommodate the entire latent load, the RTU needs pick the residual load up. Figure 67 is an example of condensate pump application. Each “+” means that the pump switches on once, and the density of “+” reflects the frequency of the pump operation.

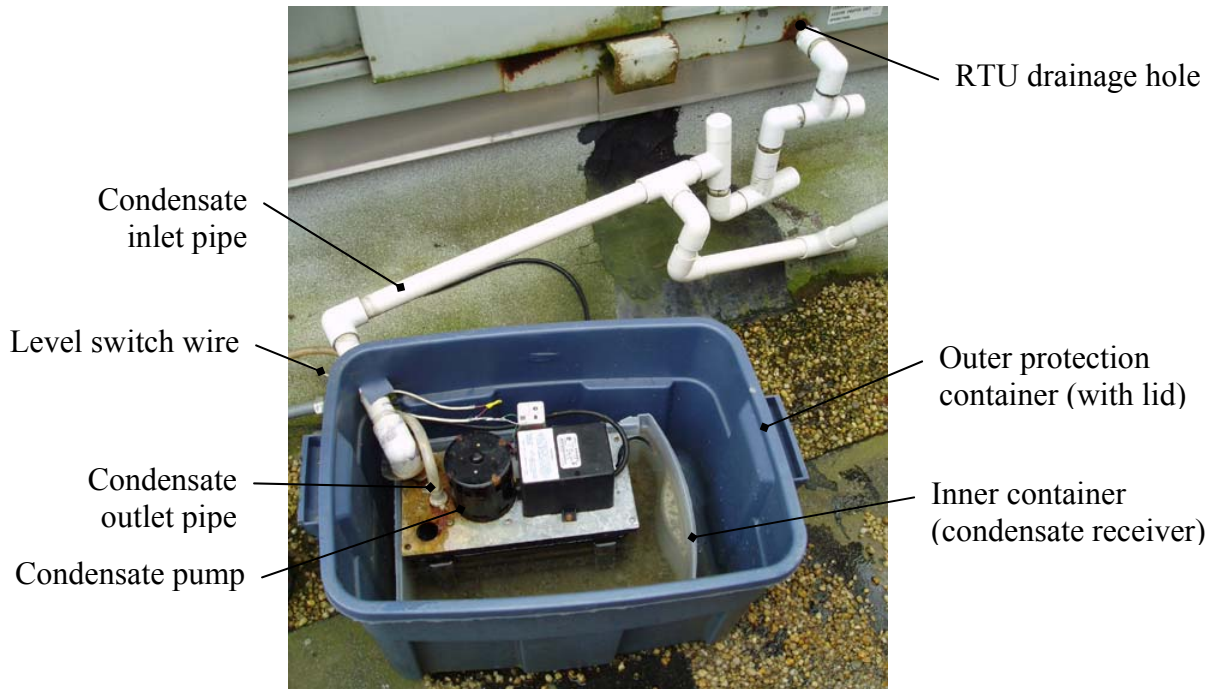


Fig. 12. Condensate collection device

Normally the pump needs about 40 seconds to pump the water out from the high limit to the low limit. If no logic is programmed in HP VEE, the DAS might miss some operations, e.g. the first minute in Fig. 13 (a) because it happens between the interval of DAS data logging, in which the shading represents the period when condensate pump is running and the dashed lines mean at that time the DAS writes the data into a log file. The former researchers installed a time delay relay, and tried to avoid the problem. The relay can purposely make up the high voltage time to 60 seconds, as shown in Fig. 13 (b), even after the pump is off. But it may cause the opposite problem; that is, the DAS might count the high voltage signal twice, for example the fifth minute in Fig. 13 (b).

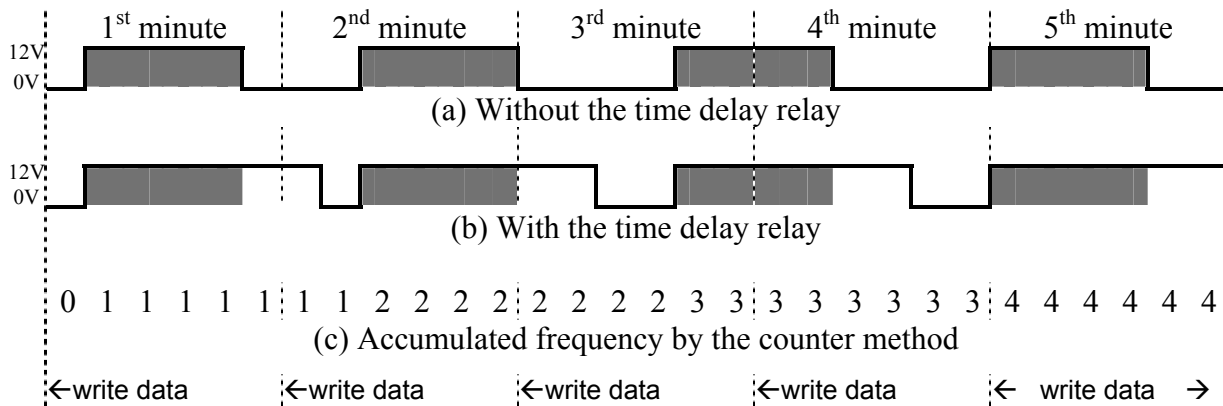


Fig. 13. Saving the operation of condensate pump w/o HP VEE logic

The author designed a logic algorithm in the HP VEE program, which solves the problem without using any time delay relay. See Fig. 14. The pump voltage signal is input to the 'Data' of Shift Register, and then copied to the "current" output terminal. Data that was in the current output is moved to the "1 Prev" output. The next 2 objectives compared their signal “a” to 10V respectively. If “a” is greater than 10V, the result is 1; otherwise 0. The third step is to compare the 2 results “A” and “B”. When $A > B$, that means the pump starts, the last object “CP1” counts once. By using this logic, the DAS can record the accumulated frequency that the pump runs without any miscounting problem. An example of the counter method is illustrated in Fig. 13 (c).

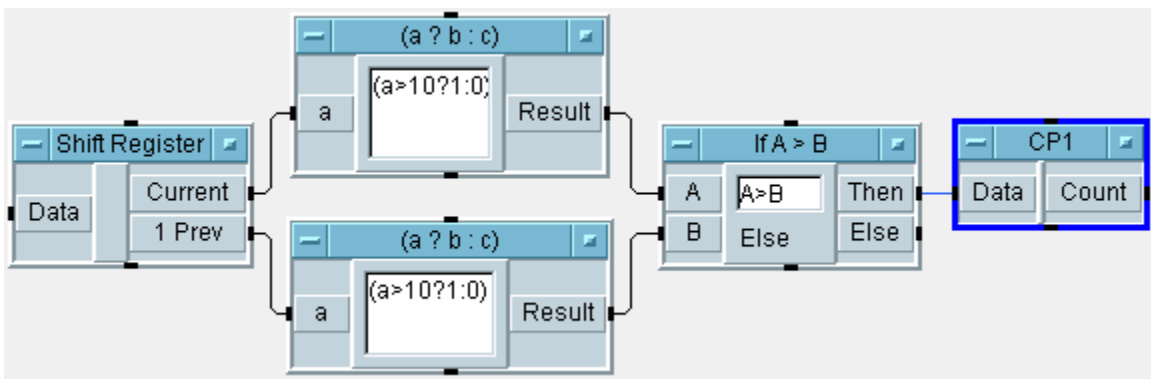


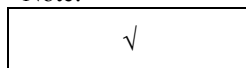
Fig. 14. Saving operation of condensate pump with HP VEE logic

Custom developed Matlab programs process the log files to make the data more meaningful and presentable. For example, Appendix B – Weather in Three Locations gives the weather data (dry-bulb, dew point and relative humidity) acquired by the DAS in College Park in a whole year. The data plots of two nearby cities, Baltimore and Dulles, published by EnergyPlus (U.S. DOE, 2004 b) are also attached afterwards for reference.

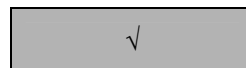
Table 5. Sensor installation for absorption chiller and its accessories

State point	Flow rate	Temperature	Pressure
1	√	√	
2		√	
3		√	
4		√	
5		√	
6		√	
7		√	
8	√	√	√
9		√	√
10		√	
11	√	√	
12		√	
13	√	√	
14		√	
15	√	√	
16		√	
17	√	√	
18		√	

Note:



Sensors preferred, but not provided



Sensors provided in test setup

Instrumentation Setup

Ideally it is better to have as many and as comprehensive sensors as possible for the purpose of system monitoring, controlling or data acquisition. Table 5 lists the preferred sensors for an absorption chiller and its accessories along with the sensors that

exist in the test center. However, in the real application the implementation is unfortunately restricted by the feasibility, availability and budget.

Figure 15 shows the exhaust heat recovery integration, cooling supply integration and instrumentation designed for the second-generation microturbine-based system. The mechanical connections between the equipment consist of ductwork, dampers, actuators and fans. These components are necessary in order to allow proper control of the exhaust from the microturbine before entering the absorption chiller. The dampers are needed to allow the microturbine exhaust gas to either flow to the chiller or to be rejected to the atmosphere depending on the chiller cooling load. When there is more of a demand for cooling, the dampers allow more exhaust gas to enter the chiller. When cooling demand decreases, the dampers reverse and allow more exhaust gas to be rejected. The make-up air fan is required in order to maintain the chiller exhaust inlet temperature. Since the microturbine exhaust temperature exceeds 600° F (316°C), it is necessary to mix in a small amount of outside air to the temperature below 550° F (288°C) before it enters the chiller due to safety concerns.

In addition, the exhaust heat management and safety control for the second-generation microturbine-based CHP system are displayed in Fig. 16.

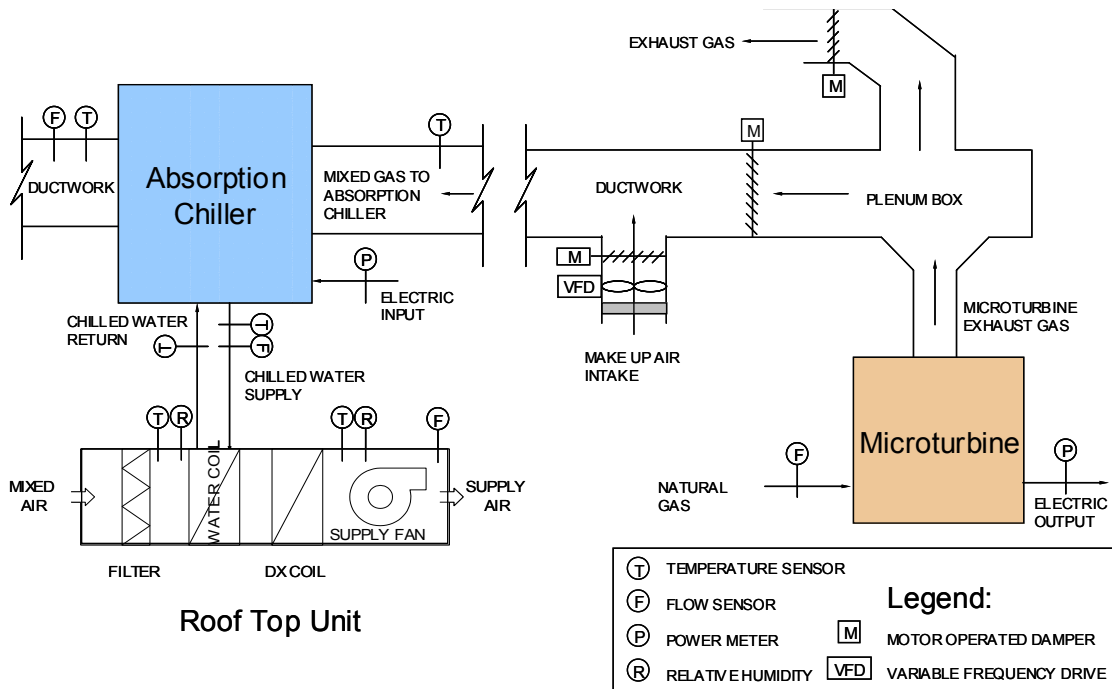


Fig. 15. P&I Diagram for the second-generation microturbine-based system

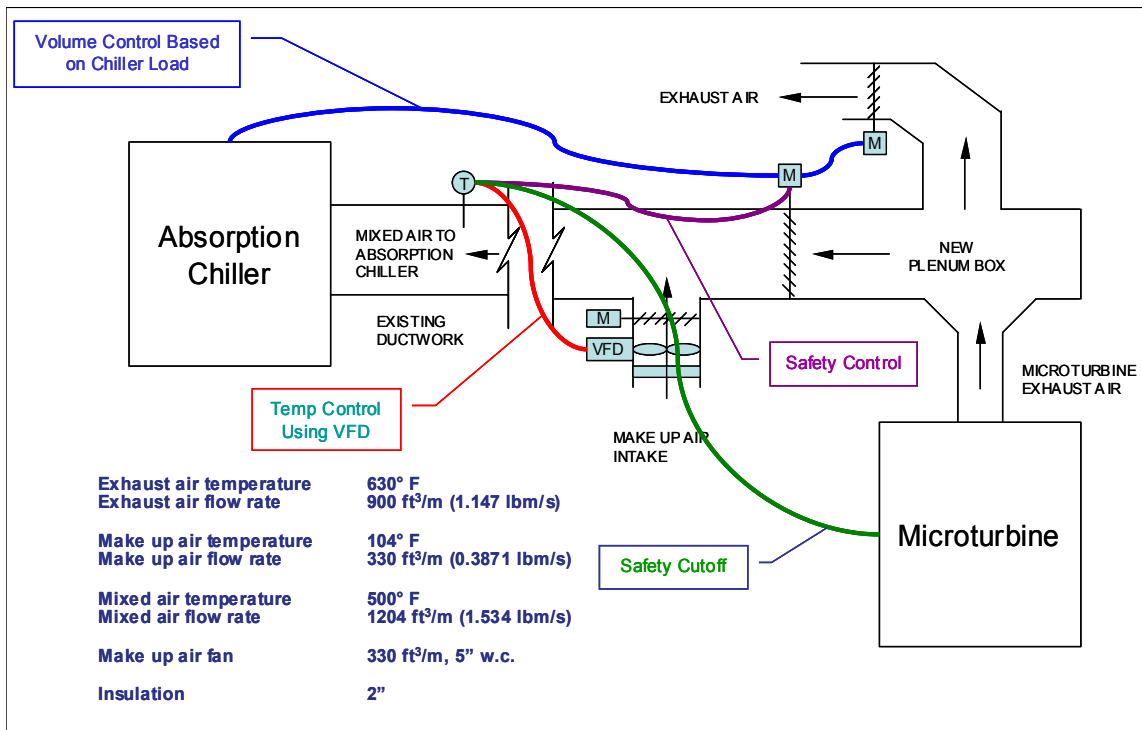


Fig. 16. Exhaust heat management and safety control for the second-generation microturbine-based CHP system

Since the chilled water coil is installed on the upstream of the existing DX coil of RTU#2 (see Fig. 15), almost in all tests the chiller was running at full capacity because its capacity is far below the demand of Zone 2. It implies that the total flow rate of exhaust gas to the chiller is constant in this investigation. However, under a specific mixed exhaust temperature setting, for example at 260°C, the constituents of the mixed exhaust vary with the ambient temperature. That is, when the weather gets hotter less exhaust gas is utilized and more make-up air is sucked in. See Fig. 17.

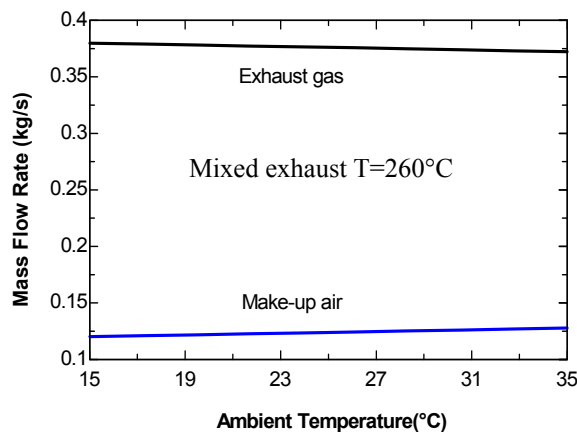


Fig. 17. The flow rate of exhaust gas and make-up air

Sensor Calibration in HP VEE

Need and Method

Numerous factors contribute to errors in measurements; a sensor device must be calibrated periodically to adjust its accuracy against the expected measurement scale. The existing conventional correction techniques are essentially based either on the hardware adjustment of the sensor response, or on lookup tables. The calibration of sensors using these methods is usually of a high cost and time consuming (Kouider, 2003). In this research, a new, economic and massive productive method is proposed and used upon the

calibration of temperature and humidity sensors, both sensors nearly cover 60% of the measurements in the Chesapeake Building.

The detailed procedure is: install a reference sensor and the sensors need to be calibrated in a closed chamber, and tie them close together. A fan is used to keep the air uniform and flowing if necessary. The chamber needs no insulation, so the temperature changes with the environment. DAS records their readings over days with the aim of collection a maximum operation range. Plot the readings of calibrated sensor over the readings of reference sensor, as the top part of Fig. 18 shows, and find the correlation for each line/curve. The last step is to update the equations inside the HP VEE program.

Determination of the Calibration Correlation

Ratio estimation works best if the data are well described by a straight line through the origin. Sometimes, data appears to be evenly scattered about a straight line that does not go through the origin. That is, the data looks as through the usual straight-line regression model: $Y = B_0 + B_1X$ would provide a good fit (Lohr, 1999). According to the least squares method, the coefficients are:

$$B_1 = \frac{\sum(X_i - \bar{X})(Y_i - \bar{Y})}{\sum(X_i - \bar{X})^2}$$

$$B_0 = \bar{Y} - B_1\bar{X}$$

X: reading of reference sensor

Y: reading of calibrated sensor

Hint: an easier way to avoid the tedious calculation and find the correlations is to use the curve fitting options in MS Excel or Matlab.

After obtaining the correlation, update the equations inside the HP VEE program for each calibrated sensor:

$$f(Y') = \frac{f(Y) - B_0}{B_1},$$

where:

f(Y)= old equation of calibrated sensor in HP VEE

f(Y')= new equation of calibrated sensor in HP VEE.

Calibration Samples

The lower part of Fig. 18 shows an obvious improvement after the calibration; all sensors were still put in the same chamber and measured the temperature at the same location, and the errors dropped from $\pm 3^\circ\text{F}$ to $\pm 1^\circ\text{F}$. The system data now have much more significance and the possibility of misinterpretations has been reduced.

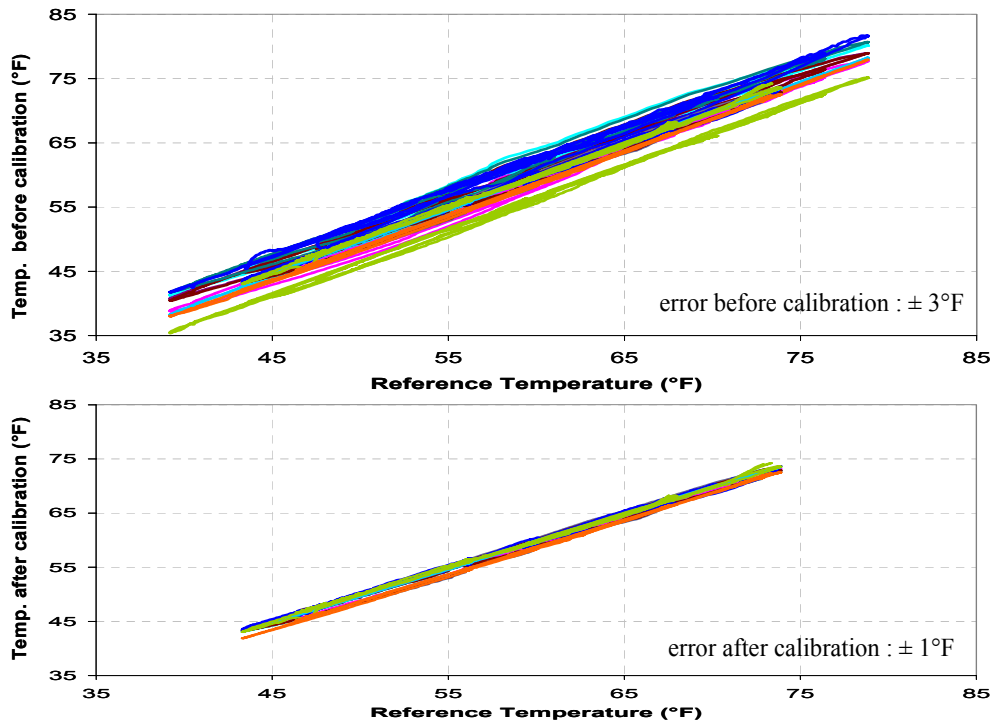


Fig. 18. A calibration sample of temperature sensor

Chapter 4 – Performance Tests on Components and CHP

System

Exhaust Temperature Profile

Since the integration of the absorption chiller with other CHP components is an important part of the research, performance tests on each component and the whole CHP system were conducted for this purpose.

In a CHP system, the generator exhaust flows through and links all components. Figure 19 depicts the temperature profile of exhaust flowing through each component on a typical operation day. Points ① and ② represent the exhaust entering and leaving the absorption chiller; points ③ and ④ represent the exhaust entering and leaving the solid desiccant unit, and point ⑤ is the ambient condition. The disparity between point ② and point ③ is caused by the heat loss from ducting due to the restriction of equipment weight on the building roof. SI and English temperature units are shown on the left and right y-axis, respectively. The dashed lines with arrows show the exhaust heat, in which there is totally ~140 kW exhaust * leaving the MT, and ~66% (92kW) is consumed by the absorption chiller, and ~16% (22kW) residual consumed by the SDU. The rest is lost during the exhaust transportation.

* The reference point is the ambient condition, i.e. Point ⑤.

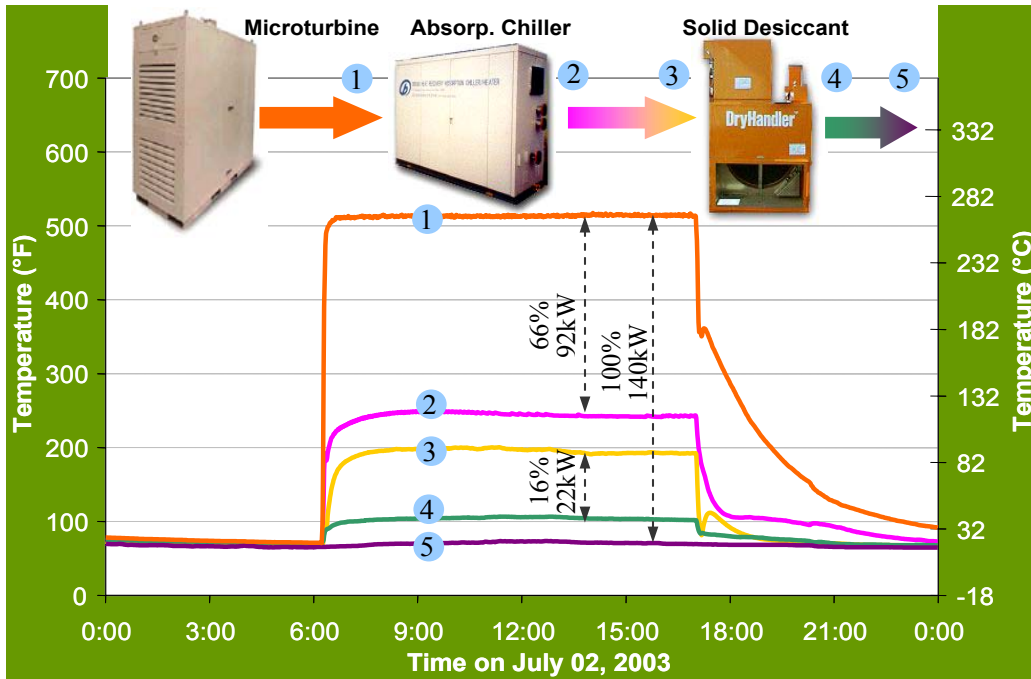


Fig. 19. Temperature profile of CHP system at UMD on a typical day of cooling season

Microturbine Performance

Extensive tests have been conducted over a wide ambient temperature span in the CHP Integration Test Center. Figure 20 shows the performance plots of MT on a typical day. From the top to the bottom they are:

- natural gas consumption;
- measured net power delivered; note that it is lower than the 60kW power demand because of the lighter air density caused by the higher ambient temperature. The ambient temperature is plotted on the middle panel of the same figure.
- microturbine efficiency.

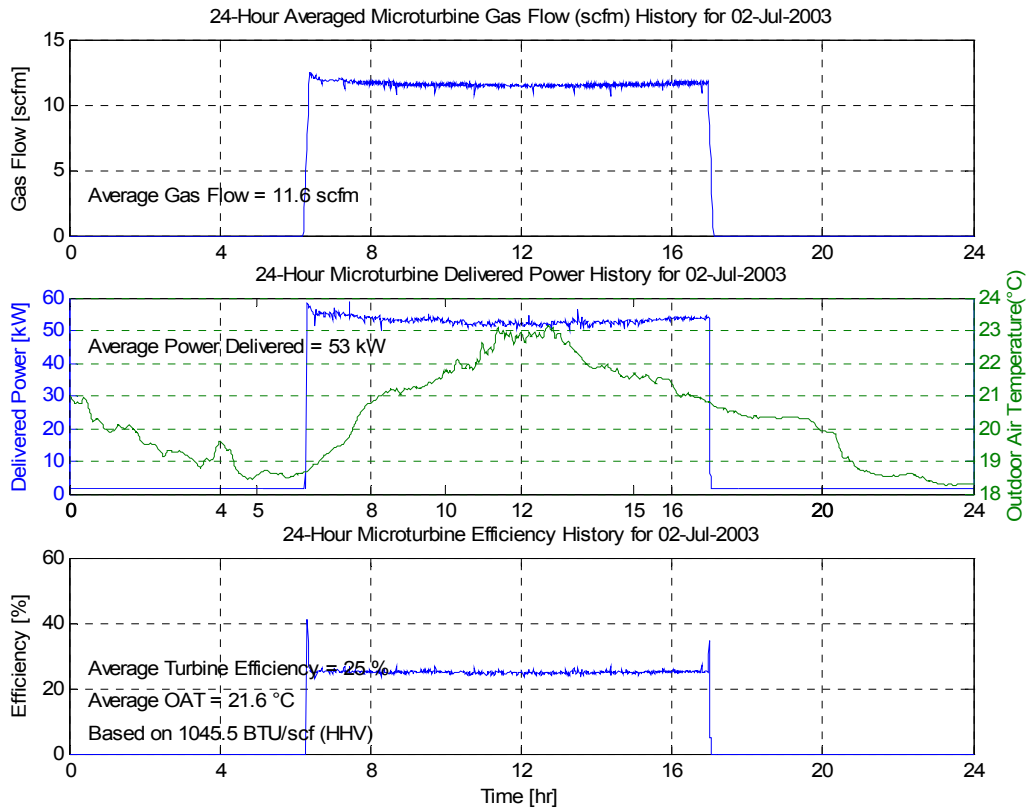


Fig. 20. Microturbine operating profiles for a typical day

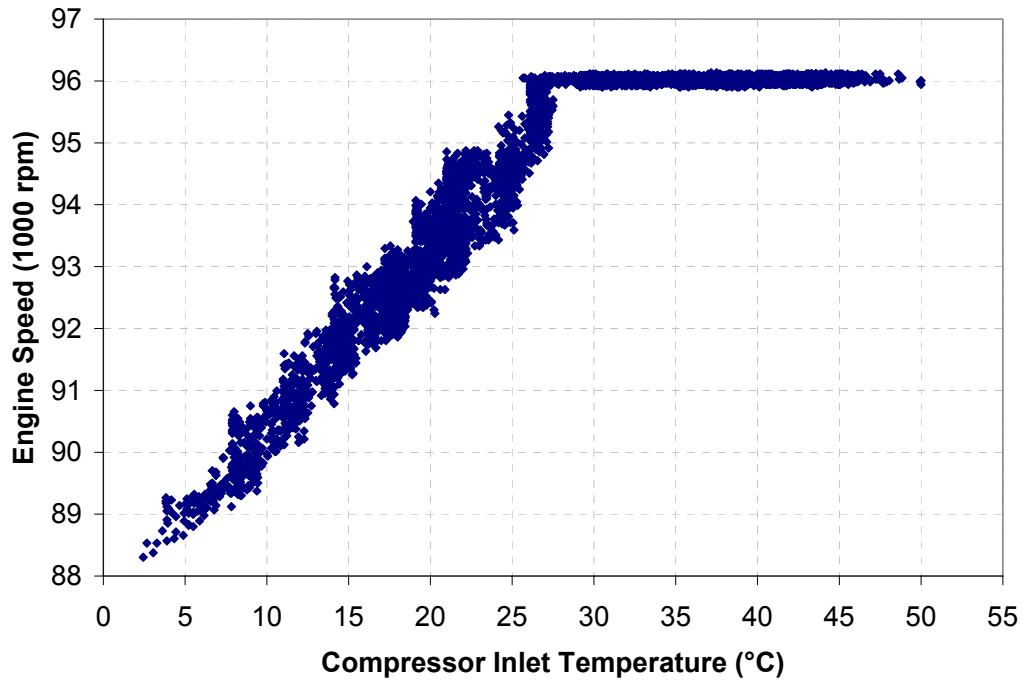


Fig. 21. Microturbine engine speed vs. compressor inlet air temperature

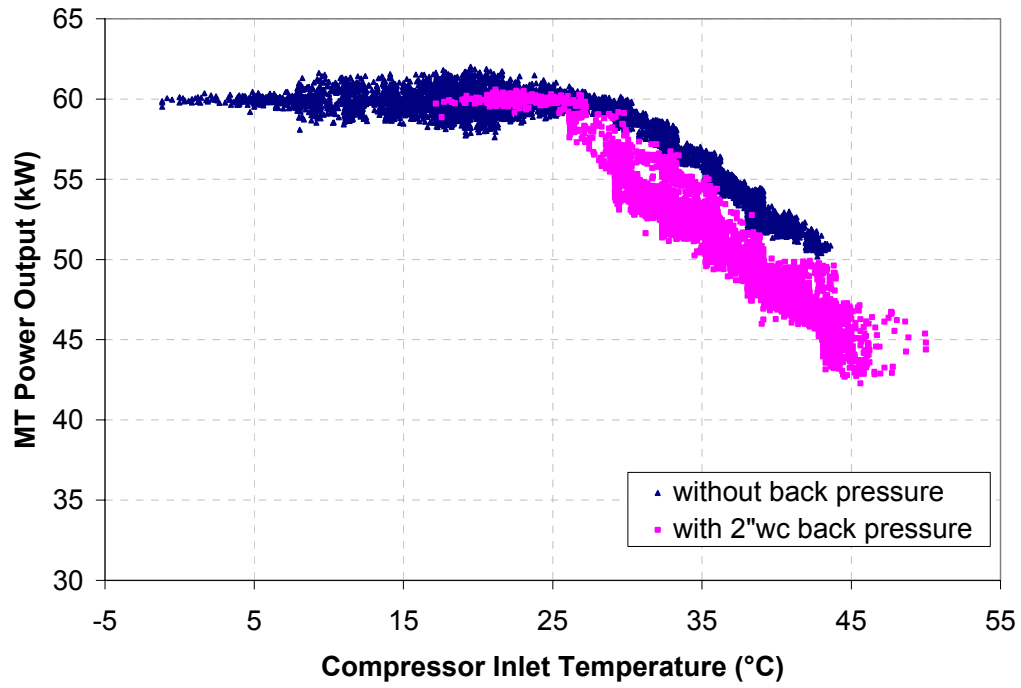


Fig. 22. Microturbine output vs. compressor inlet air temperature

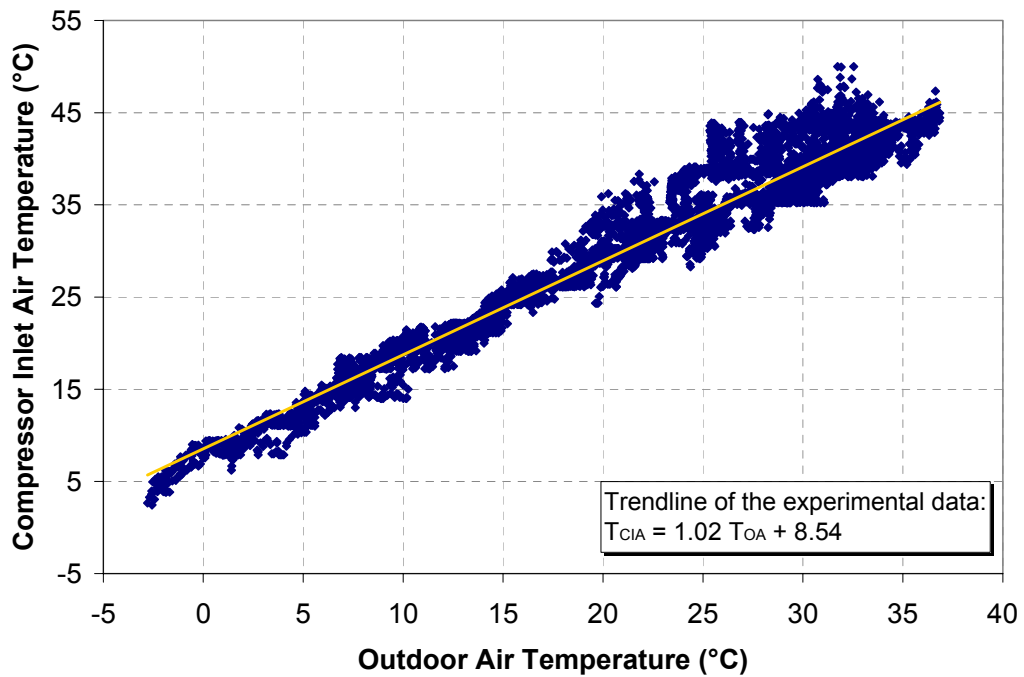


Fig. 23. Microturbine compressor inlet air temperature vs. ambient temperature

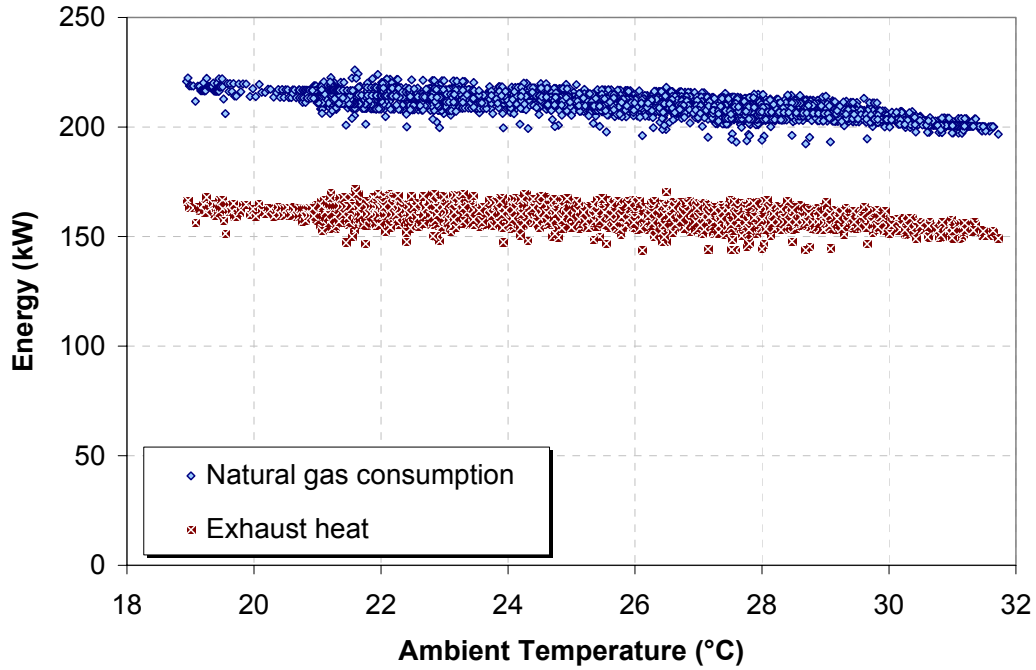


Fig. 24. Microturbine natural gas and exhaust heat vs. ambient temperature

The microturbine energy input Q_{in} is calculated by the product of natural gas flow rate and high heating value (HHV) of natural gas.

$$Q_{in} = \dot{V}_{NG} \cdot HHV \quad (2)$$

in which

Q_{in} = Microturbine natural gas consumption;

\dot{V}_{NG} = Natural gas flow rate (sCFM);

HHV = high heating value, 1103 kJ/sCFM for natural gas.

Note: sCFM is cubic feet per minute at the standard condition.

According to the energy conservation law, the exhaust heat vented by microturbine Q_{out} is the difference of natural gas energy input and the electricity output produced by the microturbine.

$$Q_{out} = Q_{in} - P_e \quad (3)$$

The microturbine efficiency η is the ratio of electricity output P_e to natural gas energy input Q_{in} .

$$\eta = \frac{P_e}{Q_{in}} \quad (4)$$

in which

Q_{out} = Microturbine exhaust heat (kW);

P_e = Microturbine electricity output (kW);

η = Microturbine efficiency (%).

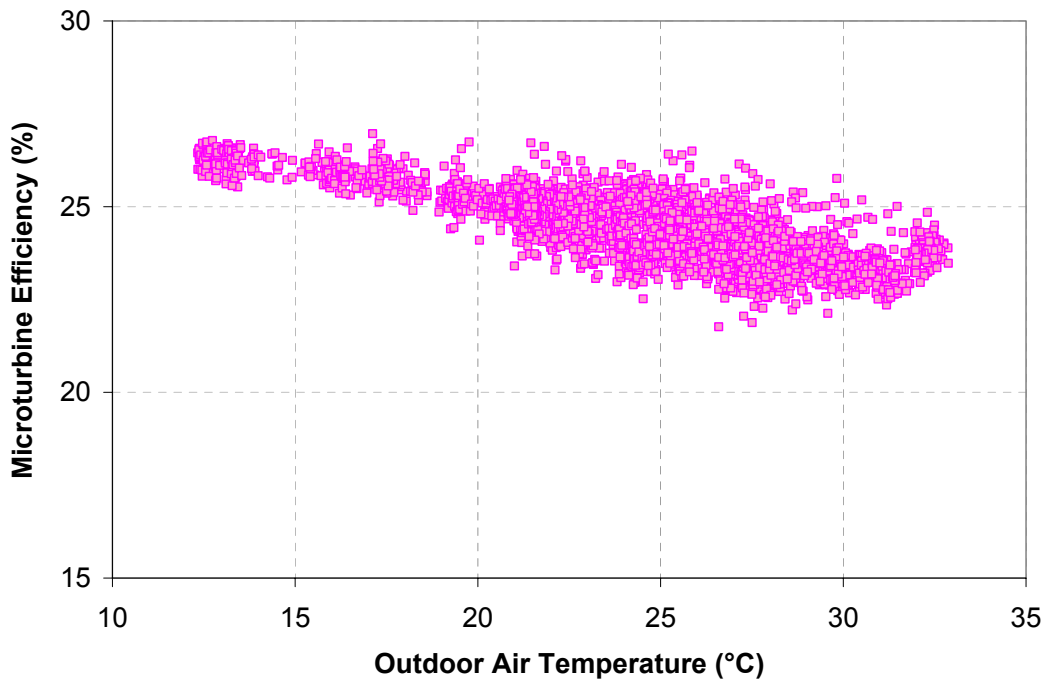


Fig. 25. Microturbine efficiency (HHV) vs. ambient temperature

The experimental results acquired in the CHP Integration Test Center are summarized in Figures 21 ~ 25. In summary, the microturbine exhibits the following performance:

- Exhaust emission: 150~160 kW
- Natural gas consumption: 200~220 kW
- MT efficiency: 23~27% (in HHV – high heating value)

Water-cooled Absorption Chiller Performance

Figure 26 shows the chiller performance on a typical day (07/02/2003). From the top to the bottom the graphs display: cooling capacity, power consumption by pumps and fans, chilled water return/supply temperature, exhaust gas inlet/outlet temperature and ambient temperature. The fan of the cooling tower was switched on and off to maintain the coolant temperature automatically; this is the reason why the power consumption and cooling capacity fluctuated.

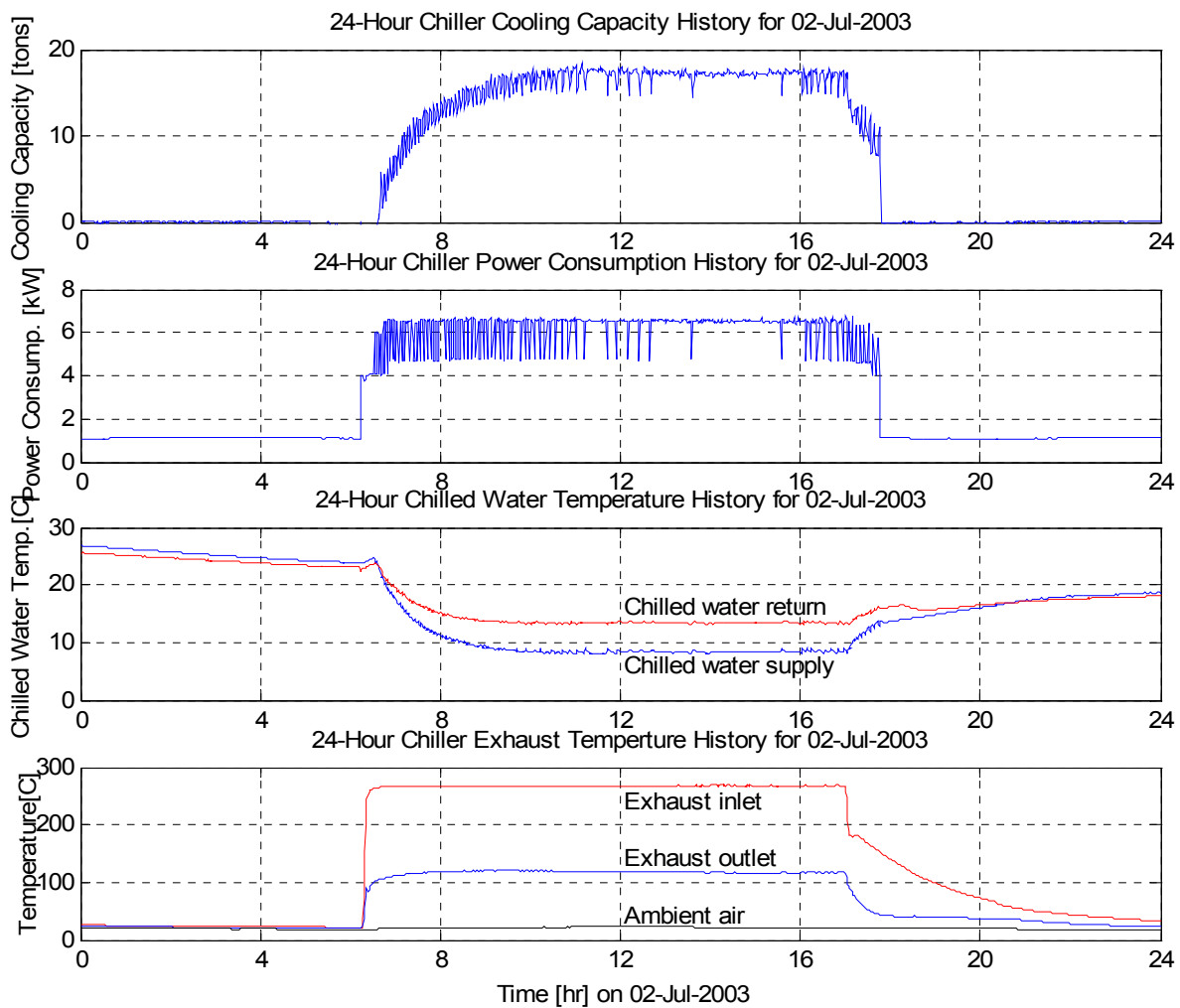


Fig. 26. The absorption chiller operating profiles for a typical day

The absorption chiller is somewhat of a thermal flywheel due to a large amount of metal hardware and the solution contents. For example, there is at least a one hour transient period after the chiller is started. However, the experimental validation is based on the performance at the steady state.

More test results are detailed in the following Chapter 7 – Absorption Chiller Validation.

Solid Desiccant Unit Performance

Approximately 350 hours of tests on SDU have been conducted over a wide ambient temperature span (15 ~ 35°C). Figure 27 shows the performance plots of SDU on a typical day. In each plot, the order of the legend entries from top to bottom corresponds to the curves from top to bottom.

The schematic drawing of the solid desiccant unit is shown in Fig. 9. The moistures removed by the enthalpy wheel and desiccant wheel are calculated by:

$$\dot{m}_{EW} = \dot{m}_{OA} \cdot (w_1 - w_2) \quad (5)$$

$$\dot{m}_{DW} = \dot{m}_{OA} \cdot (w_2 - w_3) \quad (6)$$

in which

\dot{m}_{EW} = Moisture removed by the enthalpy wheel (kg/hr);

\dot{m}_{DW} = Moisture removed by the desiccant wheel (kg/hr);

\dot{m}_{OA} = Outdoor air flow rate (kg/hr);

w_1 = Humidity ratio of outdoor air (kg/kg dry air);

w_2 = Humidity ratio of intermediate air (kg/kg dry air);

w_3 = Humidity ratio of process air (kg/kg dry air) .

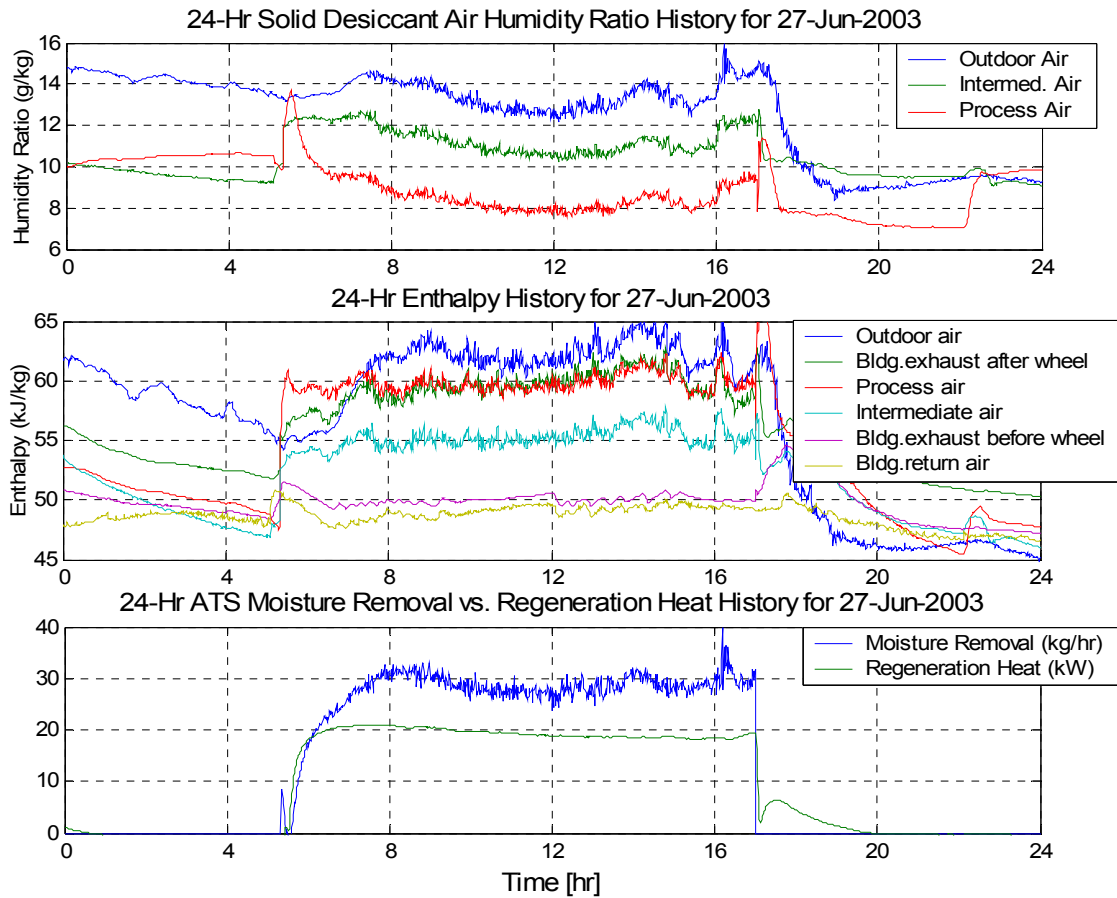


Fig. 27. Solid desiccant unit operating profiles for a typical day

The experimental results acquired in the CHP Integration Test Center are summarized in Figures 28 and 29. In summary, the 3000 sCFM SDU exhibits the following performance:

- Enthalpy wheel effectiveness: 0.75 ~ 0.8
- Desiccant wheel latent COP: 1.3 .

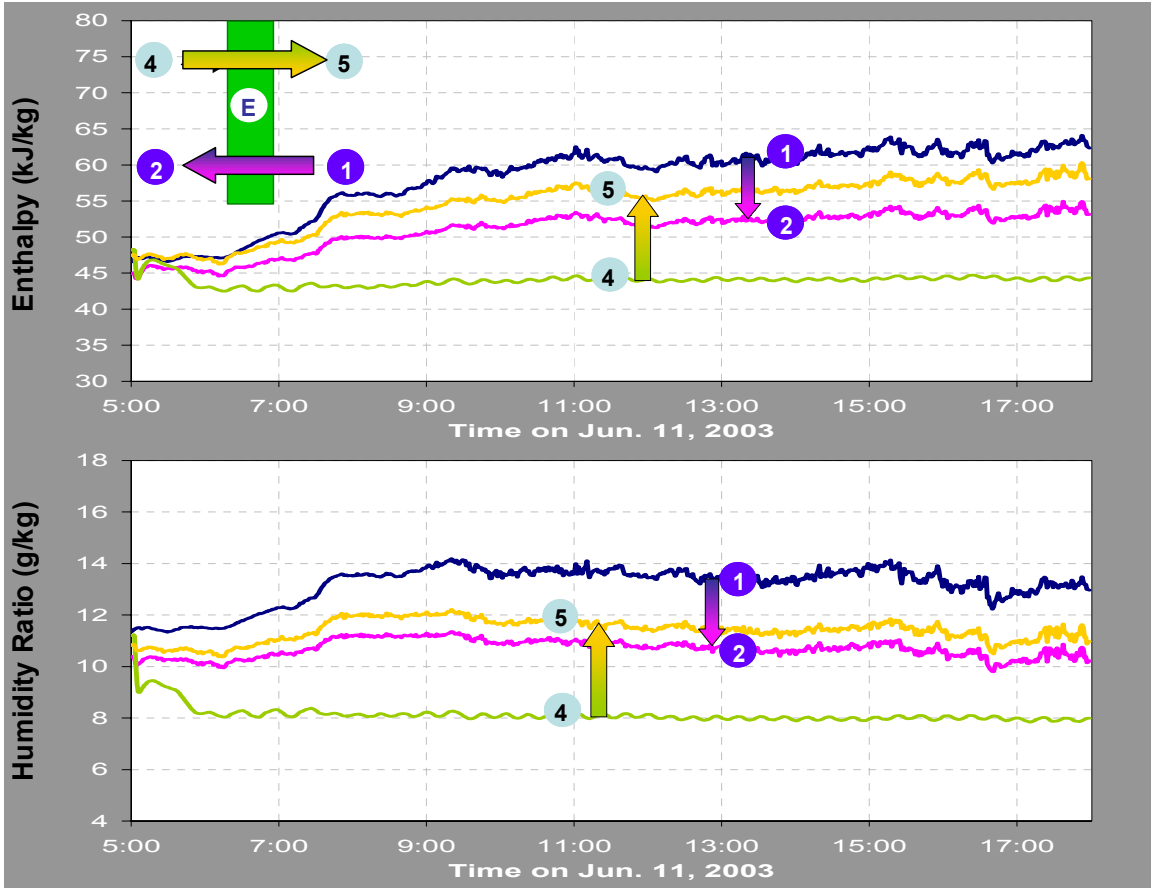


Fig. 28. Enthalpy wheel performance on a typical day

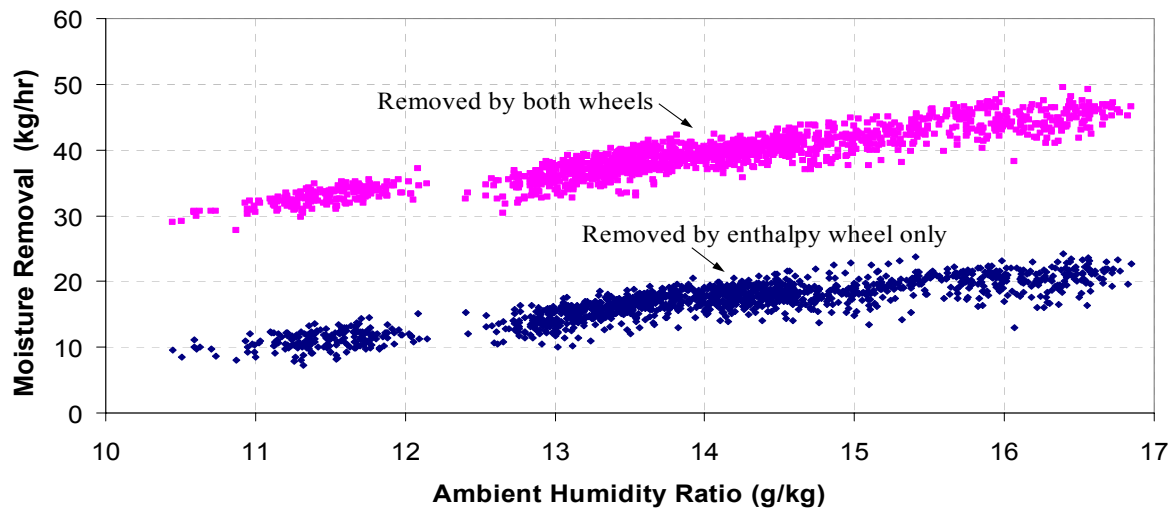
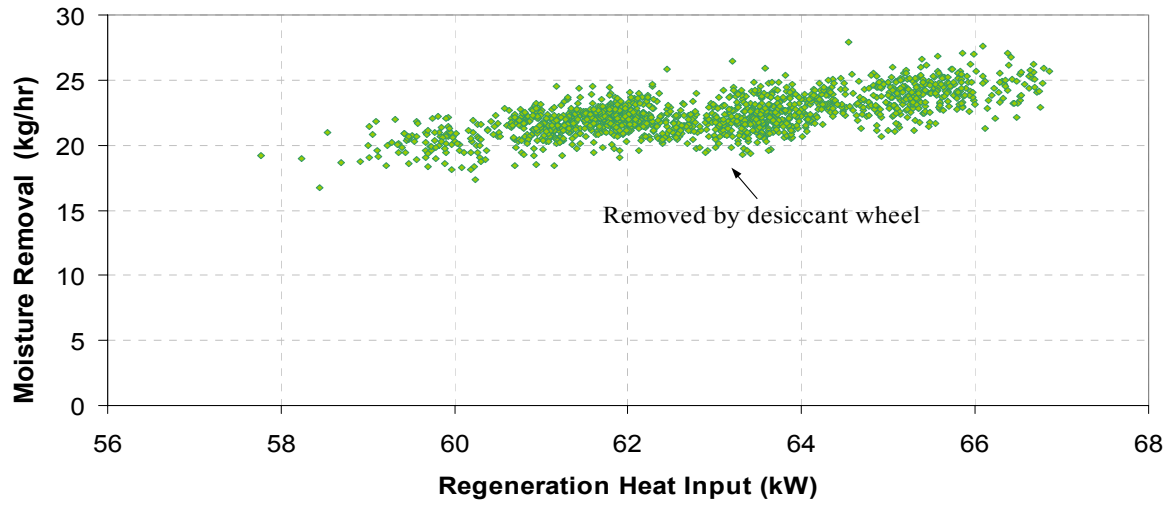


Fig. 29. Moisture removal capacity of SDU

Chapter 5 - Air-cooled Absorption Chiller Modeling

Principles of Single Effect LiBr Air-cooled Absorption Chillers

A model of a single-effect LiBr-H₂O air-cooled system is developed to investigate the performance, crystallization issues and precautions of air-cooled absorption chillers, and eventually to validate the theoretical results with simulated experiments on a water-cooled absorption chiller. Figure 30 is a flow diagram for the absorption chiller. The main components of an absorption chiller include the absorber, generator, condenser, evaporator, and solution heat exchanger.

With reference to the numbering system in Fig. 30, first, the LiBr-H₂O solution in the absorber, at point (1), gets pumped through the solution heat exchanger (2) into the generator (3). Heat input (11) to the generator allows the water to boil off from the solution into vapor (7). For the refrigerant loop, the water vapor is condensed in the condenser by ambient air (15). The water (8) then passes an expansion valve and continues to the evaporator (9) where it evaporates and provides the desirable cooling effect. The water vapor (10) then gets reabsorbed into the solution in the absorber with the help of the external coolant – ambient air (13) again. For the solution loop, the remaining solution in the generator (4) passes through the solution heat exchanger (5) before re-entering the absorber (6). In Fig. 30, the dashed lines stand for the solution loop and solid lines for the refrigerant loop.

Usually the absorption cycle is plotted in a Dühring P-T chart, a pressure-temperature graph where the diagonal lines represent constant LiBr mass fraction, with

the pure water line at the left and crystallization line at the right. A typical cycle and some state points are shown in Fig. 31.

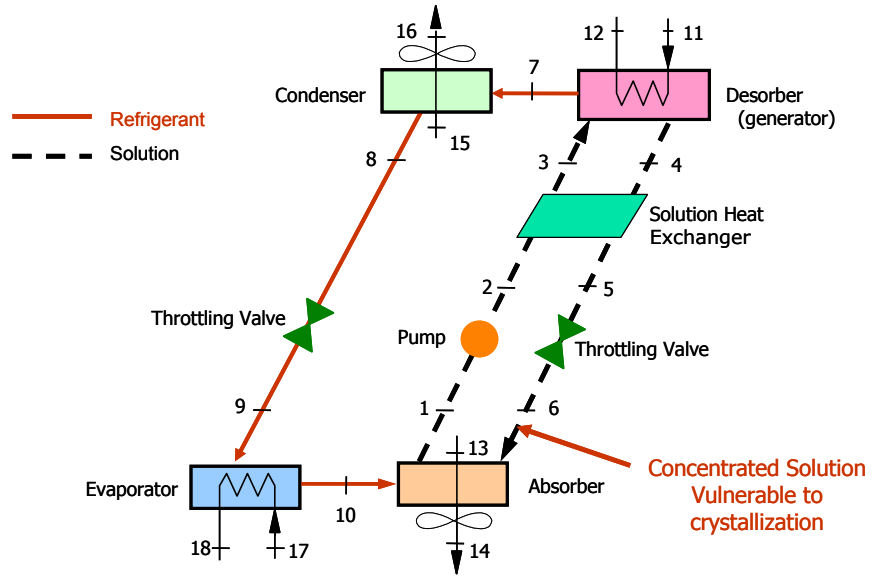


Fig. 30. Diagram of single-effect air-cooled absorption chiller

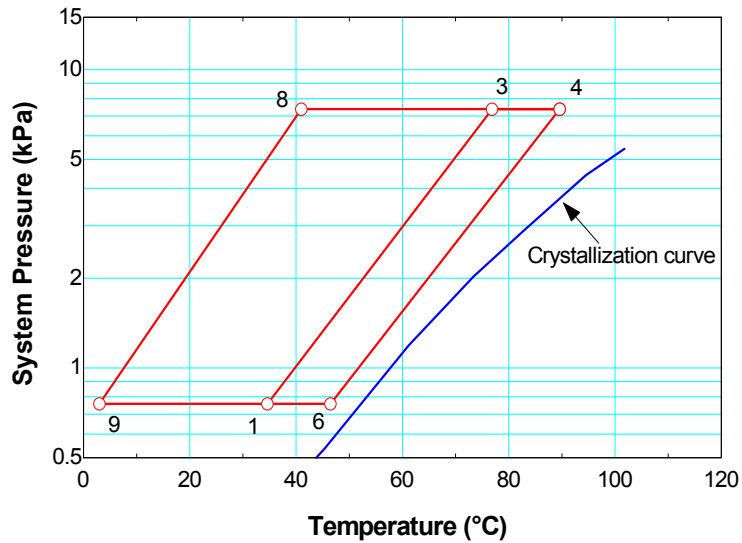


Fig. 31. The Dühring P-T chart of absorption cycle

Software Selection

The EES (Engineering Equation Solver) and ABSIM (ABsorption SIMulation) are most commonly used to simulate the operation of absorption chillers. The basic function provided by EES is the numerical solution of a set of algebraic equations. EES can also be used to solve differential and integral equations, conduct optimization, provide uncertainty analyses and linear and non-linear regression, build a simple interface and generate plots. There are two major differences between EES and other equation-solving programs or software. First, EES allows equations to be entered in any order with unknown variables placed anywhere in the equations; EES automatically reorders the equations for efficient solution. Second, EES provides many built-in mathematical and thermo-physical property functions of working fluids useful for engineering calculations.

ABSIM is a user-oriented computer code designed for simulation of absorption systems at steady state. A graphical user interface permits the user to construct the cycle diagram on the computer screen, enter the input data, run the program and view the results either in a tabular format or superimposed on a cycle diagram (Grossman, 2001 and 1994; ORNL, 1998). Like EES, ABSIM has a built-in property database and mathematical solver routine also. But it is more tedious to do the parametric study in ABSIM.

The capability of implementing control strategies in both EES and ABSIM is limited. Other common software, such as MatLab, can implement the control strategies easily, but they do not include any property database. External fluid property databases like REFPROP (REFerence fluid PROPERTIES) must be plugged in, and the LiBr/H₂O

solution properties (McNeely, 1979, Herold et al., 1987 a) together with the mathematical solver need be programmed.

By comparing the pros and cons of the above three software candidates, we chose EES to create models and predict the performance.

UA-LMTD Method

In this investigation, the UA-LMTD method is adopted. That is, the overall heat transfer coefficient (UA) of each heat exchanger is known and can be considered constant after the chiller is built. LMTD is the temperature difference at one end of the heat exchanger minus the temperature difference at the other end of the heat exchanger, divided by the natural logarithm of the ratio of these two temperature differences. The UA-LMTD method involves two important assumptions: (1) the fluid specific heats do not vary significantly with temperature, and (2) the convection heat transfer coefficients are relatively constant throughout the heat exchanger.

Assumptions

Table 6. Thermodynamic state point summary

Point	State	Notes
1	Saturated liquid solution	Vapor quality = 0
2	Sub-cooled liquid solution	State calculated from pump model, enthalpy $h_2 \approx h_1$
3	Sub-cooled liquid solution	State calculated from solution heat exchanger model
4	Saturated liquid solution	Vapor quality = 0
5	Sub-cooled liquid solution	State calculated from solution heat exchanger model
6	Vapor-liquid solution state	Vapor flashes as liquid passes through expansion valve, $h_6 \approx h_5$
7	Superheated water vapor	No salt content
8	Saturated liquid water	At pressure P_{high}
9	Vapor-liquid water state	Vapor flashes as liquid passes through expansion valve, enthalpy $h_9 \approx h_8$
10	Saturated water vapor	At pressure P_{low}

The following assumptions are used in the modeling of single-effect absorption chillers, and Table 6 summarizes the thermodynamic status of each state point:

- The system is operating in a steady state;
- There are 2 pressures (P_{high} and P_{low}) in the system: the pressure in the generator and condenser is at P_{high} , while the pressure in the evaporator and absorber is at P_{low} , and there is no pressure drop or heat transfer in the piping network;
- The throttling device is isoenthalpic;
- The solution pump is adiabatic, and it is used to maintain the constant solution level in the desorber.
- The UA for each heat exchanger is constant.

Equations of Component

Generator / Desorber

The energy balances on the solution side and heat source are:

$$Q_g = m_4 \cdot h_4 + m_7 \cdot h_7 - m_3 \cdot h_3 \quad (7)$$

$$Q_g = m_{11}(h_{11} - h_{12}) \quad (8)$$

The heat transfer rate is calculated by

$$Q_g = UA_g \cdot LMTD_g \quad (9)$$

where

$$LMTD_g = \frac{(T_{11} - T_4) - (T_{12} - T_7)}{\ln\left(\frac{T_{11} - T_4}{T_{12} - T_7}\right)} \quad (10)$$

The mass and salt should balance to satisfy the conservation law:

$$m_3 = m_4 + m_7 \quad (11)$$

$$m_3 \cdot x_3 = m_4 \cdot x_4 \quad (12)$$

Condenser

The energy balances on the solution side and cooling air are:

$$Q_c = m_7(h_7 - h_8) \quad (13)$$

$$Q_c = m_{15}(h_{16} - h_{15}) \quad (14 \text{ a})$$

$$\text{or } Q_c = m_{15}C_p(T_{16} - T_{15}) \quad ((14 \text{ b}))$$

The heat transfer rate is calculated by

$$Q_c = UA_c \cdot LMTD_c \quad (15)$$

where

$$LMTD_c = \frac{T_{16} - T_{15}}{\ln\left(\frac{T_8 - T_{15}}{T_8 - T_{16}}\right)} \quad (16)$$

Evaporator

The energy balances on the solution side and chilled water are:

$$Q_e = m_9(h_{10} - h_9) \quad (17)$$

$$Q_e = m_{17}(h_{17} - h_{18}) \quad (18)$$

The heat transfer rate is calculated by

$$Q_e = UA_e \cdot LMTD_e \quad (19)$$

where

$$LMTD_e = \frac{T_{17} - T_{18}}{\ln\left(\frac{T_{17} - T_{10}}{T_{18} - T_{10}}\right)} \quad (20)$$

Absorber

The energy balances on the solution side and cooling air are:

$$Q_a = m_{10} \cdot h_{10} + m_6 \cdot h_6 - m_1 \cdot h_1 \quad (21)$$

$$Q_a = m_{13}(h_{14} - h_{13}) \quad (22 \text{ a})$$

$$\text{or } Q_a = m_{13}C_p(T_{14} - T_{13}) \quad (22 \text{ b})$$

The heat transfer rate is calculated by

$$Q_a = UA_a \cdot LMTD_a \quad (23)$$

where

$$LMTD_a = \frac{(T_6 - T_{14}) - (T_1 - T_{13})}{\ln\left(\frac{T_6 - T_{14}}{T_1 - T_{13}}\right)} \quad (24)$$

Solution Heat Exchanger

The energy balances on the cold and hot solution side are:

$$Q_{hx} = m_1(h_3 - h_2) \quad (25)$$

$$Q_{hx} = m_4(h_4 - h_5) \quad (26)$$

The heat transfer rate is calculated by

$$Q_{hx} = UA_{hx} \cdot LMTD_{hx} \quad (27)$$

where

$$LMTD_{hx} = \frac{(T_4 - T_3) - (T_5 - T_2)}{\ln\left(\frac{T_4 - T_3}{T_5 - T_2}\right)} \quad (28)$$

Efficiency Evaluation

The desired output of an absorption chiller is to produce cooling capacity, while the input to the absorption chiller is heat input to the desorber and parasitic power consumed by its fans and pumps. To evaluate the thermodynamic performance of a single absorption chiller, we adopt the following thermal COP:

$$COP = \frac{Q_e}{Q_g} \quad (29)$$

However, if the exhaust is assumed freely available, then the denominator can also be replaced by the input that is paid for; that is the parasitic power. The electric COP defined by equation 30 can be even as high as 10, which is incomparable by the conventional vapor compression system. It proves why the combination of prime movers and absorption chiller can definitely save energy:

$$COP_{electric} = \frac{Q_e}{Parasitic \ Power} \quad (30)$$

Another common term to evaluate the CHP system or other energy conversion systems is heat utilization (equation 31); the problem with this definition is the lack of

regard for outputs from the system. It is a poor measure to compare dissimilar systems, since two systems can absorb the same amount of heat but produce very dissimilar outputs (Cowie, 2002). However, with the same COP of absorption chiller, it is fair to use heat utilization because the improvement in heat utilization within an existing system will generally indicate improved system performance and greater output.

$$\text{Heat utilization} = 1 - \frac{\text{Heat rejected from the system}}{\text{Heat Input}}. \quad (31)$$

Sensitivity Analysis

Baseline at Design Conditions

There is a total of 18 state points in the computational model, and each state point consists of a temperature, pressure, enthalpy, flow rate, and concentration. In the real operation, the system performance is determined by the dynamic interaction of all these parameters and variables. The baseline performance of the absorption cycle at the design condition is showed in the following Table 7, while Table 8 summarizes the heat duty and UA of each heat exchanger component.

Table 7. State points for the single effect air-cooled LiBr absorption chiller baseline at design condition

State point	h(kJ/kg)	T(°C)	m(kg/s)	x(%)	P(kPa)
1	89.1	34.6	0.31	56.7	0.758
2	89.1	34.6	0.31	56.7	7.381
3	148.1	63.9	0.31	56.7	7.381
4	221.7	89.6	0.2817	62.4	7.381
5	156.8	54.4	0.2817	62.4	7.381
6	156.8	46.5	0.2817	62.4	0.758
7	2618.7	76.9	0.0283	0	7.381
8	167.5	40	0.0283	0	7.381
9	167.5	3	0.0283	0	0.758
10	2506	3	0.0283	0	0.758
11	558.1	280	0.5372		
12	389.3	115	0.5372		
13	52.9	25	5.683		
14	68.3	40	5.683		
15	52.9	25	6.763		
16	63.2	35	6.763		
17	50.4	12	3.161		
18	29.4	7	3.161		

Table 8. Heat duty and UA of each component at design condition

Component	Heat duty (kW)	UA (kW/K)
Evaporator	66.2	10.740
Desorber	90.7	0.958
Condenser	69.4	7.626
Absorber	87.5	10.970
Solution HX	18.3	0.808

Effect of Exhaust Temperature into Desorber

In the performance simulation of an absorption chiller with respect to the exhaust heat temperature into the desorber, all parameters (all UA, m_{11} , m_{13} , m_{15} , m_{17} , T_{17} and ambient temperature) are fixed except the exhaust temperature T_{11} , that is:

- Ambient temperature = $T_{13} = T_{15} = 25^{\circ}\text{C}$; Chilled water return temperature $T_{17} = 12^{\circ}\text{C}$;
- All flow rates are the same as those in Table 7;
- All UAs are the same as those in Table 8.

The performances of the absorption chiller vs. T_{11} are plotted in Figures 32 ~ 35. When the exhaust temperature T_{11} increases, the condenser pressure increases slightly, while the evaporator pressure decreases at an insignificant level. Both strong and weak solutions become more concentrated, which may cause crystallization. The VFD (variable frequency drive) solution pump has to increase its flow rate to maintain the solution level in the desorber. In Fig. 34, the difference between the weak solution and strong solution is the flow rate of refrigerant water. As a result of the increase of T_{11} , more refrigerant is generated, therefore, the capacity of each heat exchanger improves, but the COP decreases slightly.

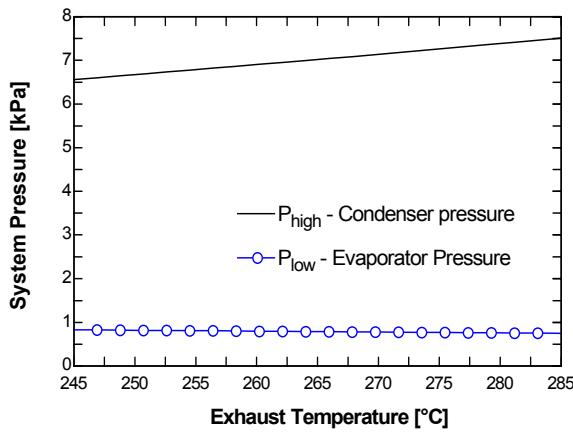


Fig. 32. System pressure vs. exhaust temperature into desorber

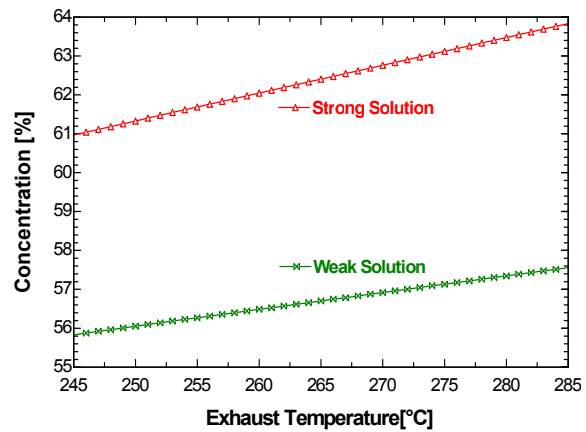


Fig. 33. LiBr concentration vs. exhaust temperature into desorber

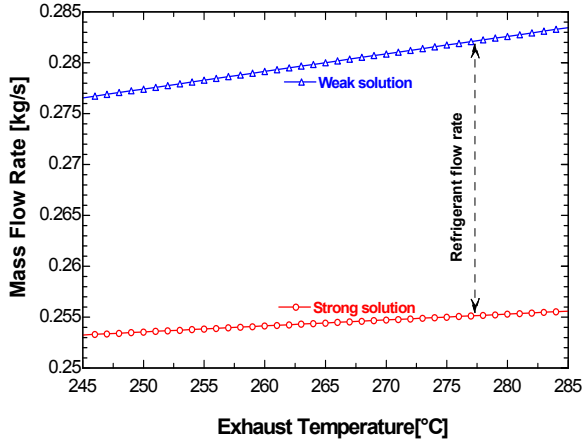


Fig. 34. Solution mass flow rate vs. exhaust temperature into desorber

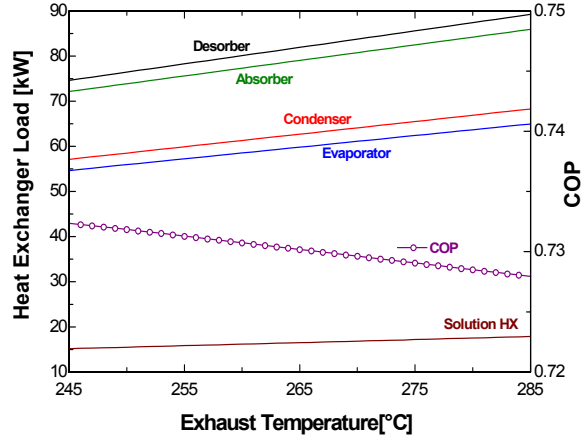


Fig. 35. Heat exchanger load and COP vs. exhaust temperature into desorber

Having the T_{11} being as high as possible is the best design to achieve higher cooling capacity and heat utilization. However, the crystallization may occur when the exhaust is too hot. More details will be discussed in Fig. 47.

Effect of Exhaust Flow Rate into Desorber

When the chilled water temperature is fixed, the control method of the chiller cooling capacity is usually to adjust either the exhaust temperature or exhaust flow rate into the desorber. In practical applications, exhaust flow rate control is often used. To simulate the performance of an absorption chiller with respect to the exhaust flow rate into the desorber, the following parameters are input:

- Ambient temperature = $T_{13} = T_{15} = 25^{\circ}\text{C}$; Chilled water return temperature $T_{17} = 12^{\circ}\text{C}$; Exhaust temperature $T_{11} = 280^{\circ}\text{C}$;
- Flow rates m_{13} , m_{15} , m_{17} are the same as those in Table 7;
- All UAs are the same as those in Table 8.

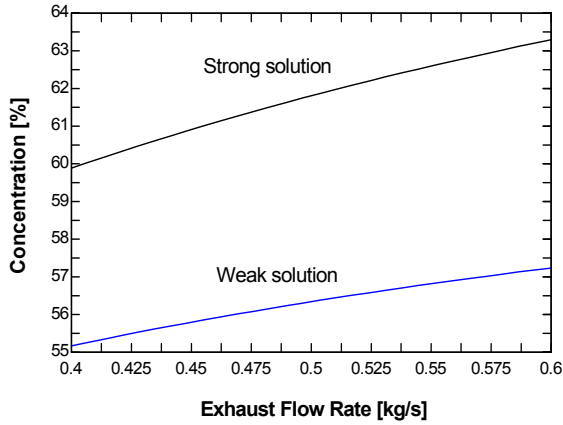


Fig. 36. Solution mass flow rate vs. exhaust flow rate into desorber

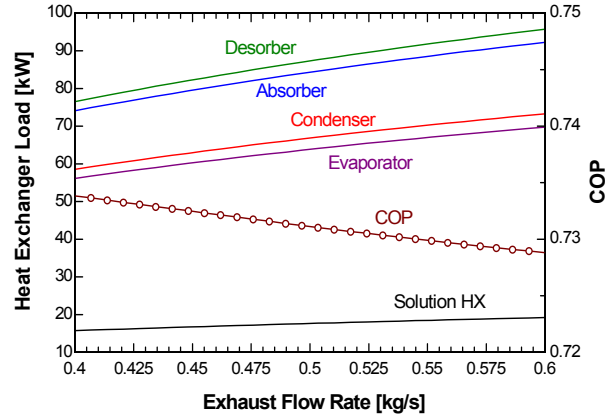


Fig. 37. Heat exchanger load and COP vs. exhaust flow rate into desorber

Figures 36 and 37 are two plots of the performance. The absorption chiller exhibits performance similar to that shown on page 50 - Effect of Exhaust Temperature into Desorber. Therefore, in the later discussion of Chapter 6 – Crystallization Control Strategies the two effects are addressed together.

Effect of Ambient Temperature

For the air-cooled absorption chiller, the ambient air is used as a coolant to cool down the condenser and absorber. In the performance simulation of an absorption chiller with respect to the ambient temperature, the following parameters are input:

- Chilled water return temperature $T_{17} = 12^{\circ}\text{C}$; Exhaust temperature $T_{11} = 280^{\circ}\text{C}$;
- Flow rates m_{11} , m_{13} , m_{15} , m_{17} are the same as those in Table 7;
- All UAs are the same as those in Table 8.

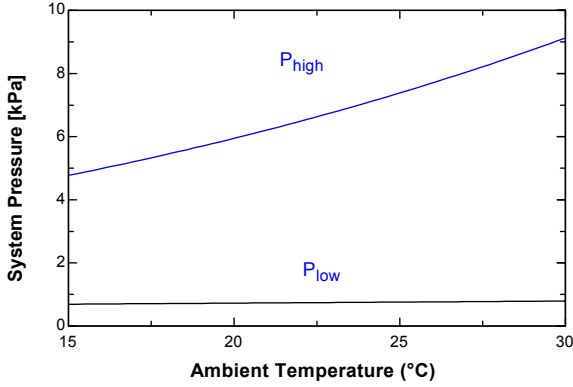


Fig. 38. System pressure vs. ambient temperature

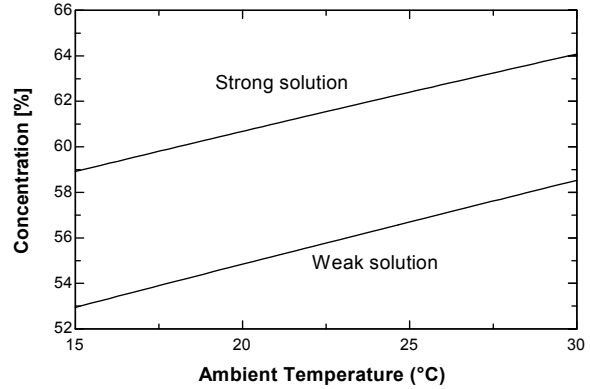


Fig. 39. LiBr concentration vs. ambient temperature

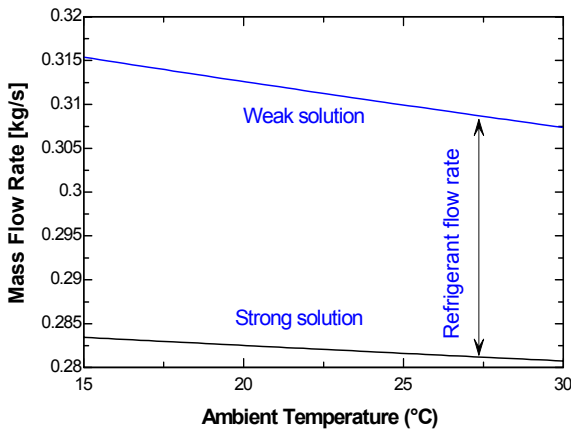


Fig. 40. Solution mass flow rate vs. ambient temperature

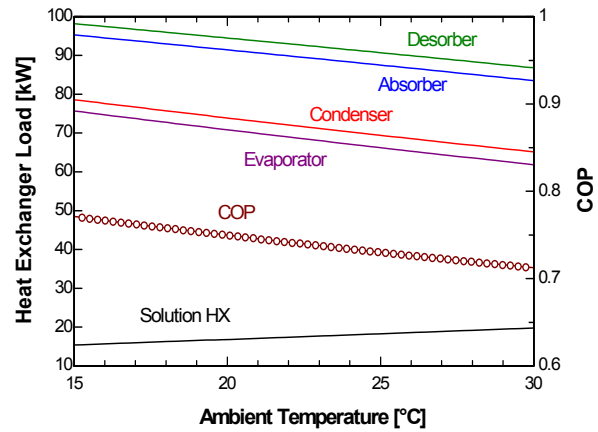


Fig. 41. Heat exchanger load and COP vs. ambient temperature

The performances of the air-cooled absorption chiller vs. ambient temperature are plotted in Figures 38 ~ 41. When the ambient temperature increases, the condenser pressure increases considerably, while the evaporator pressure increases at an insignificant level. Both strong and weak solutions become more concentrated, which may cause crystallization. This will be discussed in more detail in Fig. 46. In Fig. 40 the difference between the weak solution and strong solution is the flow rate of refrigerant water. The flow rates of weak solution, strong solution and refrigeration all drop when

the outdoor conditions hotter. The hot weather will also cause the decrease of chiller cooling capacity and COP.

Effect of Chilled Water Temperature

Usually the chilled water flow rate is not allowed to vary, but the supply temperature T_{18} can be set by the control system. To check this effect, the following input parameters were assumed:

- Ambient temperature = $T_{13} = T_{15} = 25^{\circ}\text{C}$; Exhaust temperature $T_{11} = 280^{\circ}\text{C}$;
- Flow rates m_{11} , m_{13} , m_{15} , m_{17} are the same as those in Table 7;
- All UAs are the same as those in Table 8.

The dependency of the air-cooled absorption chiller performance vs. chilled water supply temperature are plotted in Figures 42 ~ 45. When the chilled water supply temperature increases, the system pressure increases slightly, and solution concentration drops. In addition, the chiller cooling capacity and COP all improve. Higher chilled water temperature setting can also prevent the incident of crystallization.

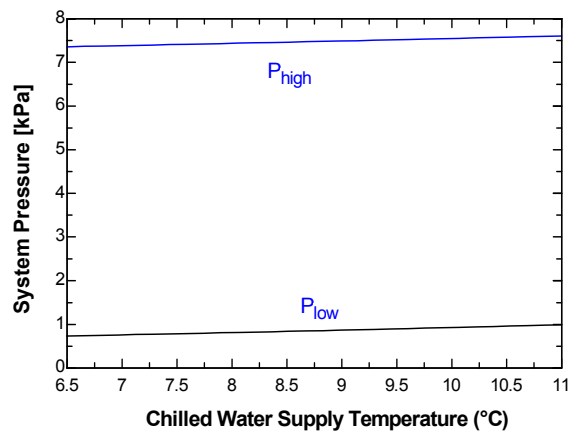


Fig. 42. System pressure vs. chilled water supply temperature

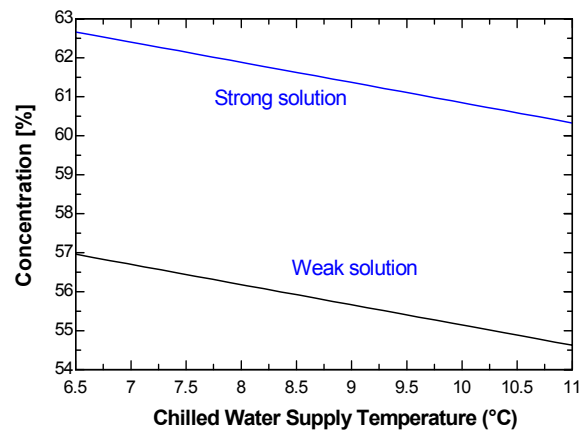


Fig. 43. LiBr concentration vs. chilled water supply temperature

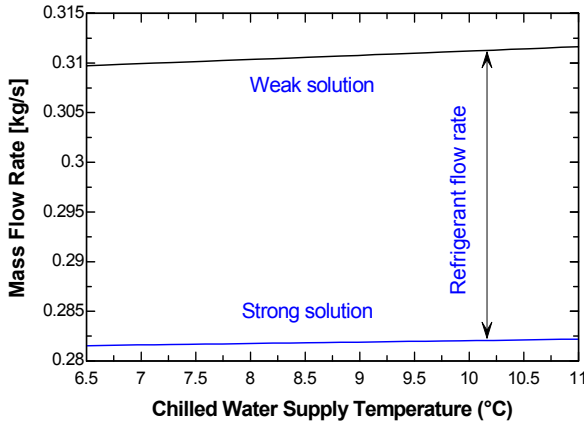


Fig. 44. Solution mass flow rate vs. chilled water supply temperature

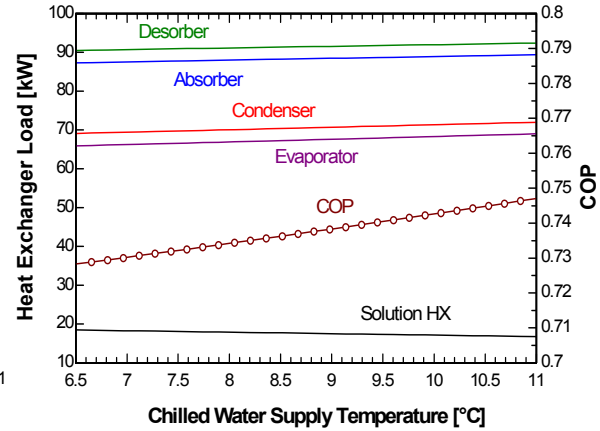


Fig. 45. Heat exchanger load and COP vs. chilled water supply temperature

Summary of Simulation Results

In the above sensitivity analysis, only one variable is considered each time. In summary, major conclusions of the simulation are:

- Having the MT exhaust gas temperature or flow rate being as high as possible is the best design to achieve higher cooling capacity and better heat utilization. However, the crystallization may occur when the exhaust is too hot.
- Cold weather decreases the condenser pressure and improves the COP and cooling capacity, while hot weather may cause crystallization of the chiller.
- Higher chilled water temperature can improve the chiller performance by increasing the cooling capacity and COP. It is recommended to set higher as long as the application permits.

Chapter 6 – Crystallization Control Strategies

Crystallization Causes and Precautions

In absorption chillers, if the solution concentration is too high or the solution temperature is reduced too low, crystallization may occur and interrupt machine operation. The vulnerable location is also decided by the mechanical structure of pipes and fittings; this is most likely to occur in the strong solution entering the absorber; that is the point 6 in Fig. 30, the concentrated solution at the lowest temperature. Crystallization must be avoided because the formation of slush in the piping network over time could form a solid and block the flow. If this occurs, the concentrated solution temperature needs to be raised above its saturation point so that the salt crystals will return to the solution, freeing the machine.

The big difference between water-cooled and air-cooled LiBr-water absorption chillers is the temperature of the absorber. With air-cooling, one cannot achieve a temperature of the solution in the absorber sufficiently low to maintain the evaporator pressure. The only way to compensate for the high absorber temperature is to increase the concentration of LiBr in the solution, but that brings it closer to crystallization.

One of the following five causes or a combination of those causes may trigger crystallization of air-cooled absorption chillers, and the associated precautions are also suggested as well:

1. Higher ambient temperature (it is higher condenser cooling water temperature for the water-cooled machine): The air-cooled absorbers tend to run hotter than water-cooled units due to the relatively poor heat transfer characteristics of air.

Figure 46 gives the overall impression of how each point changes when the ambient temperature increases in the Dühring P-T chart. The system runs with the same exhaust temperature and chilled water temperature setting. When the ambient temperature increases from 25°C (dashed lines) to 35°C (solid lines). Crystallization occurs.

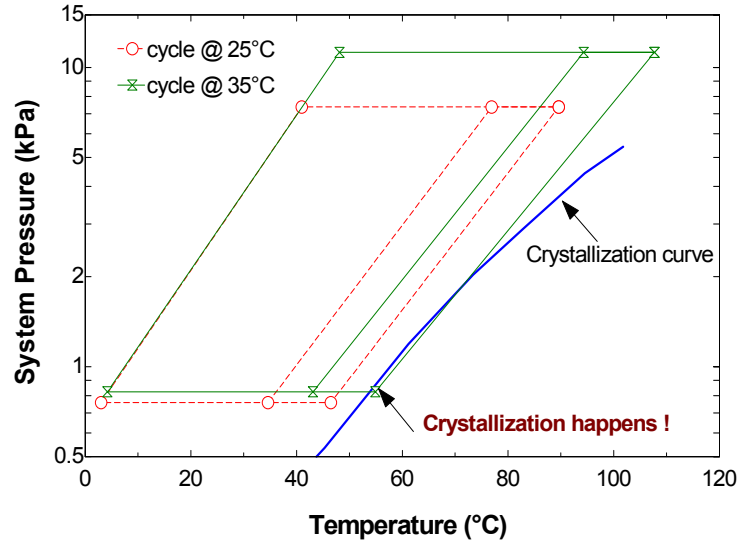


Fig. 46. The Dühring P-T chart of absorption cycle (dashed line) @ ambient 25°C and cycle (solid line) @ ambient 35°C

2. Air leak into the machine or non-absorbable gases produced during corrosion: Both deteriorate the UA and cause higher system pressure, decreased capacity and COP, and higher crystallization probability. A direct method for keeping the required pressure is to evacuate the vapor space periodically with a vacuum pump. This situation can be simulated by assuming a decreased UA, which will cause x_6 , the concentration of point 6, to move closer to the crystallization line limit. As a precaution to this issue, the system should be evacuated routinely.
3. Too much heat input to the desorber: either the exhaust temperature or the flow rate is too high, which results in increased solution concentrations to the point

where crystallization may occur. As a precaution to this issue, the exhaust temperature or flow rate into the desorber should be maintained within a specific range. Figure 47 gives the overall impression of how each point changes when the exhaust temperature increases in the Dühring P-T chart. The system runs with the same ambient temperature, chilled water temperature setting and flow rates, when the exhaust temperature increases from the designed 280°C (dashed lines) to 320°C (solid lines), crystallization occurs.

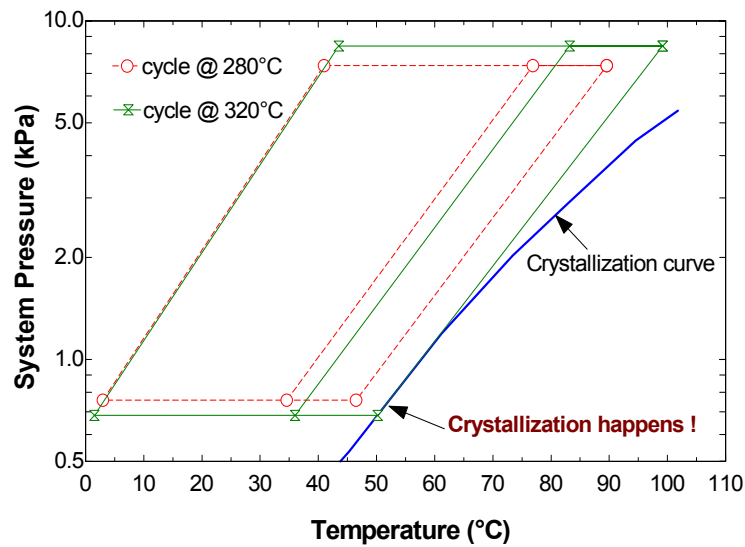


Fig. 47. The Dühring P-T chart of absorption cycle (dashed line) @ exhaust 280°C and cycle (solid line) @ exhaust 320°C

4. Failed dilution after shutdown: During normal shutdown, the machine undergoes an automatic dilution cycle, which lowers the concentration of the solution throughout the machine. In such a case, the machine may cool to ambient temperature without crystallization occurring in the solutions. Crystallization is most likely to occur when the machine is stopped due to power outage while operating at full load, when highly concentrated solutions are present in the solution heat exchanger (Florides et al., 2003).

5. Chilled water supply temperature is set too low when the weather and/or exhaust are too hot: Usually the chilled water supply temperature can be set by the control system. The darker zone in Fig. 50 represents the infeasible temperature combination. The air-cooled chiller should not run in this zone to avoid crystallization; while the lighter zone is safe for the chiller operation.

Control Strategies

Chilled Water Temperature Control

The control strategies are new approaches proposed by the author to prevent crystallization. Though hot weather may cause crystallization, increasing the chilled water temperature settings can avoid crystallization; while the byproducts include the improved cooling capacity and COP.

Assume that the exhaust gas temperature and flow rate are fixed. Then for a certain ambient temperature the minimum chilled water temperature is determined by the following two requirements: one, the refrigerant (water) should not freeze; two, the system should not be crystallized. Figure 48 shows the relation between the two temperatures, assuming the exhaust to the chiller is set at 280°C and with constant flow rate. The minimum chilled water temperature defines the crystallization prevention margin.

The chilled water temperature control strategy is shown in Fig. 49. The darker zone in the three dimensional figure (a) represents the infeasible temperature combination. The air-cooled chiller should not run in this zone to avoid crystallization; while the lighter zone is safe for the chiller operation, and the chiller can have higher

cooling capacity and COP when the weather is colder and the chilled water temperature is higher. For example, when the ambient temperature is at 35°C, the minimum chilled water supply temperature should be set at 8.5°C, and then the chiller can achieve 16.5 ton cooling capacity. The dashed lines and the star symbol (★) show how to look up the corresponding temperature setting and cooling capacity under a certain ambient temperature. As the counterpart of figure (a), figure (b) plots the cooling capacity contour to display the same conclusion quantitatively. While Fig. 50 gives the chiller COP.

The cooling capacity Q_e (in ton) and COP can be quantified by the following equations:

$$Q_e = a + bT_{CHWS} + cT_{CHWS}^2 + dT_{amb} + eT_{amb}^2 + fT_{CHWS}T_{amb} \quad (32)$$

$$COP = aa + bbT_{CHWS} + ccT_{CHWS}^2 + ddT_{amb} + eeT_{amb}^2 + ffT_{CHWS}T_{amb} \quad (33)$$

In which:

T_{CHWS} = chilled water supply temperature (°C);

T_{amb} = ambient temperature (°C);

$a=24.59688$; $b=0.24398$; $c=0.001358$; $d=-0.3143$; $e=0.001319$; $f=-0.00286$;

$aa=0.810071$; $bb=0.005651$; $cc=6.95e-5$; $dd=-0.00507$; $ee=3.72e-5$; $ff=-0.00011$.

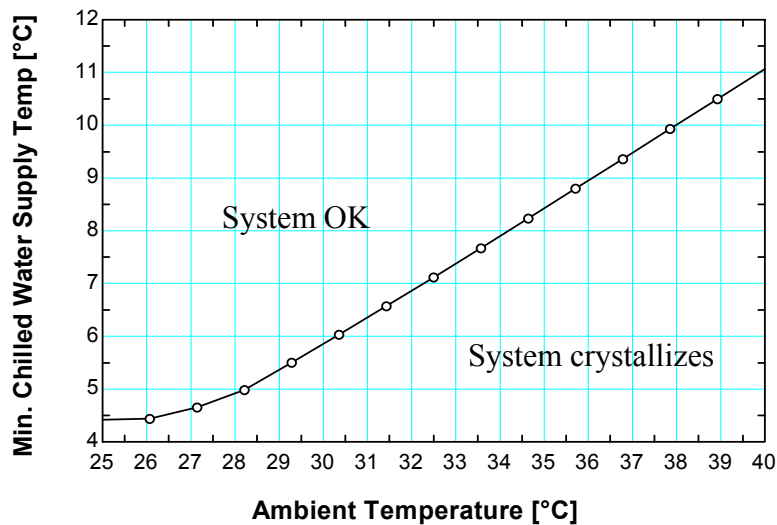
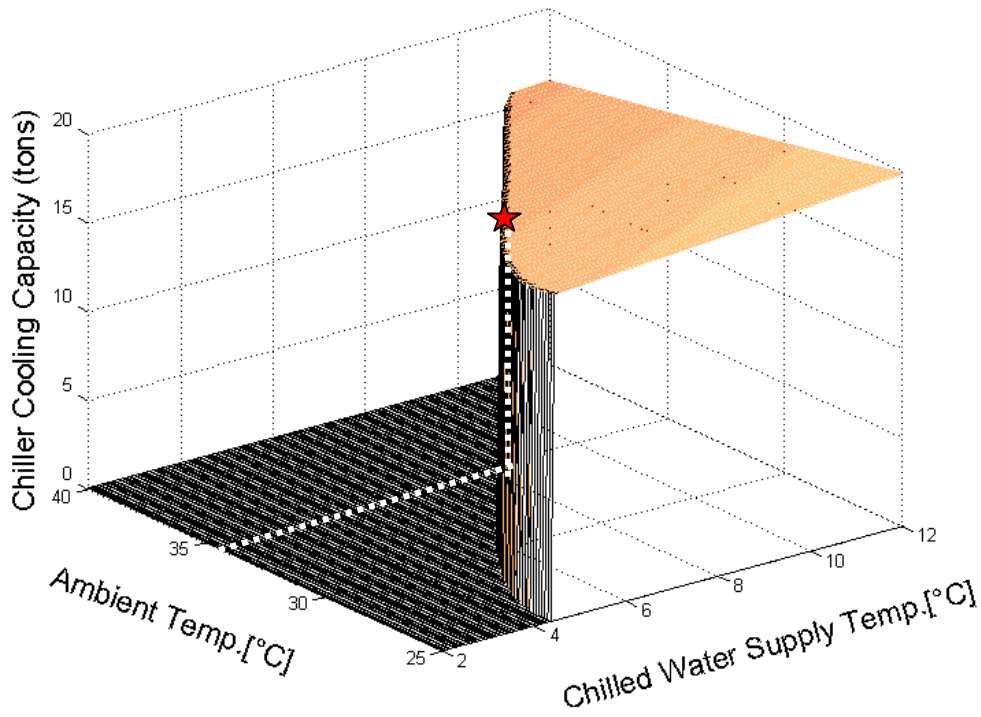
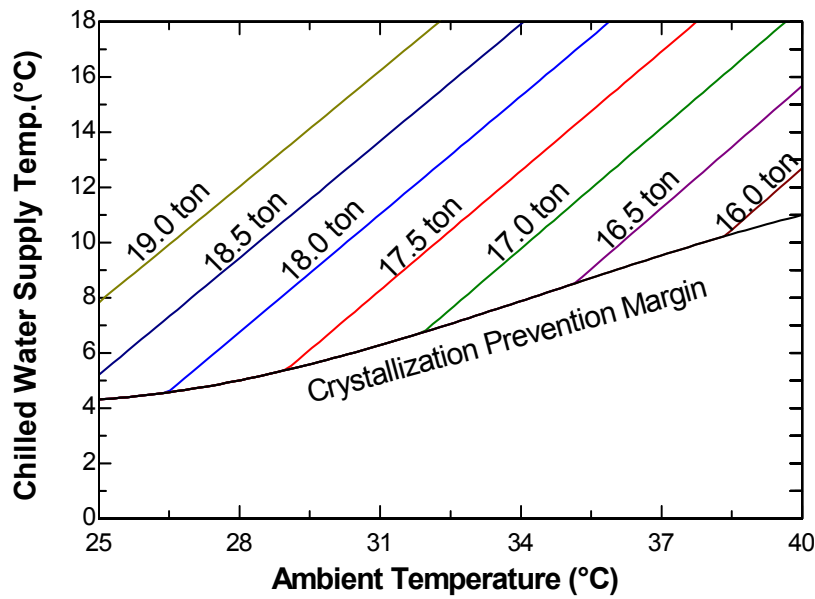


Fig. 48. Minimum chilled water supply temperature (exhaust @ 280°C and with constant flow rate)

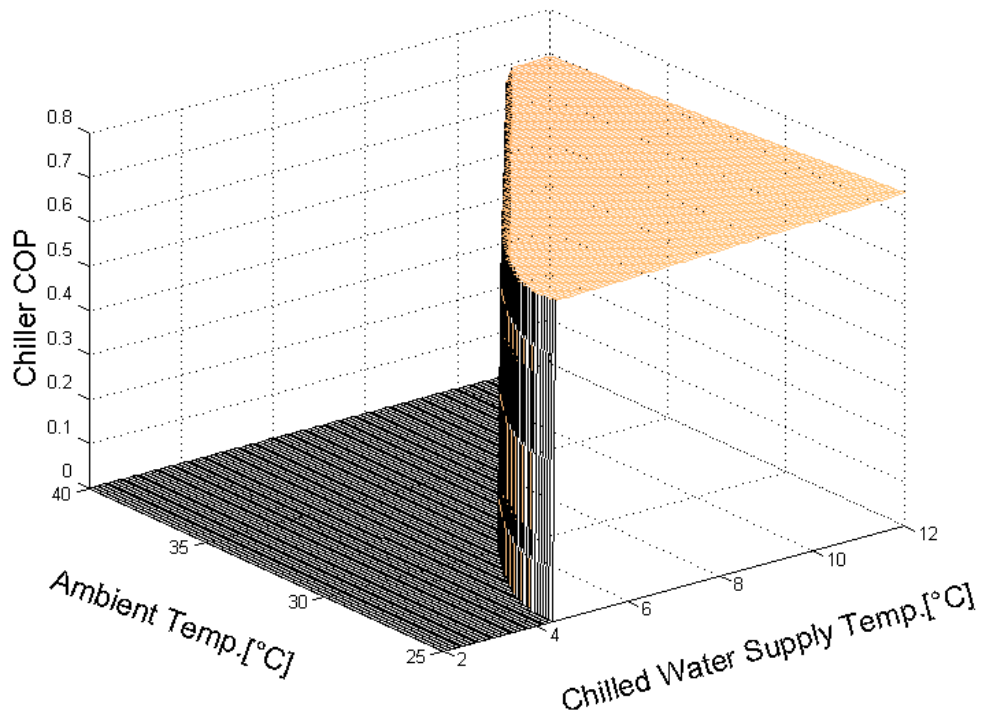


(a) Chiller cooling capacity 3D plot

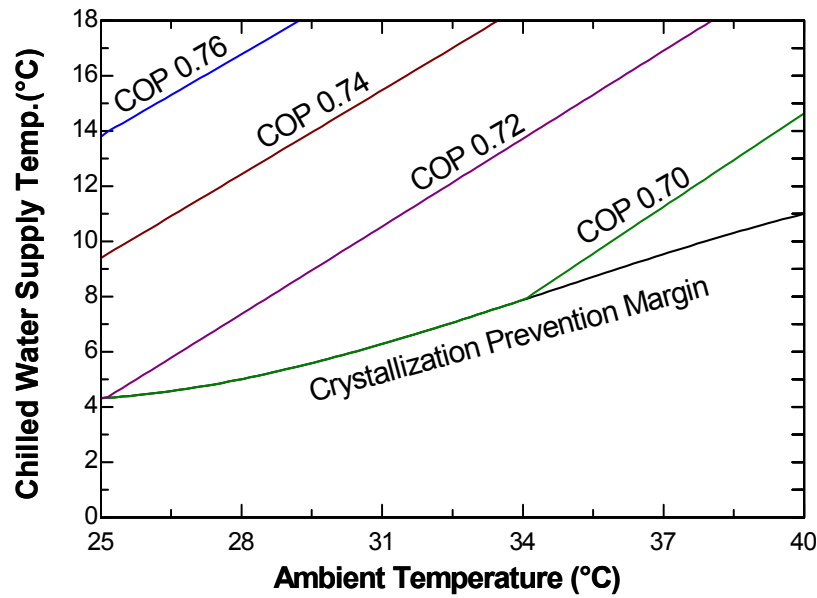


(b) Chiller cooling capacity contour

Fig. 49. Chiller cooling capacity map over the chilled water and ambient temperature combination (exhaust @ 28°C and with constant flow rate)



(a) Chiller COP map 3D plot



(b) Chiller COP contour

Fig. 50. Chiller COP map over the chilled water and ambient temperature combination

(exhaust @ 28°C and with constant flow rate)

Exhaust Temperature Control

In order to improve heat utilization in the system, the absorption chiller should use exhaust that is as hot as the component materials are able to withstand; otherwise the make-up air is needed, which makes the system clumsier, as shown in Fig. 15.

When the chilled water temperature is fixed with a constant flow rate, the highest exhaust temperature is also restricted by the ambient temperature. See Fig. 51. The darker zone represents the infeasible temperature combination. The air-cooled chiller should not run in this zone to avoid crystallization; while the lighter zone is safe for the chiller operation, and the chiller can obtain higher cooling capacity and COP when the exhaust is hotter and the weather is colder. For example, the dashed lines and the star symbol (★) in Fig. 51 (a) show how to look up the corresponding temperature setting and cooling capacity under a certain chilled water temperature. When the exhaust temperature is at 300°C, the chiller cannot run in weather that is hotter than 29°C, otherwise the crystallization may occur. At that combination, the chiller can obtain 19.4 ton cooling capacity.

On the other hand, when the ambient temperature is hot enough to cause crystallization, it can be successfully prevented by reducing the exhaust inlet temperature, assuming that the exhaust flow rate is constant.

The cooling capacity Q_e (in ton) and COP can be quantified by the following equations:

$$Q_e = a + bT_{ex} + cT_{ex}^2 + dT_{amb} + eT_{amb}^2 + fT_{ex}T_{amb} \quad (34)$$

$$COP = aa + bbT_{ex} + ccT_{ex}^2 + ddT_{amb} + eeT_{amb}^2 + ffT_{ex}T_{amb} \quad (35)$$

In which:

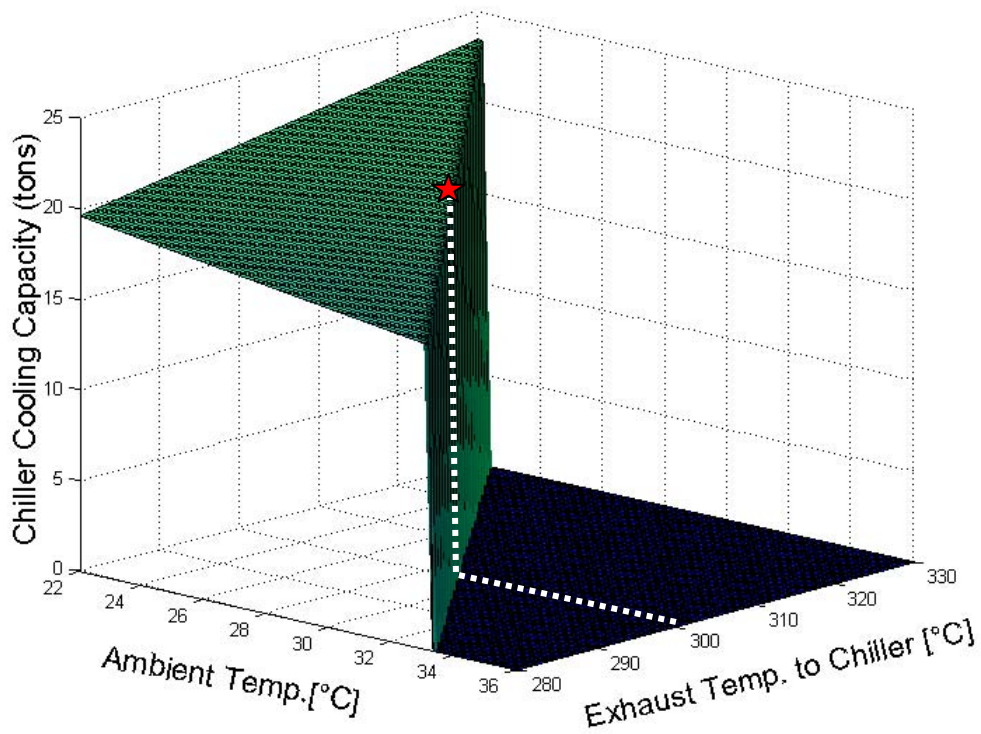
T_{ex} – exhaust temperature to chiller (°C);

T_{amb} – ambient temperature ($^{\circ}\text{C}$);

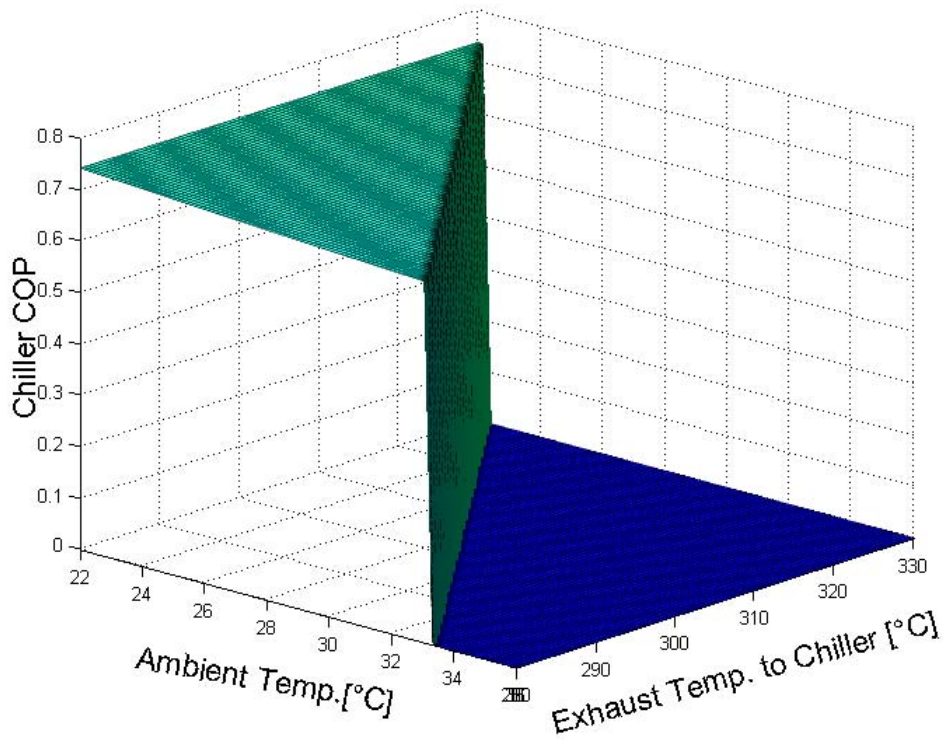
$a=3.965605$; $b=0.081376$; $c=-1.10413\text{e-}05$; $d=-0.321244$; $e=0.001059$; $f=4.58144\text{e-}05$;

$aa=1.008437$; $bb=-0.0006$; $cc=5.67978\text{e-}08$; $dd=-0.010655$; $ee=3.44788\text{e-}05$;

$ff=1.85839\text{e-}05$.



(a) Chiller cooling capacity (chilled water supply temperature @ 7°C)



(b) Chiller COP (chilled water supply temperature @ 7°C)

Fig. 51. Chiller performance over the exhaust and ambient temp. combination

Chapter 7 – Absorption Chiller Validation

Rationale for the Test Method

Since no air-cooled absorption is available, the validation tests were conducted on an 18-ton water-cooled absorption chiller driven by the exhaust from a 60 kW microturbine to validate the computer modeling. The author names them “simulated tests”; that is, we simulate air-cooled conditions with a water-cooled absorption chiller. The rationale for the simulated tests is that both the air-cooled and water-cooled chillers:

- Include identical desorbers, evaporators, solution heat exchanger, solution pumps and throttling valves;
- Comply with the same thermodynamic equations 7 ~ 29, so they should develop similar performance trends.
- Are assigned with the same parameter inputs for condensers and absorbers respectively; see In fact, for an outdoor installation it is more convenient to test a water-cooled AC than an air-cooled AC. This is because the cooling tower can maintain the cooling water temperature in a stable range, and therefore the influence of weather on the performance can be alleviated.
- Table 9. Although it may impair the feasibility of design, for example the air-cooled absorber needs to be very big to have the same UA and mC_p as those of water-cooled one, it ensures that the air-cooled chiller has the same temperature profile and the theoretical performance. In the validation, the air-cooled condenser (absorber) air inlet temperature equals the entering condenser (absorber) water temperature of Fig. 2.

In fact, for an outdoor installation it is more convenient to test a water-cooled AC than an air-cooled AC. This is because the cooling tower can maintain the cooling water temperature in a stable range, and therefore the influence of weather on the performance can be alleviated.

Table 9. Parameter settings for condensers and absorbers

Chiller type Parameters	Air-cooled (simulation)	Water-cooled (experiment)
Condenser inlet T_{15}	Ambient air temperature=	Cooling tower leaving water temperature
Absorber inlet T_{13}	Ambient air temperature=	Cooling tower leaving water temperature
Condenser UA, mC_p	$UA_{c air-cooled} =$ $M_{15}C_{p air-cooled} =$	$UA_{c water-cooled}$ $m_{15}C_{p water-cooled}$
Absorber UA, mC_p	$UA_{a air-cooled} =$ $m_{13}C_{p air-cooled} =$	$UA_{a water-cooled}$ $M_{13}C_{p water-cooled}$

Data Processing

The data process is based on the steady state period, and it uses the same equations 7 ~ 29. However, the total length of the 2-1/2" chilled water pipes is longer than 60 meters without counting the pipe length of the water coil and chiller evaporator. With the flow rate of 54 gpm (12.3 m³/hr), any control volume of chilled water needs about 2 minutes to travel the whole loop. That is to say, the return temperature has 2 minutes delay after the supply temperature. See Fig. 15 for the thermometer location. The data acquired in Fig. 52 proves the delay. Chilled water return temperatures A', B', C'... correspond to supply temperatures A, B, C... The peaks are caused by the on/off switchover of the cooling tower fan. Therefore, when using equation 18 to calculate the cooling capacity, the corresponding return temperature of 2 minutes later should be used.

The cooling tower fan is switched on and off to maintain the cooling water temperature within the setting range. The switchover is determined by the outdoor

temperature, chiller load and the settings of cooling water temperature. When the fan is on, the total chiller power consumption is about 6.8 kW; when the fan is off, the total power consumption is about 4.8 kW. See the top plot of Fig. 53. The fluctuation comes from the switchover of the cooling tower fan. But the fan may also run continuously in some tests, such as the middle and bottom plots of Fig. 53. Since extensive tests were conducted in the summer of 2003, in the following experimental validation the author uses the data when the fan was running continuously to avoid the transient effect caused by the fluctuation.

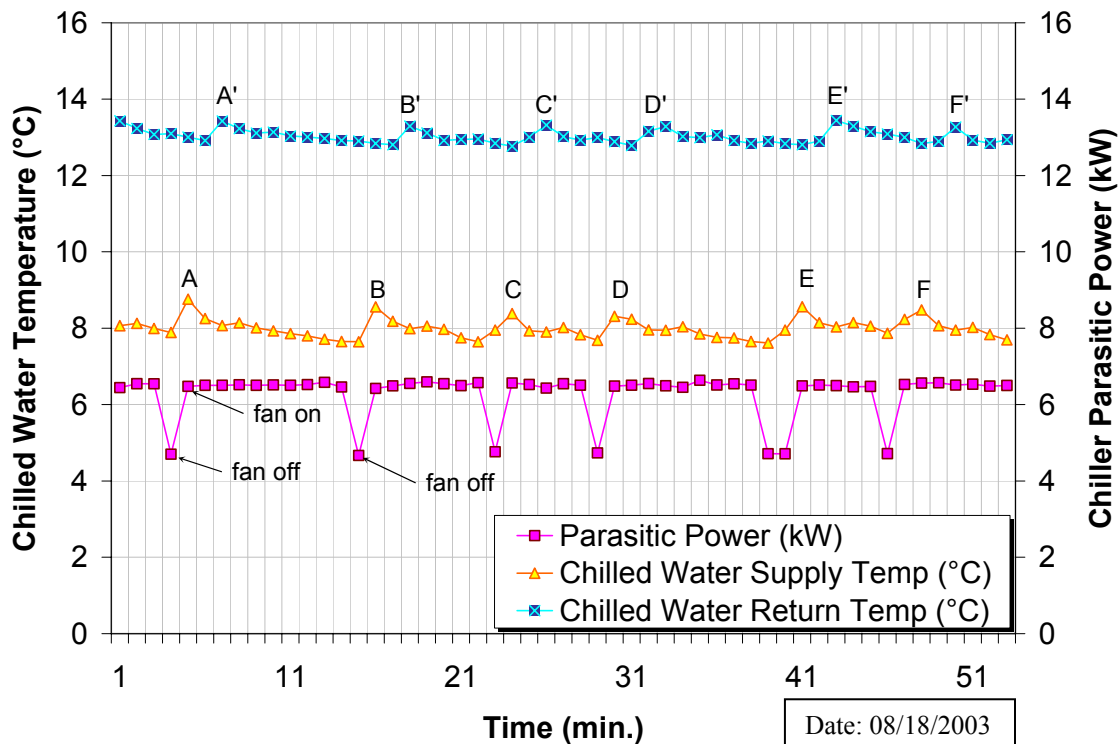


Fig. 52. Detailed chilled water temperatures and parasitic power in steady state at 1 minute interval

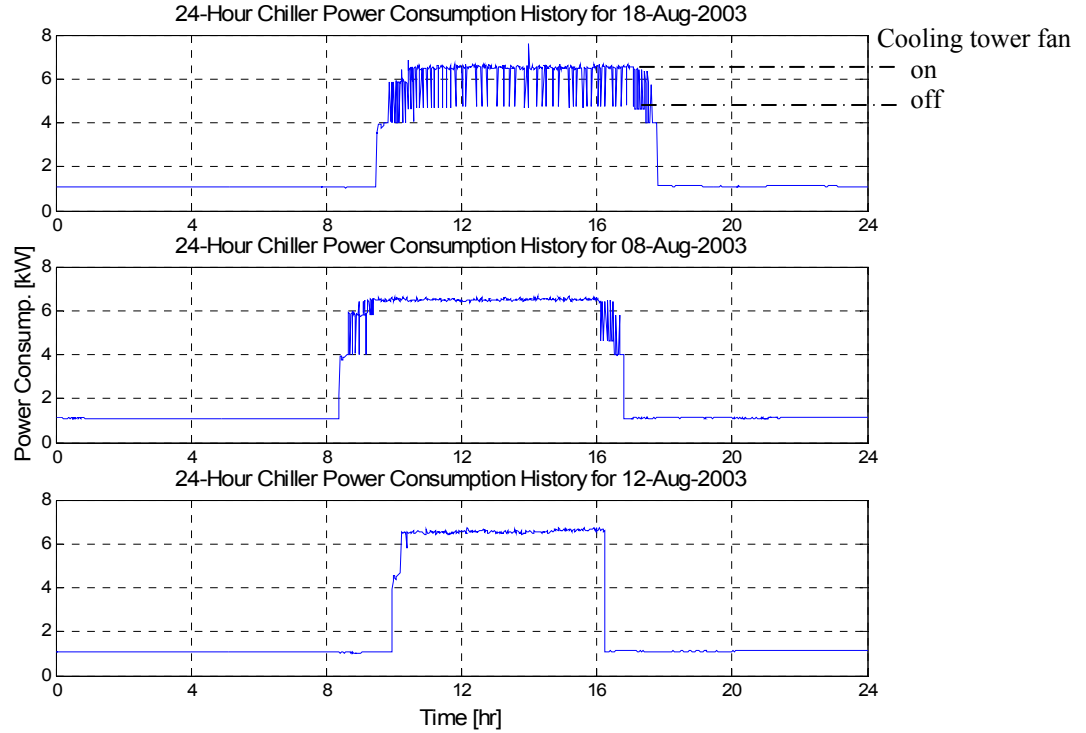


Fig. 53. Cooling tower fan operation comparison

The average relative error between simulation and experimental data was calculated as:

$$\varepsilon[\%] = \frac{1}{N} \sum \frac{| \text{Calculated Value} - \text{Measured Value} |}{\text{Measured Value}} \cdot 100 \quad (36)$$

where N is the number of samples.

Chiller Validation

Altering the Exhaust Temperature

The temperature of exhaust into desorber can be adjusted by mixing the exhaust from microturbine and outdoor make-up air. The validation is based on extensive experimental data from the operation on August 8th, 11th, 12th, 13th and 14th, 2003 when the cooling tower fan was running continuously. A Matlab data processing program was

programmed to sort out all steady state data points which satisfy the same conditions: 9°C chilled water supply temperature and the cooling tower fan turns on/off at 32.2/29.4°C.

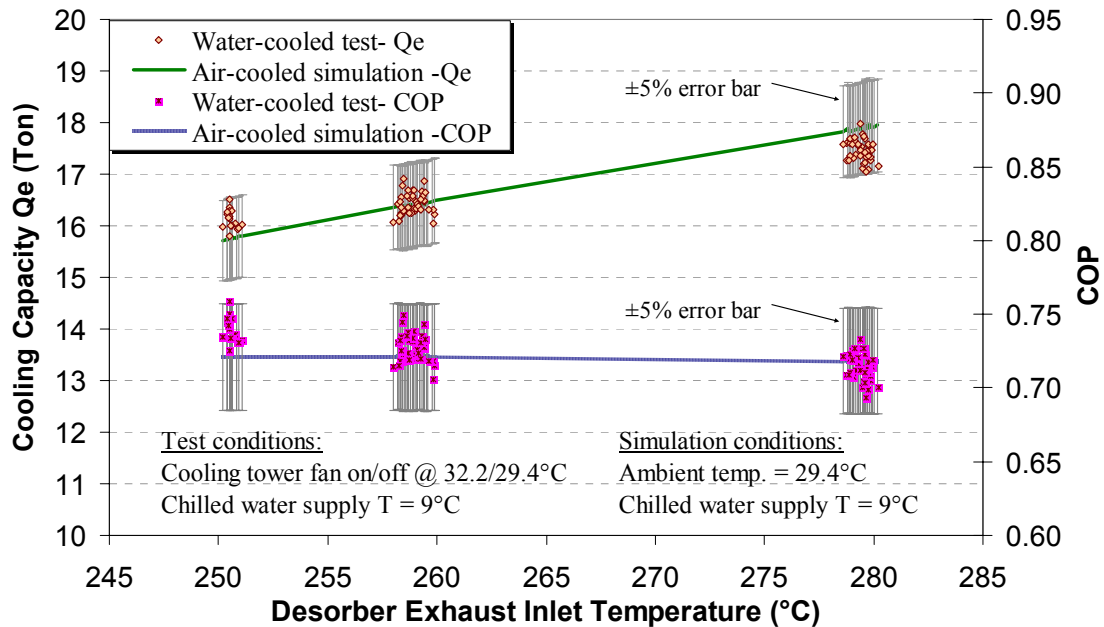


Fig. 54. The experimental validation by altering the exhaust temperature

Since the air-cooled chiller needs no cooling tower, the simulation conditions are set at: 29.4°C ambient temperature and 9°C Chilled water supply temperature. Figure 54 demonstrates the experimental validation of the air-cooled simulation by the water-cooled tests. When the desorber exhaust inlet temperature increases, the cooling capacity increases and the COP decreases slightly. A good agreement of validation was observed for all data points and the average deviation was $\pm 5.0\%$ for both cooling capacity and COP.

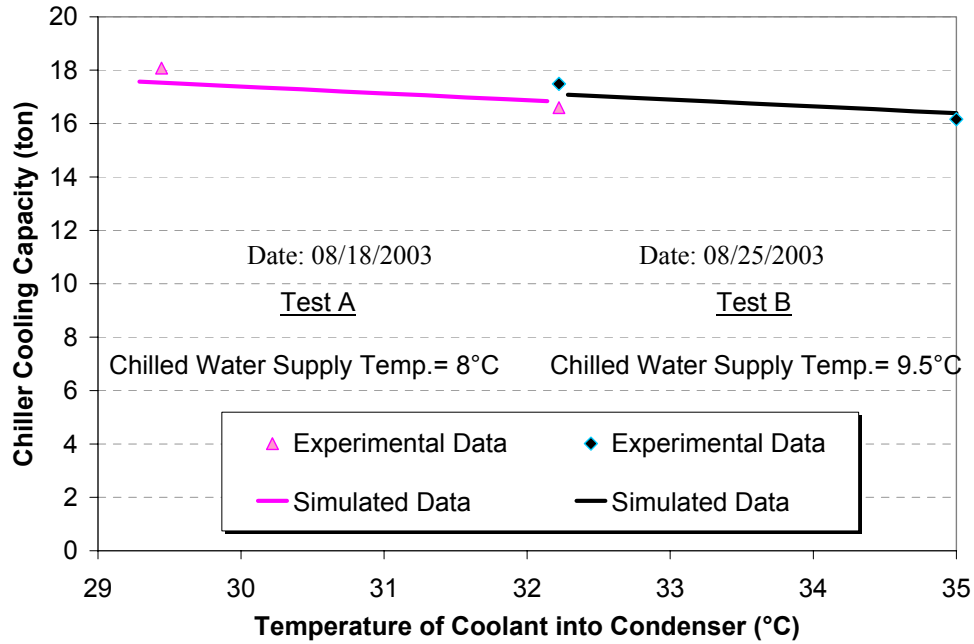
No tests have been conducted on the varied exhaust flow rate, because the system controls make it impossible to manually adjust the exhaust flow rate.

Altering the Coolant Temperature

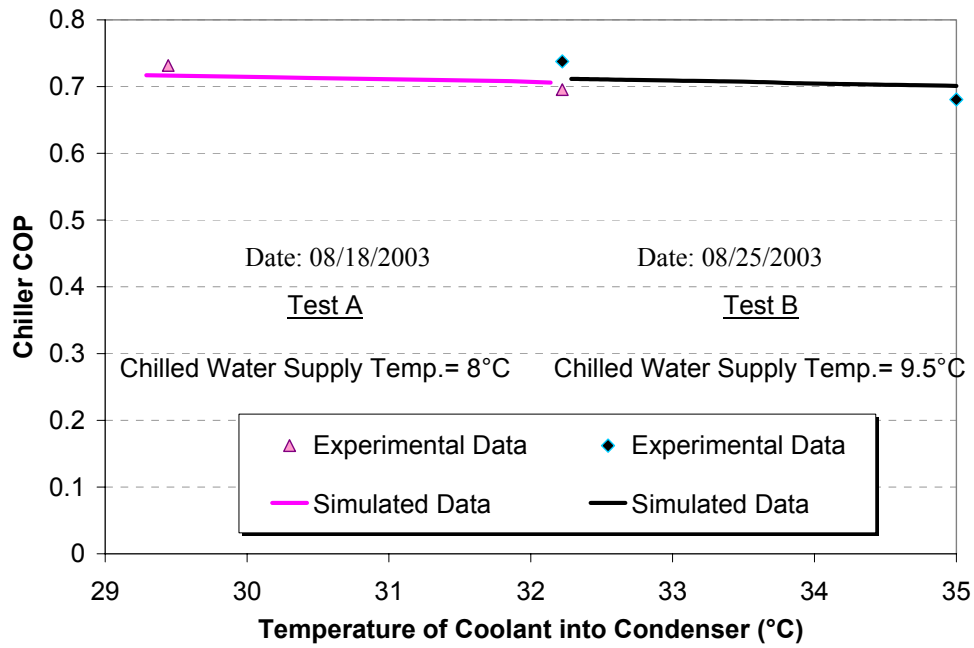
In the validation of proposed crystallization control strategies, the chiller was tested under two different conditions, both having the same exhaust inlet temperature (276°C) but different chilled water supply temperatures and cooling water temperatures. In Test A, the chilled water supply temperature was set at 8°C, and when the cooling water temperature increased the cooling capacity dropped. In Test B, as the cooling water temperature continued to increase (above 32.2°C), the chilled water supply temperature was set to 9.5°C, and the chiller could still run decently without a crystallization issue.

Figure 55 (a) and (b) show the experimental validation of chiller cooling capacity and COP under the two conditions, respectively. The dots are the average of experimental data, and the solid lines are simulation results. A good agreement of validation was observed for all data points and the average deviation was $\pm 3.0\%$ for cooling capacity and $\pm 3.6\%$ for COP. When the coolant temperature increases, the cooling capacity and the COP drop.

The deviation stems from the accuracy of instrumentation, the degree of vacuum in the system, and the fact that in the tests the cooling water temperature is only maintained in a range (e.g. 29.4~32.2°C) due to the on/off control of cooling tower fan.



(a) Chiller cooling capacity



(b) Chiller COP

Fig. 55. The experimental validation under 2 different conditions for the crystallization control strategies

Altering the Chilled Water Temperature

In addition to the above validations shown in Fig. 55 which involve the varied chilled water temperature, more extensive tests have been conducted. Figure 56 shows the validation of chiller performance on a range of chilled water temperatures when the chiller was running in a steady state period. The experimental data in the plots was acquired on July 2nd, 3rd, 8th, 9th, 10th and 11th, 2003 when the exhaust temperature into chiller was at 267°C and the cooling tower fan turned on/off at 32.2/29.4°C. The simulation of the air-cooled absorption chiller uses the same operation conditions of tests: 29.4°C ambient temperature, 7.5~11.5°C chilled water supply temperature, and 267°C exhaust temperature.

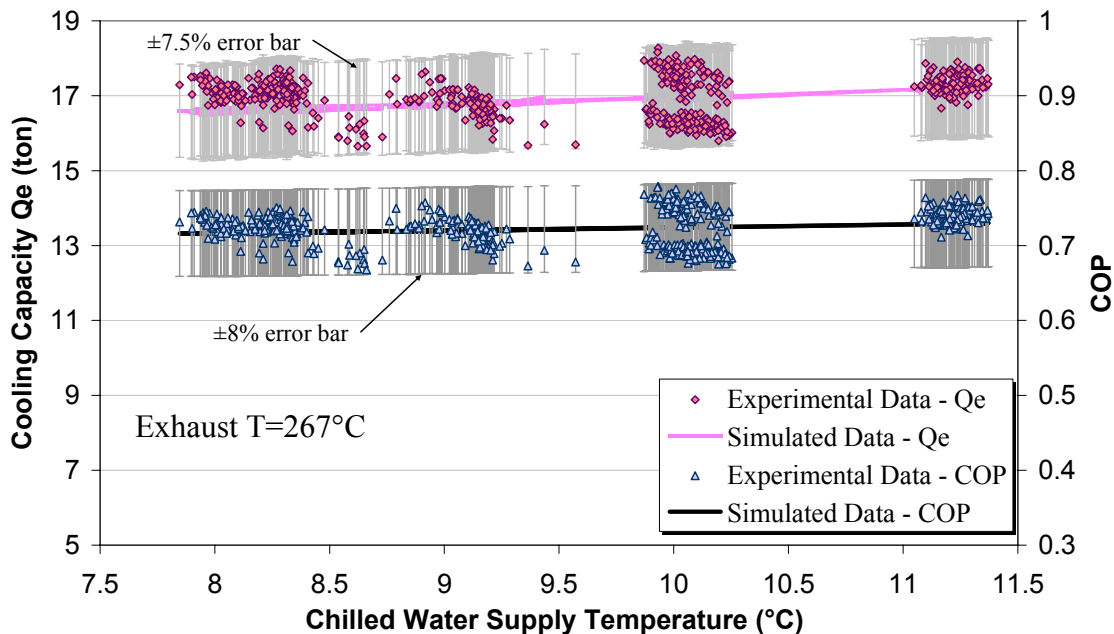


Fig. 56. The experimental validation by altering the chilled water temperature

A moderately good agreement of validation was observed for all data points and the average deviation was $\pm 7.5\%$ for cooling capacity and $\pm 8.0\%$ for COP respectively. When the chilled water supply temperature increases, both the cooling capacity and COP

improves. Again, the sources for the deviation include: the accuracy of exhaust flow rate measurement, the degree of vacuum in the system, the cooling water temperature is only maintained in a range (e.g. 29.4~32.2°C) due to the on/off control of cooling tower fan.

Chapter 8 – Integration of Air-cooled Absorption Chillers in CHP Systems

Operating Hours of Mechanical Cooling Equipment

The real HVAC or CHP system loads are determined by the building function, local weather conditions, outdoor air ratio (the ratio of the outdoor air mass flow rate to that of the supply air), operation schedule and building envelope. This investigation focuses on a commercial office building.

The psychrometric chart of Fig. 57 illustrates the weather data in College Park in a mixed year*, which was recorded by the weather station in the CHP Integration Test Center. Each dot represents the hourly data, and there are totally 8760 hours in a year. The density of dots implies the frequency of a particular weather condition.

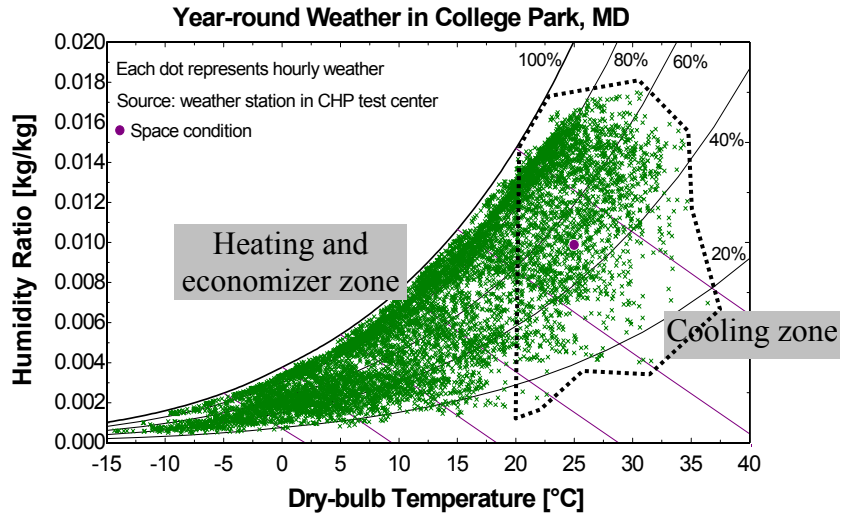
Most commercial buildings generally have a cooling requirement even during mild and cold weather conditions, because of the internal loads. A HVAC system with an economizer uses controllable dampers to increase the amount of outside-air intake into the building when the outside air is cool to meet all or part of the cooling demand. When outside-air conditions are not favorable for economizing, the outside-air damper system is positioned to provide the minimum outside-air intake required to meet the fresh-air ventilation requirements for occupants, and at the same time mechanical cooling is required. Based on the control criterion, it is classified as dry-bulb temperature-based

* Although theoretically 4 years of data has been acquired in the CHP Integration Test Center at one-minute interval, data breakdown happened sometimes due to the power outage, DAS maintenance, sensor installation, and bad sensors. Therefore, a mixed year was selected, which covers each day from January 1st to December 31st, but they may be in different year. The mixed year comprises 30% days from 2004, 60% from 2003, 7% from 2002 and 3% from 2001.

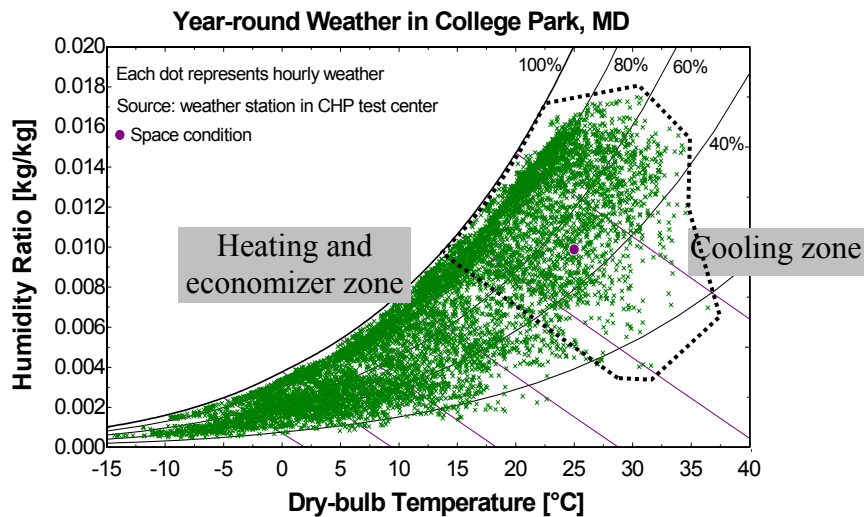
economizer and enthalpy-based economizer. The former one is cheaper, and therefore more common in applications.

In Fig. 57 (a) and (b), a dashed polygon divides the psychrometric chart into 2 zones respectively. In the left zone where the ambient dry-bulb temperature is less than 20°C or ambient enthalpy is less than 38 kJ/kg, the building needs either heating or ventilation; that is, no mechanical cooling is needed, assuming that the economizer can meet all of the cooling demand. In the highlighted zone, the building needs cooling and/or dehumidification. Since cogeneration has been developed and has mature commercial market already, only the applicability of air-cooled absorption chillers tackling the cooling load is investigated in this work.

Assume the mechanical cooling equipment has the operating schedule of 5:00 am – 10:00 pm, that is, 18 hrs/day and 7 days/week; the coincident operating hours when the mechanical cooling is required differ from location to location. Figure 58 gives the coincident weather of 4 representative cities in the United States when mechanical cooling is needed. Each “×” symbol represents the hourly average weather. So in Fig. 58 (a) when the dry-bulb temperature-based economizer is used, there are 2039 hours in College Park MD, 1583 hours in Hartford CT, 4115 hours in Phoenix AZ and 5785 hours in Miami FL per year; in Fig. 58 (b) when the enthalpy-based economizer is used, these numbers change to 2793 hours in College Park MD, 2457 hours in Hartford CT, 3513 hours in Phoenix AZ and 6136 hours in Miami FL per year.



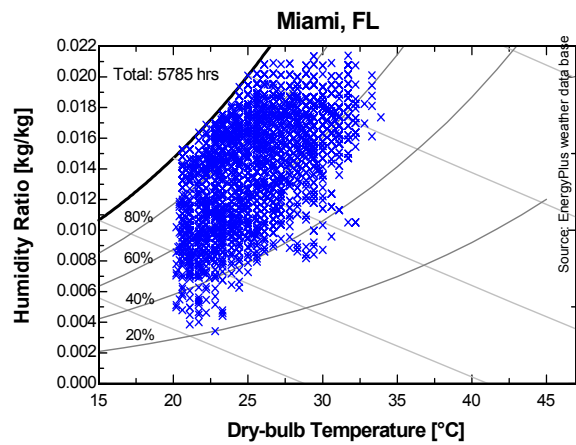
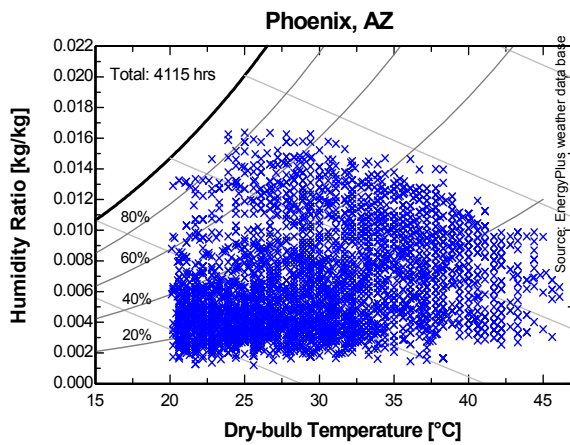
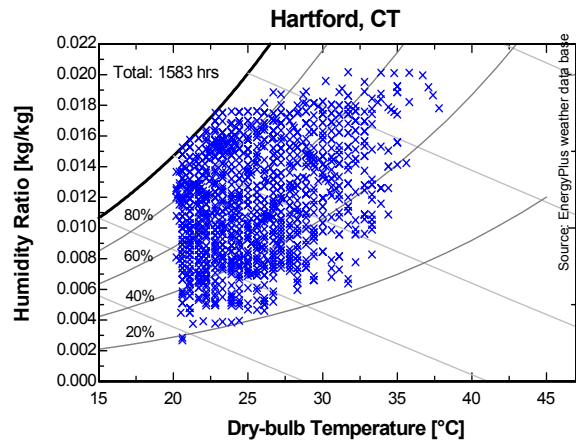
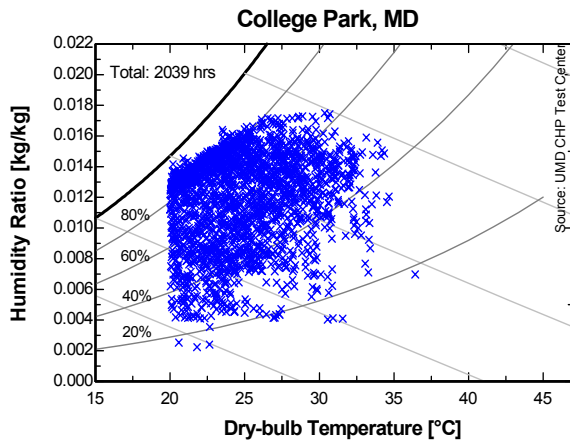
(a). Assume mechanical cooling is required when ambient temperature $\geq 20^{\circ}\text{C}$ for the system with temperature-based economizer



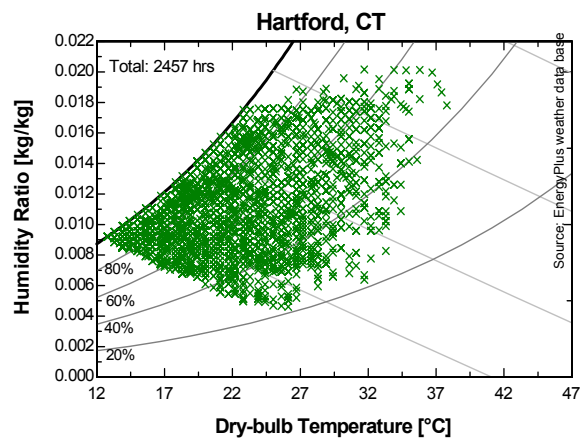
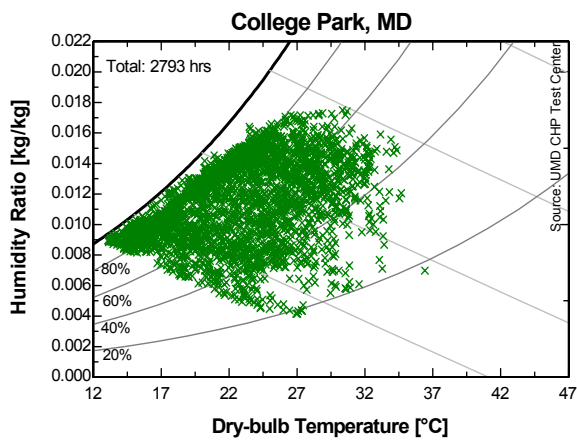
(b). Assume mechanical cooling is required when ambient enthalpy $\geq 38 \text{ kJ/kg}$ for the system with enthalpy-based economizer

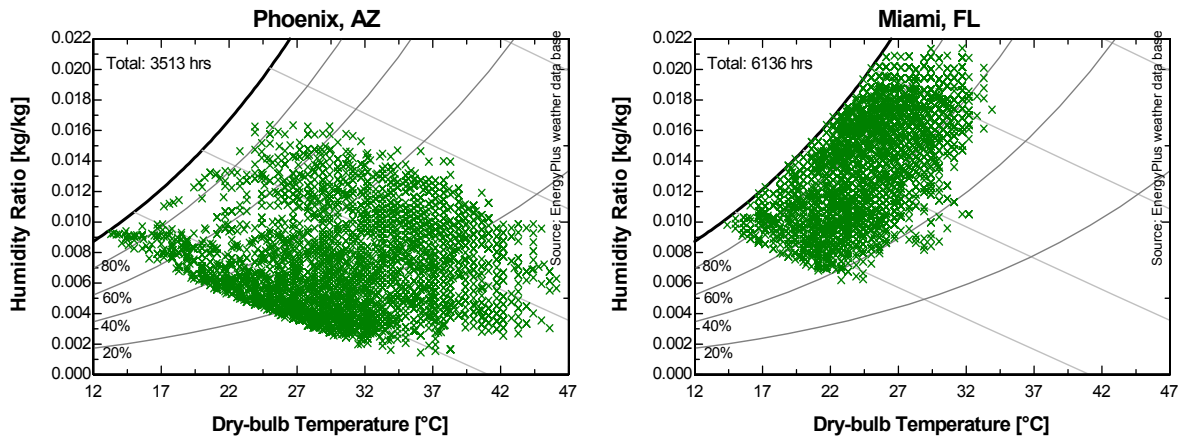
Fig. 57. Year-round weather in College Park, Maryland, USA

In addition to the difference of operating hours, the shape of the dot cluster or the weather pattern is different also. For example, Phoenix AZ is hot and dry most of the time, while Miami FL is more humid.



(a) Assume mechanical cooling is required when ambient temperature $\geq 20^{\circ}\text{C}$ for the system with temperature-based economizer





(b) Assume mechanical cooling is required when ambient enthalpy ≥ 38 kJ/kg for the system with enthalpy-based economizer

Fig. 58. The coincident weather when the mechanical cooling is required

Conventional RTU Baseline

Many commercial buildings use conventional Roof Top Units (RTUs) to supply cooling. Use the Chesapeake Building as an example: it has two 90 ton (316 kW, 1 ton = 3.516 kW) RTUs for each zone. Each RTU uses a conventional vapor compression cycle to cool air through a DX coil. Then the supply air is distributed via Variable Air Volume (VAV) boxes that modulate air volume distribution throughout each conditioned room based on wall-mounted thermostats, adjusted by the building occupants. Electric reheats within these VAV boxes provide localized heating when required. The core of the building requires cooling all year round and the supply air must be kept at a level where cooling can be provided to all areas of the building (about 15 °C). Figure 59 describes the relation of RTU, VAV and the conditioned space (building).

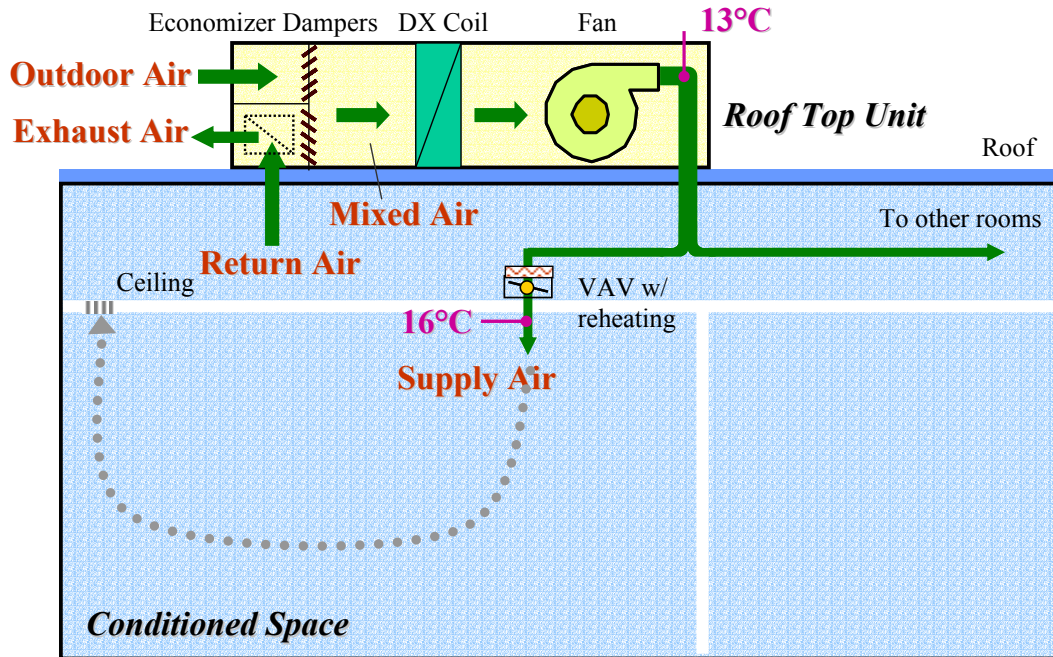


Fig. 59. Roof top unit and the conditioned space

Consider an analysis of a conventional vapor compression RTU for a commercial building, where the total 15000 CFM mixed air (MA) consists of 80% return air (RA) and 20% outdoor air (OA). The MA is cooled and dehumidified by a DX coil, then reheated to the supply air (SA), because the DX coil must overcool the air to achieve the required dehumidification. The whole process is illustrated in Fig. 60. The energy consumption to process 1 kg of Supply Air (SA) is 21.3 (cooling and dehumidifying by the DX coil) + 3.1 (reheat) = 24.4 kJ/kg of dry supply air. The moisture suppression* required is 2.63 g/kg of dry supply air.

It is believed that the dehumidification method results in extra energy consumption due to the overcooling and reheating. Ironically, the reheating is still needed even in summer when the RTU is working! The experimental data presented in Fig. 4 (b)

* Moisture depression means the difference between the moisture content (in terms of humidity ratio) of the process air entering and leaving the dehumidifier.

is good evidence. Note: the peak lighting load is about 15 kW on workdays according to the design data; no specific sensor for lighting is available.

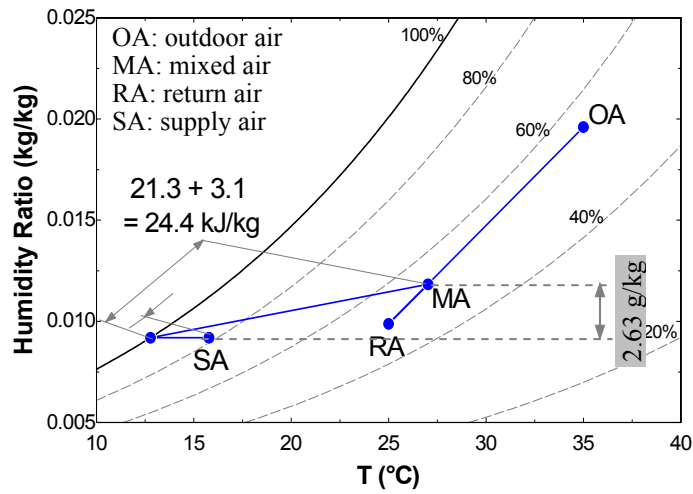


Fig. 60. The conventional vapor compression air conditioning used to remove moisture and control air temperature with reheat

In addition, the latent load and sensible load of a building zone, as shown in Fig. 61, will proportionally increase with the outdoor air ratio. The calculation uses the same OA, RA and SA assumptions as those in Fig. 60.

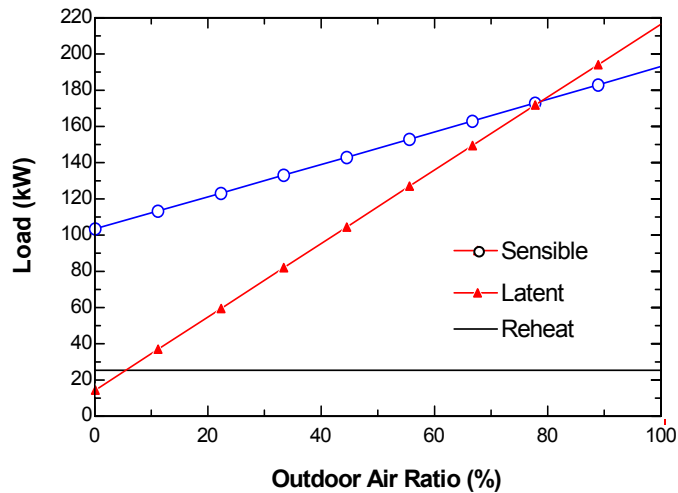


Fig. 61. Latent load, sensible load and reheat load of a building zone

Best CHP Practice

Desiccant as an Energy Transformer

Refrigeration of the air below its dew point is the most common method of dehumidification; the process is depicted from state point MA to SA in Fig. 60. Desiccant dehumidification uses a different method: the dehumidification effect is achieved by converting latent heat to sensible heat, as shown from state point MA to PA in Fig. 62. Ideally the use of desiccant systems can eliminate the reheat component of the air conditioning cycle by suppressing the humidity without overcooling the air.

By working together, conventional cooling systems and desiccant systems can accommodate the temperature and humidity loads separately and more efficiently. Since the RTU DX coils can now use a higher evaporation temperature setting as they only need to satisfy the sensible load, the COP can be higher, and the unit size can be reduced, which consequently brings the benefits of reduced capital cost, compact size, smaller resistance to air due to smaller coils, and smaller fan power required. In addition, since there will be no condensation on the coil the problem of mold growth is eliminated.

When a heat source (for instance the waste heat) is available for free, desiccant units exhibit even greater potential to reduce energy costs as utilities move commercial customers to real-time pricing which sees electrical costs increasing with outdoor temperature and humidity, since desiccants in particular will be more effective with higher inlet humidity.

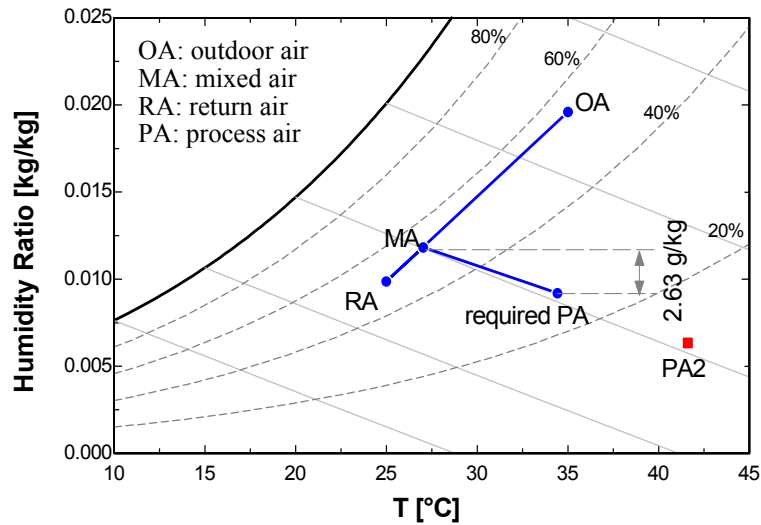


Fig. 62. Desiccant wheel delivers the required latent load at the design condition by dehumidifying the mixed air

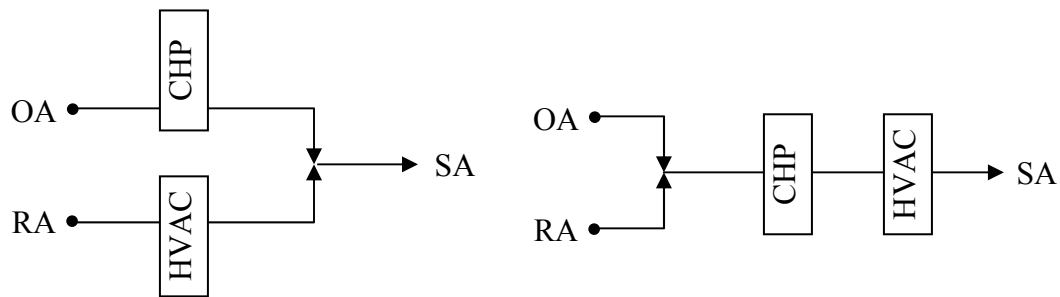
CHP Arrangements in Parallel or Series with HVAC

The building onsite generation of power provides many opportunities for energy savings if the waste heat rejected by the power generator can be effectively utilized elsewhere in the building. The least complicated application for this waste heat is for low-grade heating of either domestic water or room air in winter. The use of absorption chillers for cooling/heating and desiccants for dehumidification are two applications that can extend the time frame over which the waste heat from the power generator is useful to the building; these applications are where the research of this dissertation is focused.

An attractive CHP application would be the provision of an absolutely constant electrical and cooling/heating demand for the building, but this is almost never the case with commercial buildings. In a real commercial building, the energy consumption is dominated by building heating and cooling loads, and the plug load, which vary with times, dates and seasons. See Fig. 4.

Since CHP equipment is currently more expensive in terms of capital cost than the conventional HVAC systems, financial gain is achieved through maximizing the operating hours of the unit so that the cost savings achieved through the recovery of waste heat can help to repay its higher initial capital cost. However, the daily load fluctuation and energy diversity of a typical commercial building are great enough to severely reduce the full load operating hours of a unit sized at the peak load of the building, so the difficulty of supplying all heating, cooling and power loads from the same CHP system without having some conventional HVAC becomes apparent.

If a commercial building is served by a CHP system and conventional HVAC equipment, there are two arrangements with regard to the air streams they condition: parallel and series, as shown in Fig. 63. The CHP in the former configuration is also called a CHP Dedicated Outdoor Air System (CHP DOAS), which only conditions outdoor ventilation air separately from the conditioned space return air stream.



Legend

OA: outdoor air for ventilation purpose

RA: return air from the conditioned space

SA: supply air delivered to the conditioned space

(a) Parallel

(b) Series

Fig. 63. Configurations of CHP and HVAC in parallel or series connection

Parallel Configuration (CHP DOAS)

A Dedicated outdoor air system (DOAS) conditions outdoor ventilation air separately from the conditioned space return air and eventually handles the entire building latent load. It may have several versions (Mumma, S. 2001, Trane Company 2003), but an indispensable device is a direct expansion (DX) coil, which cools and dehumidifies the outdoor air to 7°C dew-point temperature (see Fig. 5). Then the air is mixed with the air from a smaller RTU, which conditions the return air only, before being delivered to the conditioned space.

The CHP DOAS (Cowie et al., 2003 b) at times contains a desiccant wheel to remove the latent load, while the absorption chiller supplies chilled water in summer and hot water in winter. The relation between CHP DOAS and RTU is illustrated in Fig. 64, and Fig. 65 is the configuration of the CHP DOAS.

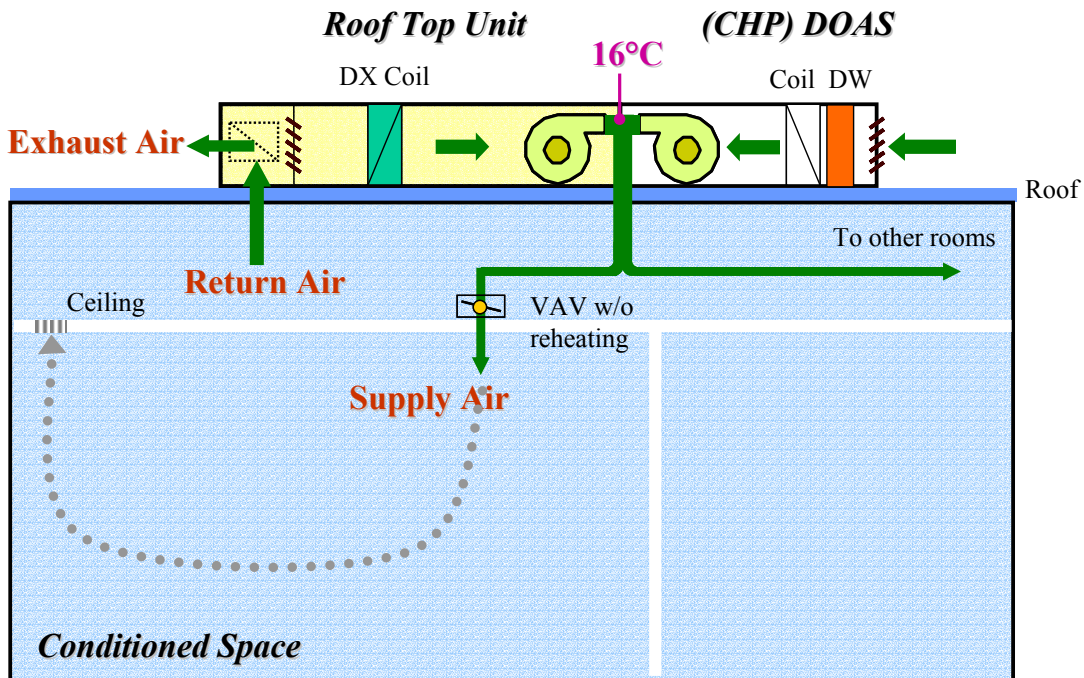


Fig. 64. Schematic drawing of the parallel configuration

Legend

- ①: Outdoor air
- ⑤: Air after desiccant wheel
- ⑦: Supply air

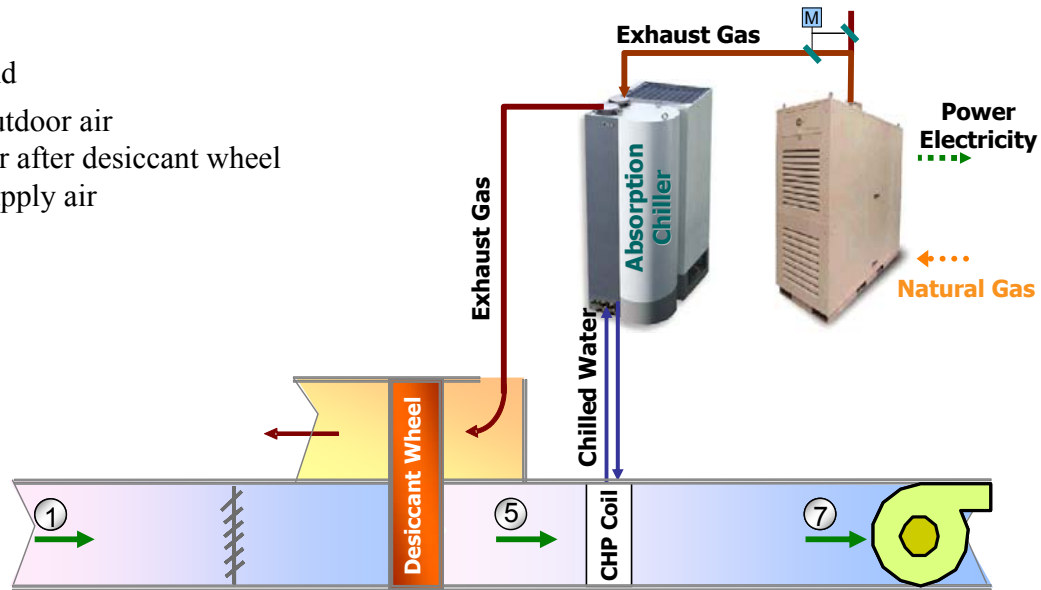


Fig. 65. CHP DOAS illustration

Assume that the outdoor air is at 20% of the supply air. If the desiccant wheel is intended to handle the entire moisture load of the building by only dehumidifying the outdoor air, it should ideally have a moisture removal capacity of 79.0 kg/hr out of 3000 CFM outdoor air at the design condition shown in Fig. 60, or moisture suppression of 12.6 g/kg dry air.

Unfortunately both the simulation by Klingenberg (2002) and the experiments conducted by the author cannot prove that the current desiccant unit in the CHP Integration Test Center can have such a high desired moisture suppression capacity (that is 12.6 g/kg). The exhaust regenerated solid desiccant unit can only provide moisture suppression of 6.9 g/kg dry air at the design condition (35°C DB and 55% RH), which is about half of the desired capacity. See Fig. 66.

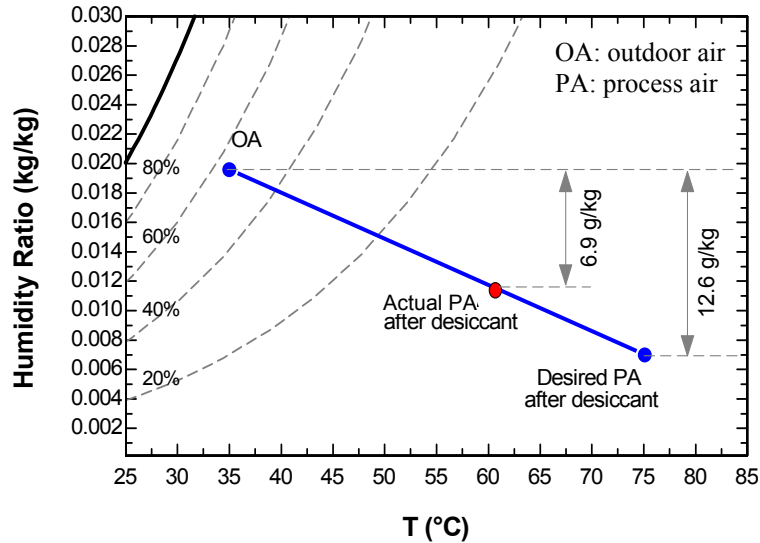


Fig. 66. Desiccant wheel takes care of the latent load at the design condition by dehumidifying the outdoor air

For example, there are two similar days (07/07/03 and 07/11/03) - the enthalpy of outdoor air was similar for most of the time, and on each day the RTU ran alone from 5:00 am to 10:00 pm, but on 07/11/03 the SDU ran from 7:00 am to 6:00 pm. Figures 67 and 68 show that, when operating together with the SDU, the RTU still needs to remove moisture even though the RTU's remaining load is about half of that as compared to its standalone operation.

Even the commercially available gas fired products can only supply moisture suppression of 8.2 g/kg dry air at the design condition. See Fig. 88. It is still not enough to remove the latent load of the whole building. Therefore, the CHP DOAS cannot be expected to satisfy the entire latent load of a building unless new desiccant technology emerges and dramatically improves its capacity in the future.

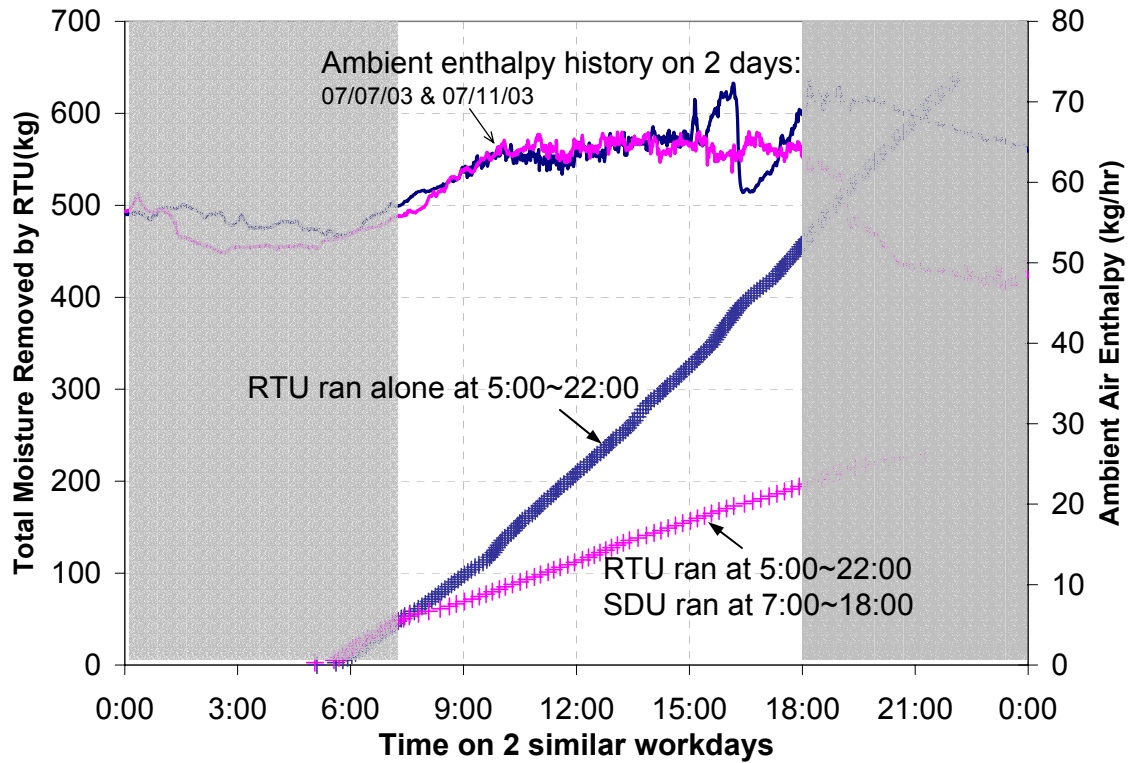


Fig. 67. Total moisture removed by RTU on 2 similar workdays

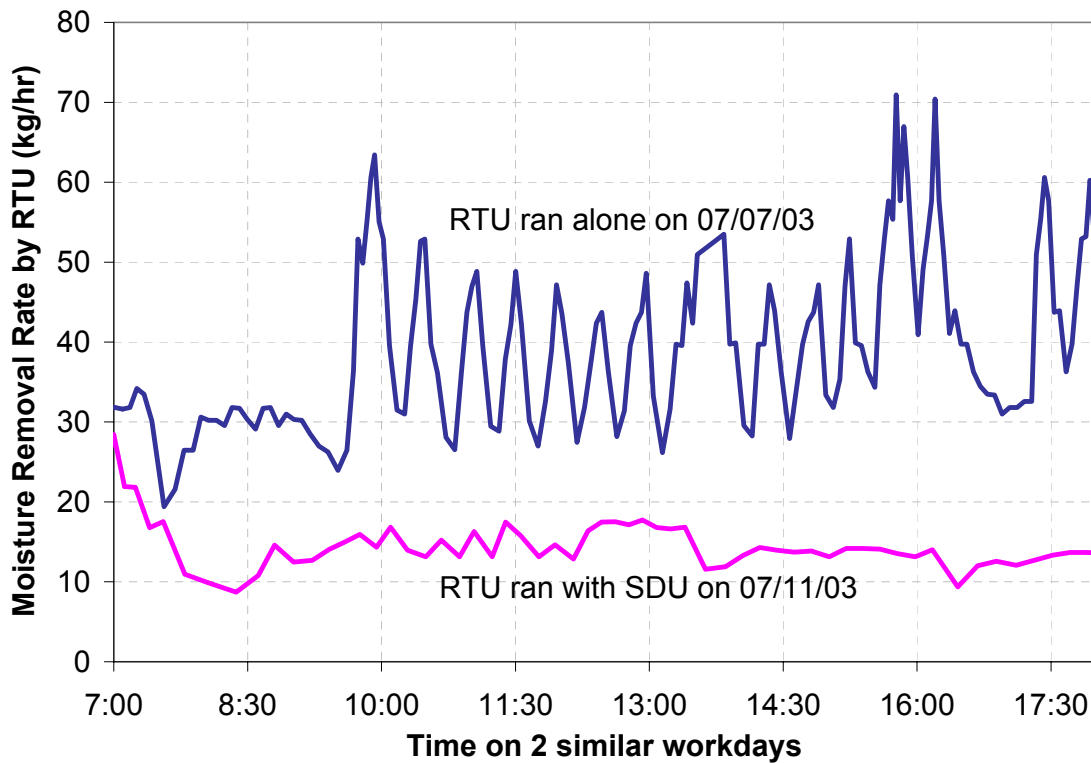


Fig. 68. The moisture removal rate by RTU on 2 similar workdays

In addition, the conditions at the air inlet vary widely during the operation of CHP DOAS as shown in Fig. 58 (that is, the CHP DOAS will encounter extreme hot, dry, or humid inlet outdoor air and different weather patterns). This will definitely increase the difficulty of designing a suitable control for CHP DOAS, and a universal CHP product for all locations, because of the various outputs of CHP systems and the exhaust distribution among the different thermally activated machines, such as absorption chillers and desiccant units. Consequently, the cost of design, training, manufacture and operation will increase, and therefore hinder the commercialization of the CHP products.

And moreover, the process air inlet moisture content affects the outlet moisture of a desiccant wheel. Usually the machine performs better at full load; that is, it has higher moisture suppression when the inlet air is more humid. So the performance of CHP DOAS will be unavoidably and unfavorably influenced by the wide range of weather conditions.

In summary, the CHP DOAS has several fatal shortcomings. One, it cannot accommodate the entire building latent load in humid weather by just dehumidifying the outdoor air (a smaller portion of the supply air) through a desiccant wheel, e.g. when the outdoor air is 20%, the CHP DOAS can only meet about half of the entire latent load at the design condition. Two, complicated controls are needed to handle various weather conditions and patterns.

Series Configuration

Being different from the parallel configuration (CHP DOAS), the series configuration can overcome all its fatal shortages. It is similar to the RTU baseline – the CHP system and conventional HVAC unit are integrated into a hybrid unit to condition

the mixed air stream. The hybrid unit may include an exhaust regenerated desiccant wheel (DW), a chilled water coil that delivers the cooling of absorption chiller to the air stream, a conventional DX coil that picks up the residual cooling load, and a supply fan. Figure 69 explains the relation between the hybrid unit and the conditioned space.

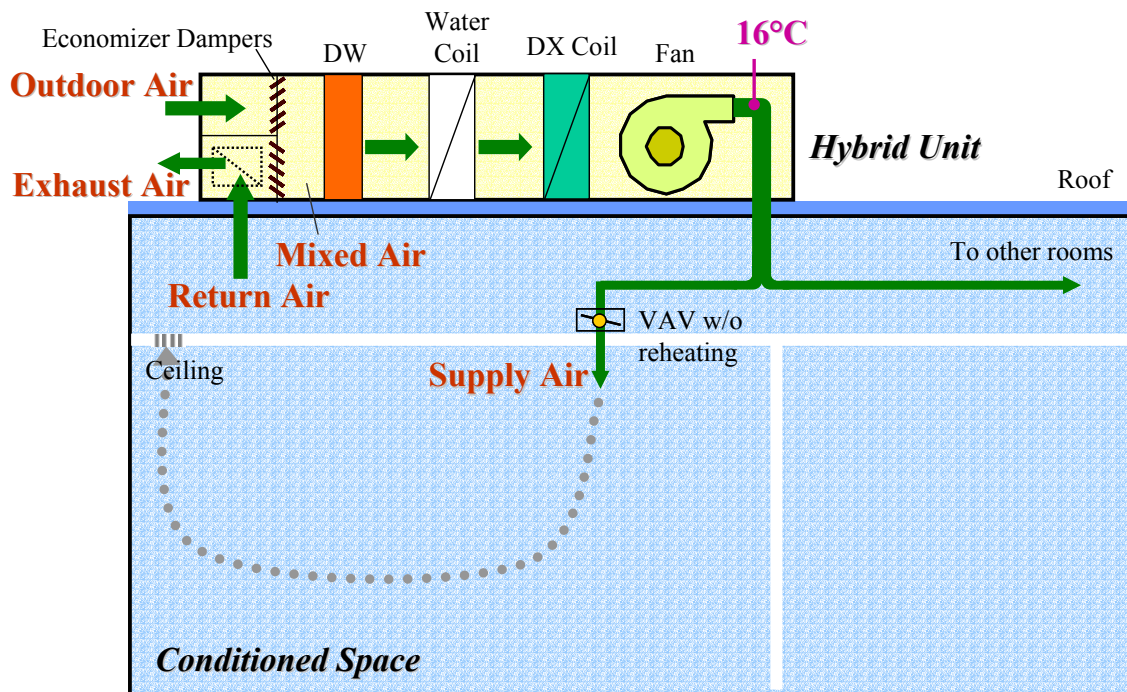
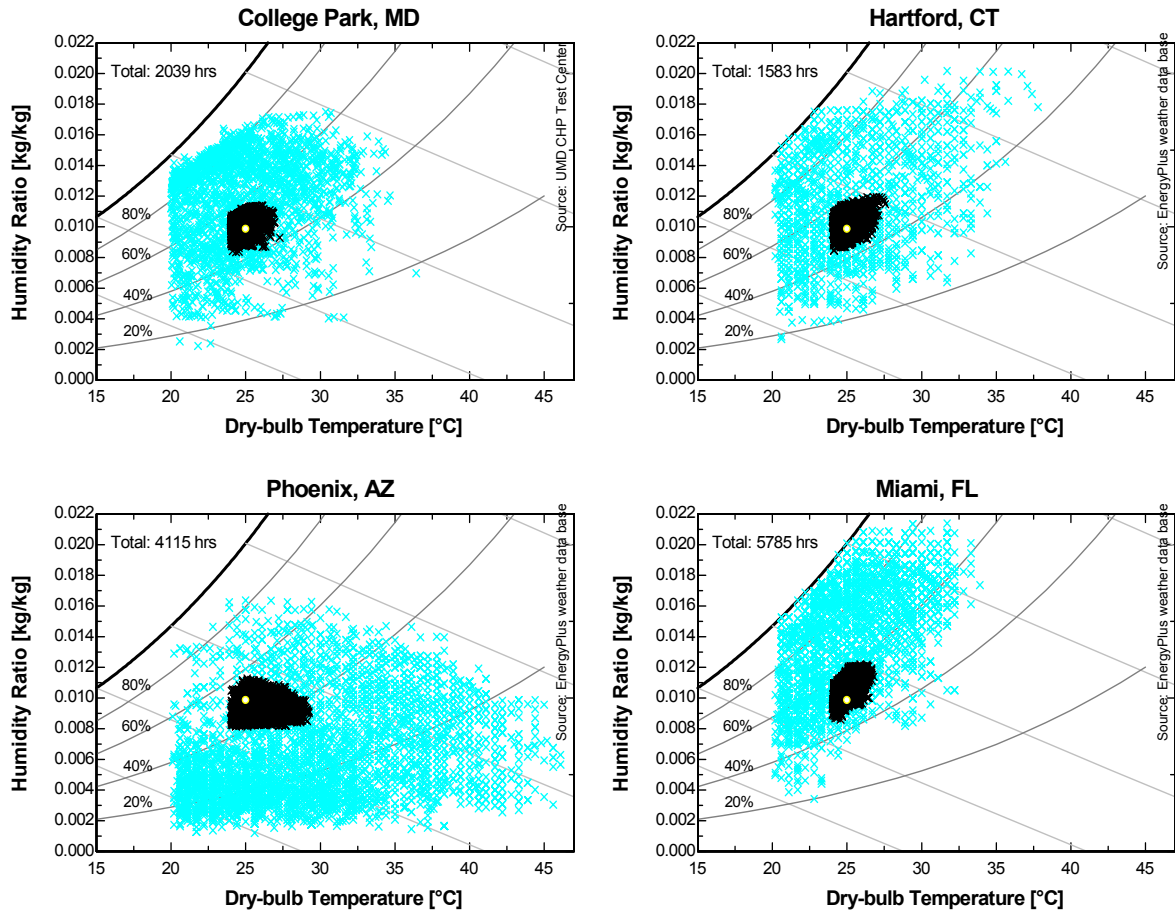


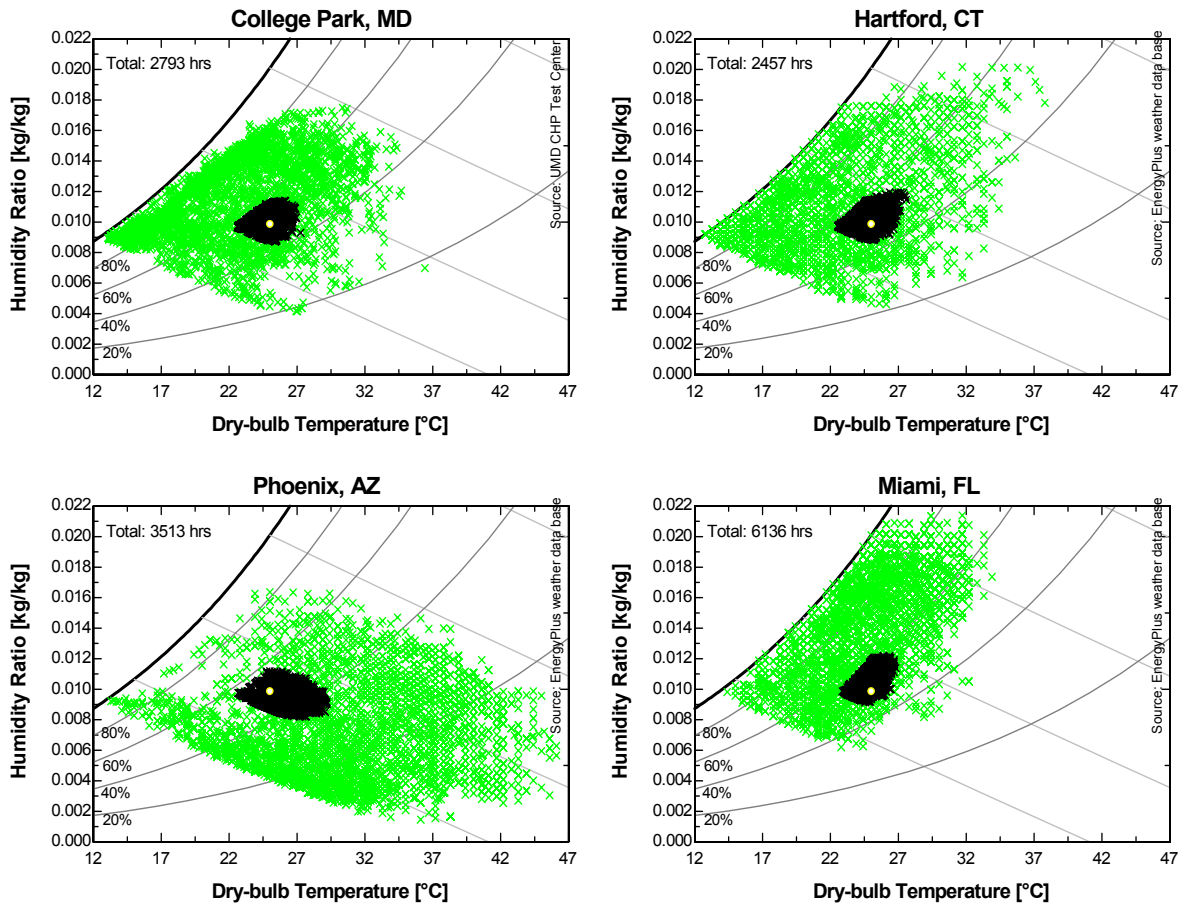
Fig. 69. Schematic drawing of the series configuration

Assume that the outdoor air is 20% in a commercial building. The coincident mixed air condition entering the CHP and HVAC series system is mapped in the darker zones of Fig. 70. The constant condition of the return air (a larger portion of the supply air) dampens the fluctuation of the outdoor air, which is a smaller portion compared with the building return air. The darker zones are concentrated, as compared to the scattered background, with similar shapes for every city. This means that, the inlet air conditions and loads for CHP, independent of location, will not vary dramatically over time and geographic location. The influence of outdoor air can be further mitigated if an enthalpy

wheel is used to recover energy from the building exhaust. Then the darker zones are more concentrated and smaller. See Fig. 71. The lighter dots within the darker zones are the state point of return air, which is set at 25°C and 50% RH in summer.



(a) Assume mechanical cooling is required when ambient temperature $\geq 20^{\circ}\text{C}$ for the system with temperature-based economizer



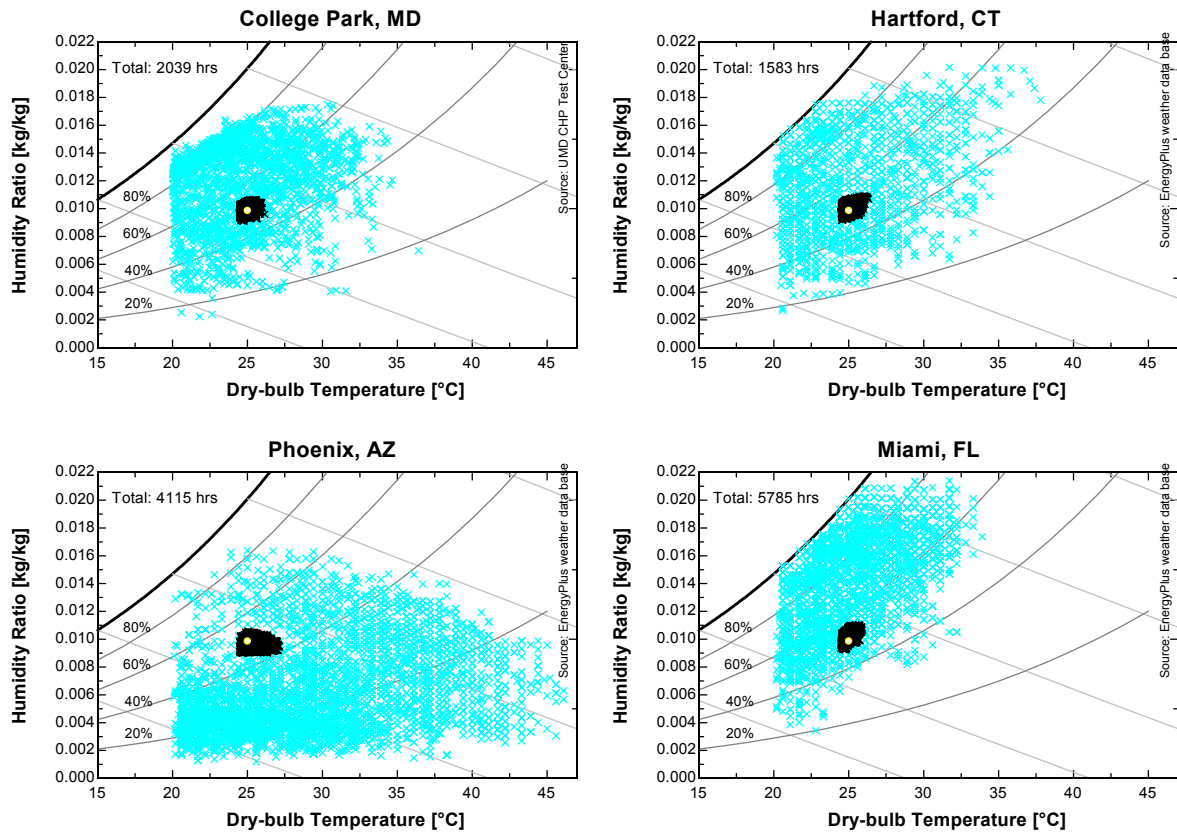
(b) Assume mechanical cooling is required when ambient enthalpy ≥ 38 kJ/kg for the system with enthalpy-based economizer

Fig. 70. The coincident mixed air condition entering the CHP and HVAC series system in the cooling season

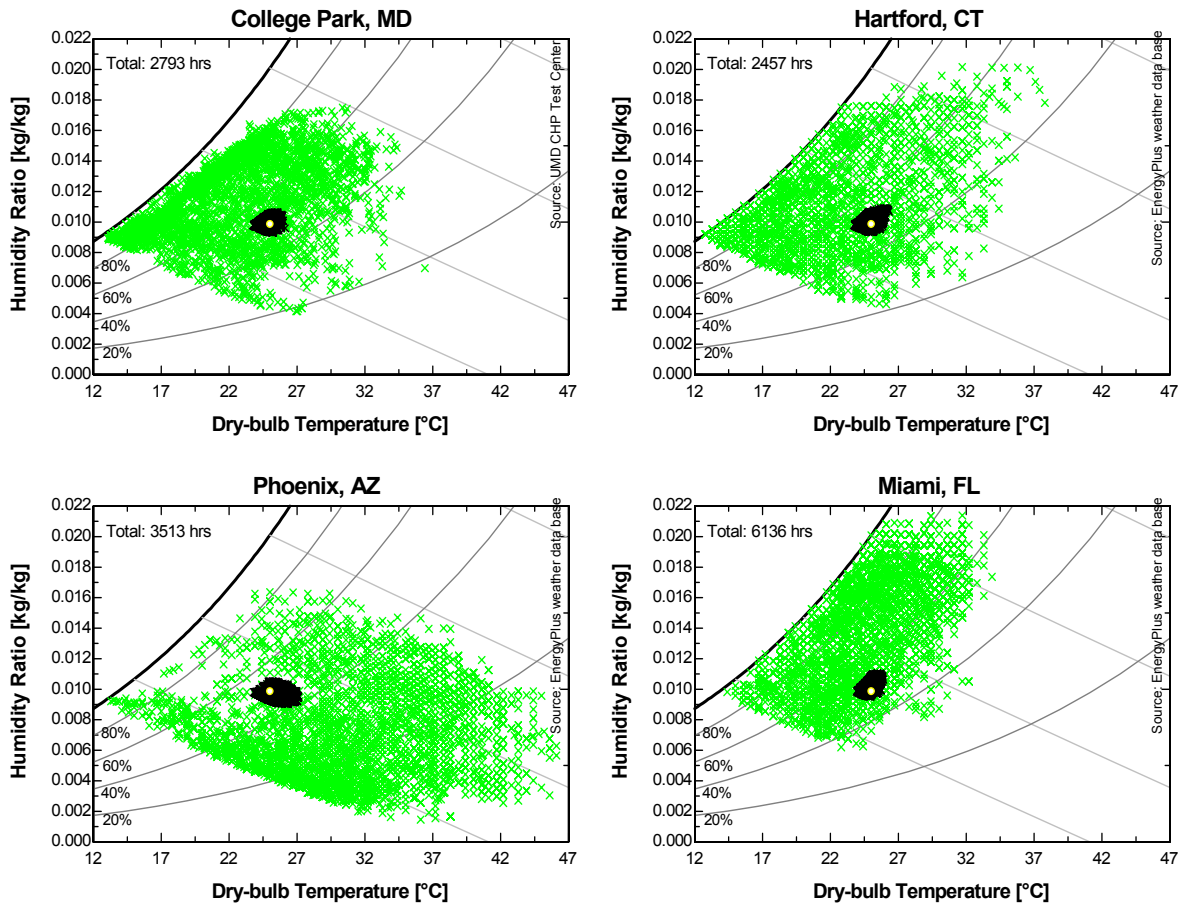
The mixed air results in a large and stable load (for the CHP system), which is less dependent on the ambient conditions and different locations. Therefore, it is possible to design and manufacture a universal CHP product for all commercial buildings in the world. Figure 62 is the simulation result, which proves that desiccant dehumidification can easily meet the entire latent load and provide the required moisture suppression of 2.63 g/kg. Commercial desiccant products can provide even larger moisture removal

capacity, for example the leaving state point of process air can reach as dry as Point PA2 in Fig. 62.

Obviously the series configuration is superior to the parallel one, because it overcomes the fatal disadvantages of the parallel design (CHP DOAS).



(a) Assume mechanical cooling is required when ambient temperature $\geq 20^{\circ}\text{C}$ for the system with temperature-based economizer



(b) Assume mechanical cooling is required when ambient enthalpy ≥ 38 kJ/kg for the system with enthalpy-based economizer

Fig. 71. The coincident mixed air condition entering the CHP and HVAC series system in the cooling season with enthalpy recovery

Proposed Application of Air-cooled Absorption Chiller in CHP Systems

Component Assumption

From the above analysis, we know that CHP introduces an innovative way to supply cooling, heating and power for a building, and the series configuration is the best method to integrate CHP with conventional HVAC units.

Assume the components in the following proposed applications include a 60 kW microturbine, a desiccant wheel and/or an enthalpy wheel with effectiveness of 0.75, an 18 ton air-cooled absorption chiller driven by the exhaust from microturbine, and a RTU air handler. The CHP system supplies cooling/heating, dehumidification and power to a zone in a building, where the total 15000 CFM supply air consists of 80% Return Air (RA) and 20% Outdoor Air (OA).

The semi-empirical model used in this research to describe the MT performance is based upon the EES program developed by Marantan, A. (2002 a) on the operating principle of the Brayton cycle, and calibrated by the experimental results - such as the heat leak from the plenum box to the engine core chamber, which reflects on the higher compressor inlet temperature than the ambient temperature, see Fig. 23.

The semi-empirical model used in the research to describe the performance of the solid desiccant wheel has been adapted from the EES program developed by Klingenberger, U. (2002) and the experimental results acquired in the CHP Integration Test Center.

The model for the air-cooled absorption chiller was described in Chapter 5 - Air-cooled Absorption Chiller Modeling. The chilled water supply temperature is set much higher than the conventional air-conditioning application to prevent crystallization. In the following simulations, the chilled water return temperature is set 7°C lower than the coil inlet air temperature. Besides, the temperature map of Fig. 50 (c) is obeyed.

System without Enthalpy Wheel

In Fig. 72, outdoor air ① is mixed with the return air ③, and becomes the mixed air ④. After being dehumidified by the desiccant wheel, it reaches a hotter and drier state

point ⑤, which satisfies the humidity content of building supply air. Both the chilled water coil of the air-cooled absorption chiller and the DX coil step take care of the sensible load only, and decrease the air temperature to ⑥ and ⑦ respectively.

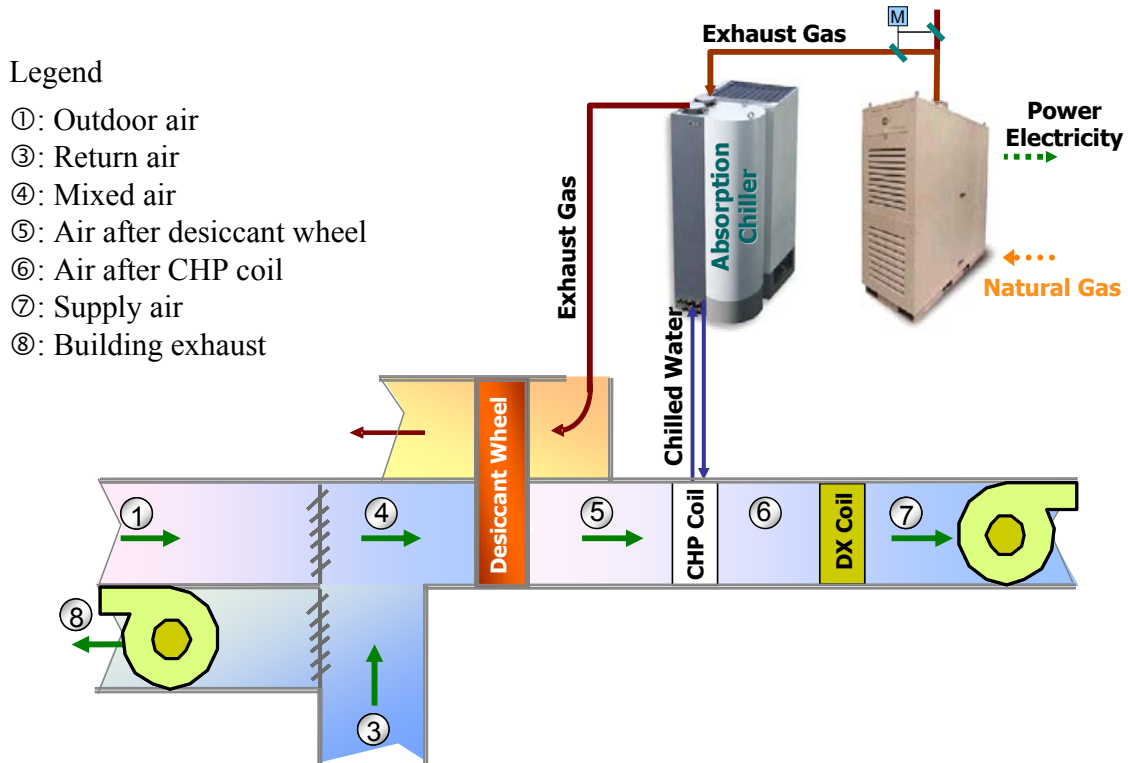


Fig. 72. Proposed CHP application without an enthalpy wheel in RTU

System with Enthalpy Wheel

In Fig. 73, an enthalpy wheel is integrated to preprocess the outdoor air to the state point ② before being mixed with the return air. Theoretically, the enthalpy wheel reduces the load on the HVAC system and boosts the efficiency in either winter or summer. However, the enthalpy wheel does not benefit in all weather. In Fig. 74, the darker dots represent the ambient conditions in the cooling season, over which the outdoor air enthalpy is equal or lower than that of the return air. Therefore the enthalpy wheel cannot save energy, but adds more load to the HVAC system instead, because it

heats up and/or humidifies the outdoor air. Note: a sensible wheel or a heat pipe has similar results.

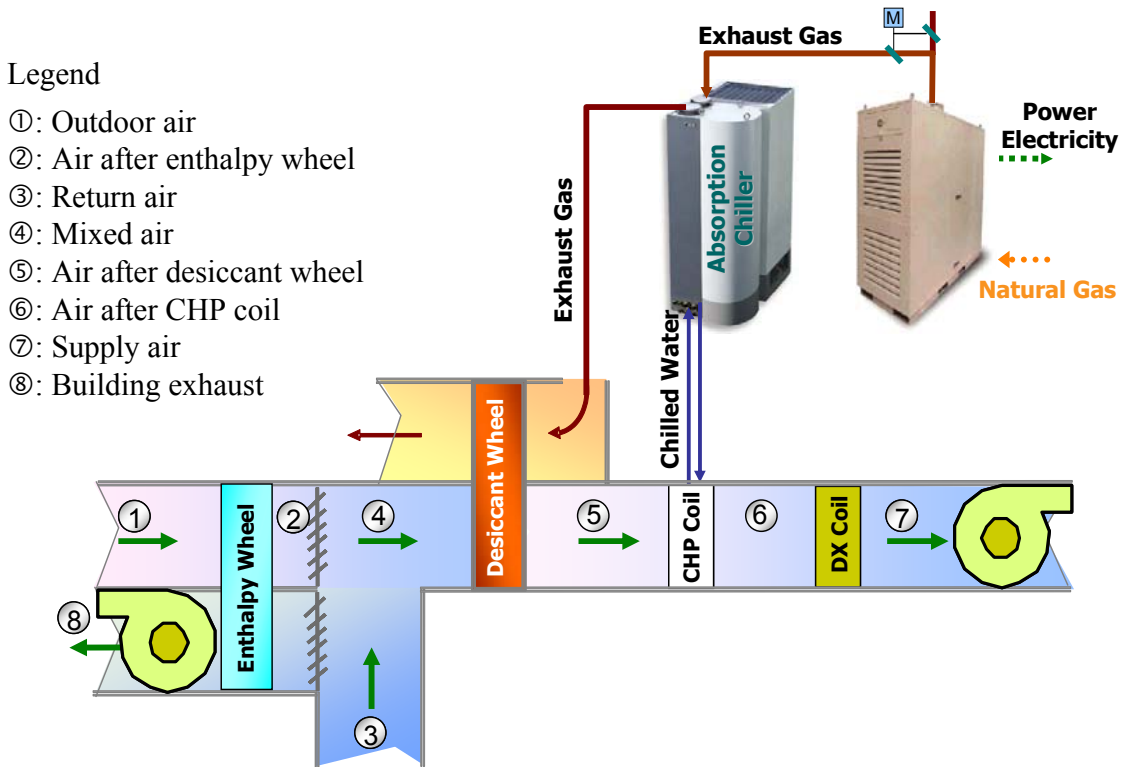


Fig. 73. Proposed CHP application with an enthalpy wheel in RTU

Energy Analysis

General

Three configurations – (1) baseline: conventional RTU, (2) hybrid system #1: CHP (w/o enthalpy wheel) in series with RTU, and (3) hybrid system #2: CHP (with enthalpy wheel) in series with RTU - in 4 representative cities in the United States are evaluated on four aspects for the entire cooling season:

- Reheat load - the additional reheat after the DX coil to reach the required supply air condition (kWh);

- RTU cooling load – the cooling load for the DX coil in RTU (Ton-hr);
- RTU moisture load – the moisture removed by the DX coil in RTU (kg);
- Primary energy consumption for each concept producing the same supply air and net electricity.

The energy analysis is based on one zone in a commercial building with 15000 CFM supply air, in which 20% (i.e., 3000 CFM) is outdoor air. The return air is set at 25°C, 50% RH, and the supply air is set at 16°C DB, 14°C WB.

The local coincident weather data shown in Fig. 58 is input. Results for different cities are plotted in Fig. 75 (when the economizer is dry-bulb temperature based) and Fig. 77 (when the economizer is enthalpy-based) respectively. The numbers in parentheses are the load percentage of a specific case to the baseline.

The primary energy consumption in the cooling season for each concept in 4 cities is plotted in Fig. 76 and Fig. 78. The assumptions in the calculation are:

- RTU COP = 3
- MT efficiency = 25% (HHV)
- Power plant efficiency = 30%
- Each case produces/purchases the same supply air and net electricity (50kW).

System with Temperature-based Economizer

Compared with the baseline, the introduction of CHP can completely satisfy the whole latent load and part of the sensible load, and no reheat is needed in the entire cooling season. The air-cooled absorption chiller operates at full load all the time, and the residual cooling load left to the RTU step is 27~37% (w/o enthalpy wheel) and 27~30% (with enthalpy wheel) of the baseline. Therefore the RTU can be much smaller and can

consume less energy than the baseline design. The primary energy consumption of hybrid systems is 60~63% of the baseline.

It is worth noting that the simulation results with the enthalpy wheel in Phoenix are somewhat against the common sense that the enthalpy wheel can always save energy. In most situations, enthalpy wheels do result in energy saving, but when most of the time the outdoor air enthalpy is below that of the return air, such as the weather pattern shown in Fig. 74, no energy saving may be expected. Since the parasitic power consumption, the capital costs, and pressure drop of air flow caused by the wheel have not been considered in the simulation, the slight energy savings over the whole year of an enthalpy wheel might be insignificant.

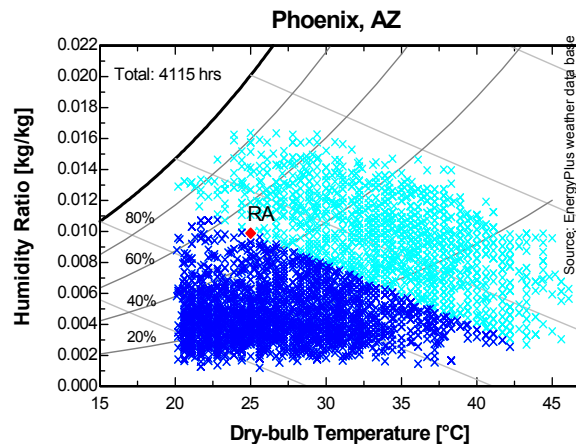


Fig. 74. Enthalpy wheel does not benefit under all weather conditions

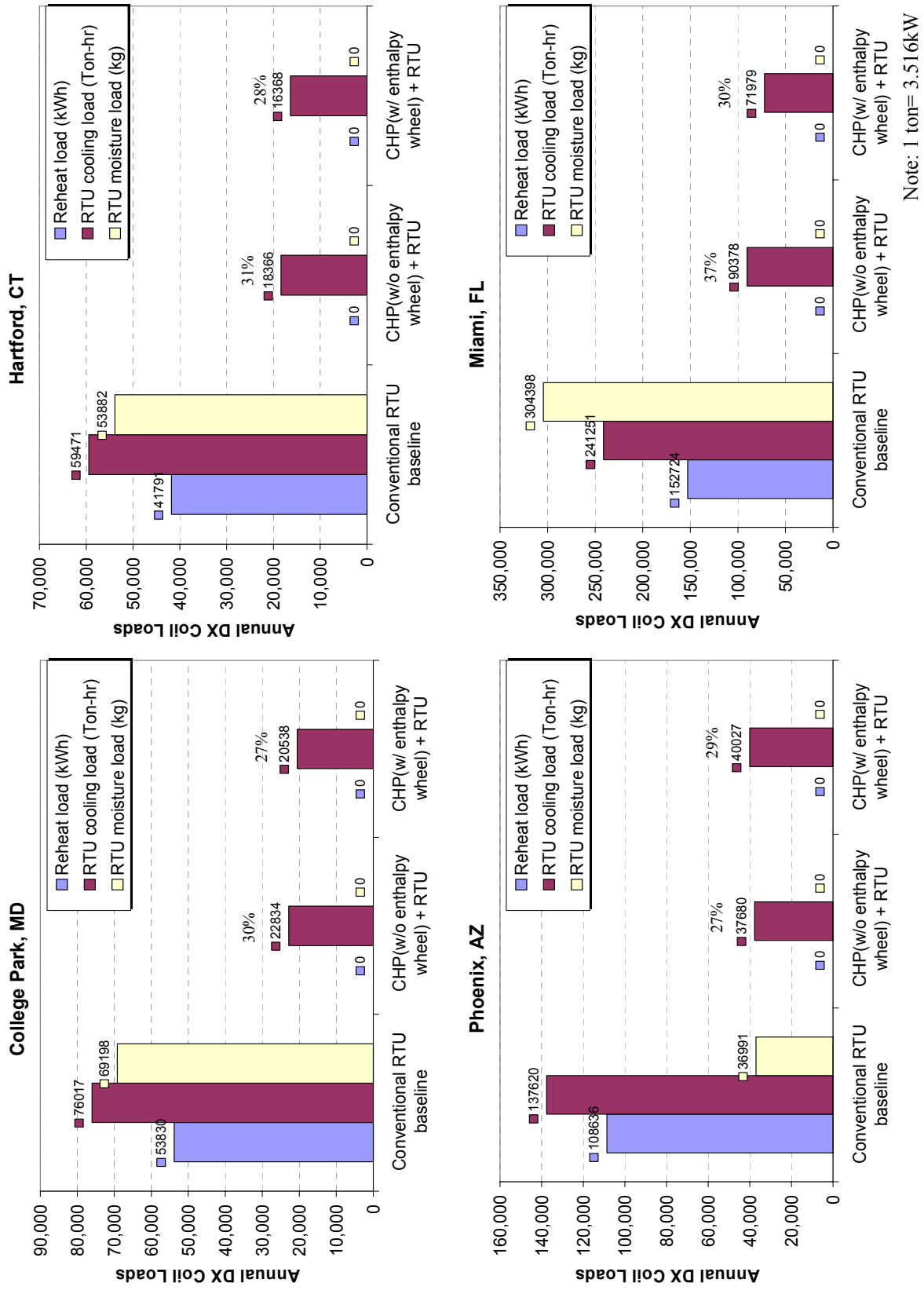


Fig. 75. Summary of RTU loads in cooling season (with temperature-based economizer)

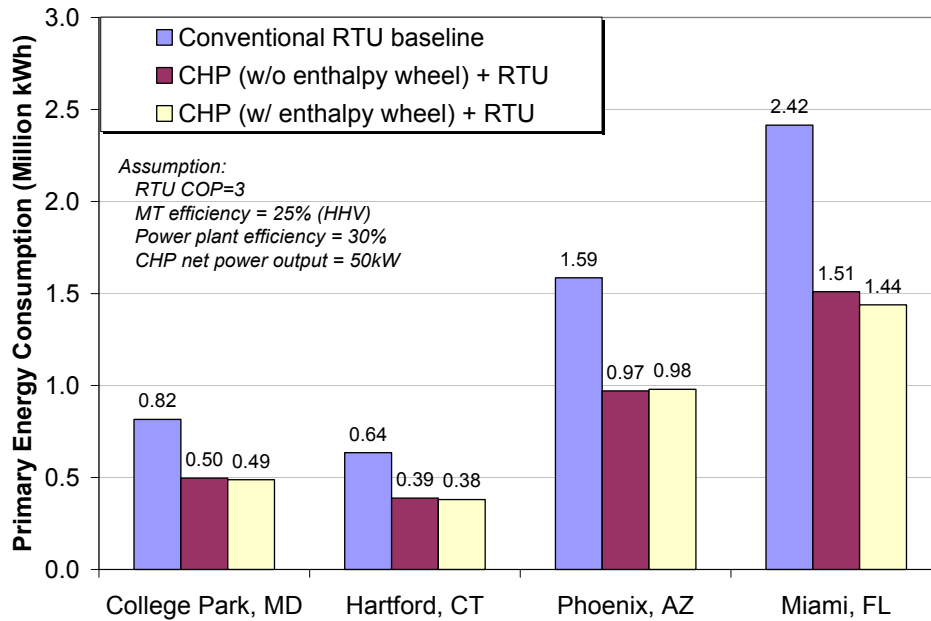


Fig. 76. Primary energy consumption for each concept producing the same supply air and net electricity in cooling season (systems with a temperature-based economizer)

System with Enthalpy-based Economizer

Again, compared with the baseline, the introduction of CHP can completely accommodate the whole latent load and part of the sensible load, and no reheat is needed in the entire cooling season. The air-cooled absorption chiller operates at full load all the time, the residual cooling load left to the RTU step is 26~36% (w/o enthalpy wheel) and 24~30% (with enthalpy wheel) of the baseline, so that the RTU can be much smaller and consume less energy than the baseline design. The primary energy consumption of hybrid systems is 59~72% of the baseline.

The results are similar to the cases with temperature-based economizer, but the phenomenon that enthalpy recovery cannot bring energy savings over the entire cooling season to cities like Phoenix is basically avoided. However, the primary energy savings introduced by enthalpy wheel are still insignificant.

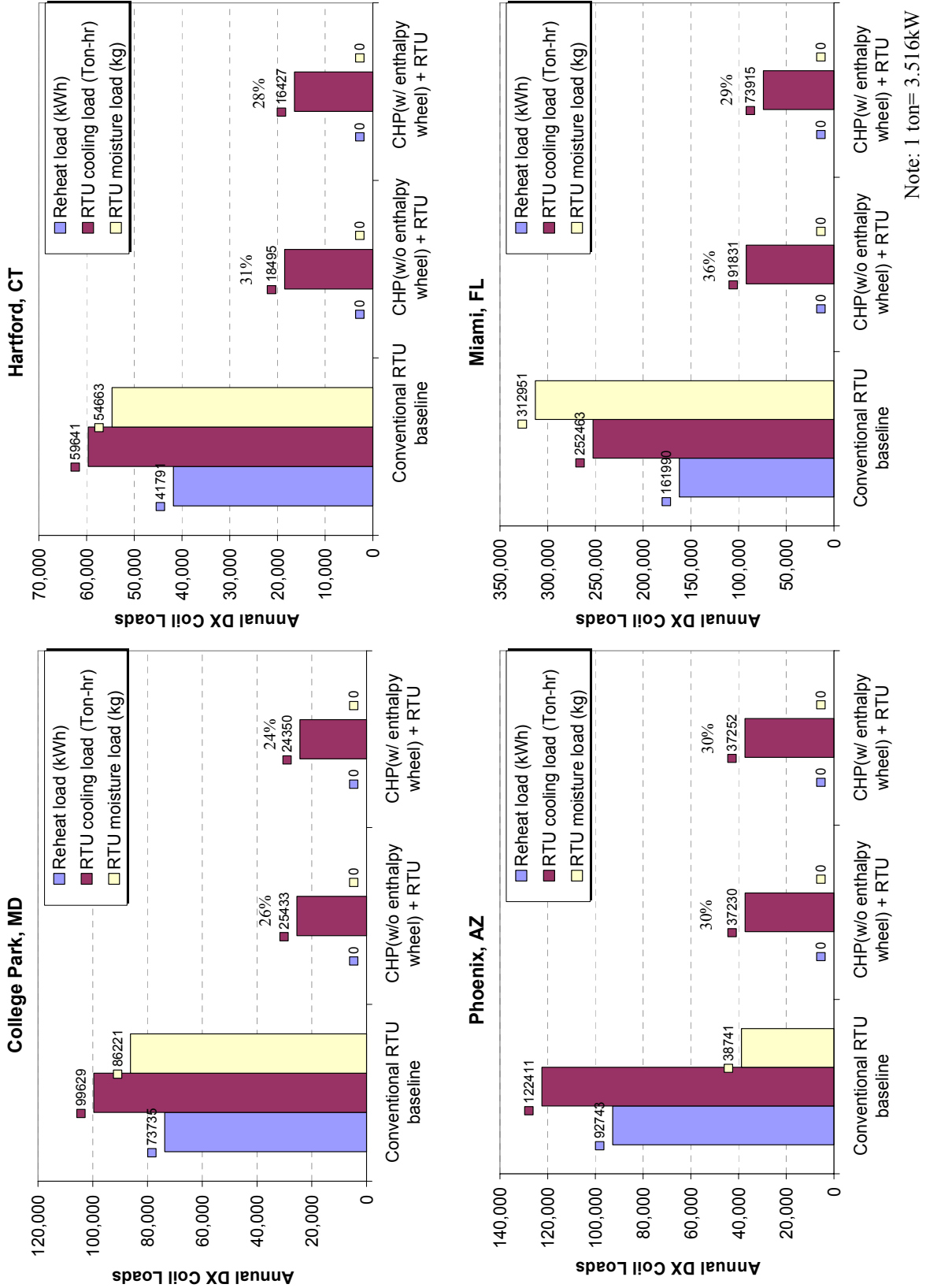


Fig. 77. Summary of RTU loads in cooling season (with enthalpy-based economizer)

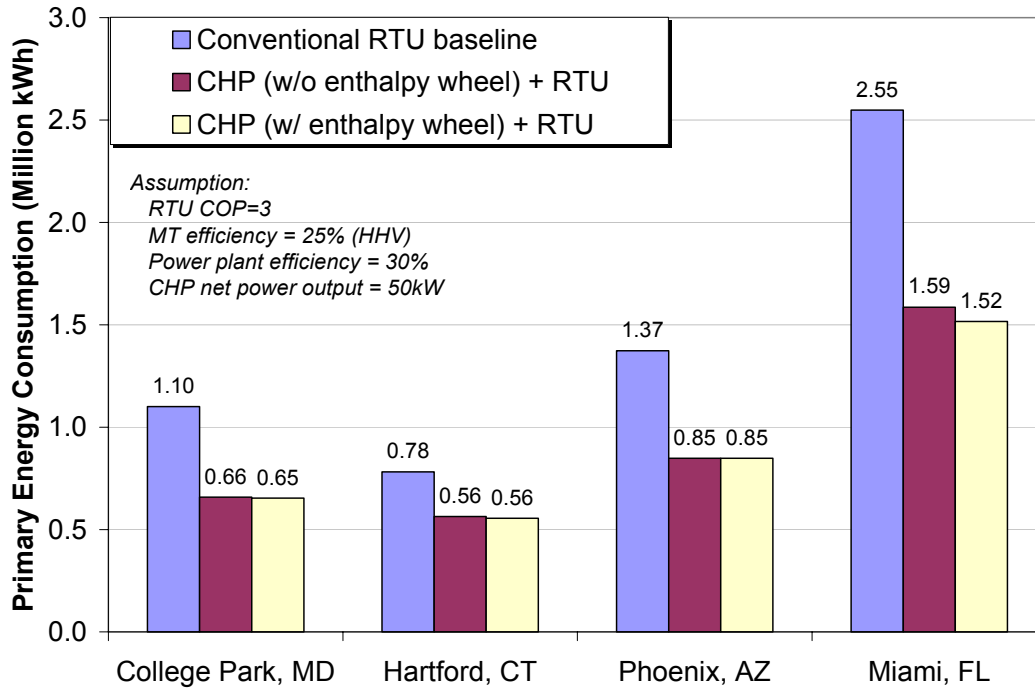


Fig. 78. Primary energy consumption for each concept producing the same supply air and net electricity in cooling season (systems with an enthalpy-based economizer)

Summary of Energy Analysis

- The series configuration is superior to the parallel configuration in the integration of CHP with conventional HVAC units. CHP is designed to meet the base load of a building.
- A CHP system in series configuration can completely satisfy the whole latent load and part of the sensible load, and no reheat is needed in the entire cooling season.
- The conventional HVAC unit can be much smaller and consume less energy than the baseline design. Since it can use a higher evaporation temperature as it only needs to satisfy the sensible load, the COP can be higher, which consequently brings the benefits of reduced capital cost, compact size, smaller resistance to air

due to smaller coils, and smaller fan power required. In addition, since there will be no condensation on the coil the problem of mold growth is eliminated.

- The primary energy consumption of hybrid systems is 60~63% of the baseline for systems with temperature-based economizers or 59~72% of the baseline for systems with enthalpy-based economizers.
- At locations where the weather conditions are mostly mild, the introduction of enthalpy wheel may not guarantee energy savings, or the savings may be insignificant.

Chapter 9 - Guidelines

General

Based on the computer simulation, extensive experiments, first hand installation, operation and maintenance experience, valuable guidelines on the operation issues, application and integration of an air-cooled absorption chiller in CHP systems are developed by the author. The following guidelines are applicable for both air-cooled and water-cooled absorption chillers.

Crystallization

New crystallization control strategies are proposed and validated in this research. The air-cooled absorption chiller may crystallize when the ambient temperature is too hot. However, increasing the chilled water temperatures can avoid crystallization; and the byproducts of this method include the improved cooling capacity and COP. Reducing the exhaust inlet temperature can also prevent the occurrence of crystallization, assuming that the exhaust flow rate is constant. However, this will reduce the cooling capacity and the heat utilization of CHP systems.

In some applications (for instance the process air after a desiccant wheel), where the chilled water supply temperature is allowed to increase appropriately with the ambient temperature, the air-cooled absorption chiller is practical. In CHP applications, the chiller is used to cool down the process air leaving a desiccant wheel, and the process air is usually at more than 40°C, so the chilled water can be set higher than the normal situation even though the temperature difference is still large enough.

Application

The capital cost of CHP equipment and the load fluctuation of a typical commercial building restrict the advantage of designing a unit sized at the peak load. Therefore a conventional HVAC system is still needed. The guideline for the CHP application is to obtain more operating hours out of the CHP equipment at full capacity, because the financial gain can be achieved through maximizing the operating hours of the unit so that the cost saving achieved through the recovery of waste heat can help to repay its higher initial capital cost.

The conventional HVAC system, which is placed to pick up the residual loads, should be arranged in series with and after the CHP equipment. The parallel configuration or CHP DOAS; that is, letting the CHP to process the outdoor air and the HVAC to process the building return air respectively, is not recommended because it has some fatal disadvantages: one, it cannot handle the entire building latent load in humid weather by just dehumidifying the outdoor air (a smaller portion of the supply air) through a desiccant wheel. Two, complicated controls are needed to satisfy various weather conditions and patterns.

The series configuration is superior to the parallel configuration in the integration of CHP with conventional HVAC units. Besides, at the locations where the weather conditions are mostly mild, the introduction of enthalpy wheel may not guarantee energy saving.

Integration

Packaged Absorption Chiller

The key for absorption chillers to be applied in CHP is integration, which implies the integration at two levels – component level and system level.

First, a packaged absorption chiller needs a built-in cooling tower, pumps, fans, and controls. Previously, even an experienced user needed to spend a lot of time and energy to design the system, order all the components from different vendors, and install everything by himself. However, the main thrust of the air-cooled absorption chiller is that the cooling tower is not necessary, and thus the associated accessories and issues can be completely avoided.

Second, the absorption chillers should not introduce too many difficulties in integrating with the prime movers or other thermally activated machines. For example, if the chiller can sustain higher exhaust inlet temperature, adjusting the exhaust flow rate to the chiller will be an easier task, because no make-up air is needed, and the associated fan and controls can be reduced.

As a part of the future research, a third-generation CHP system was designed and installed by upgrading the chiller-cooling tower to a 21 ton highly integrated absorption chiller, with a built-in cooling tower, all pumps, fans, controls and power wires, and even the water treatment. See Appendix F – BCTDE P&I Diagram. In addition, the chiller can sustain higher exhaust inlet temperature, so that, no make-up air is needed and the control is drastically simplified. The cooling capacity control is mainly accomplished by adjusting the exhaust flow rate into the desorber.

With regard to the integration at two levels, the second-generation MT-based system shown in Fig. 79 along with its exhaust heat management and safety control shown in Fig. 16 is too complicated and not feasible for the commercialization. The third-generation shown in Fig. 80 is much simplified and is very promising for future commercialization. Figure 81 displays the P&I Diagram for the third-generation system.

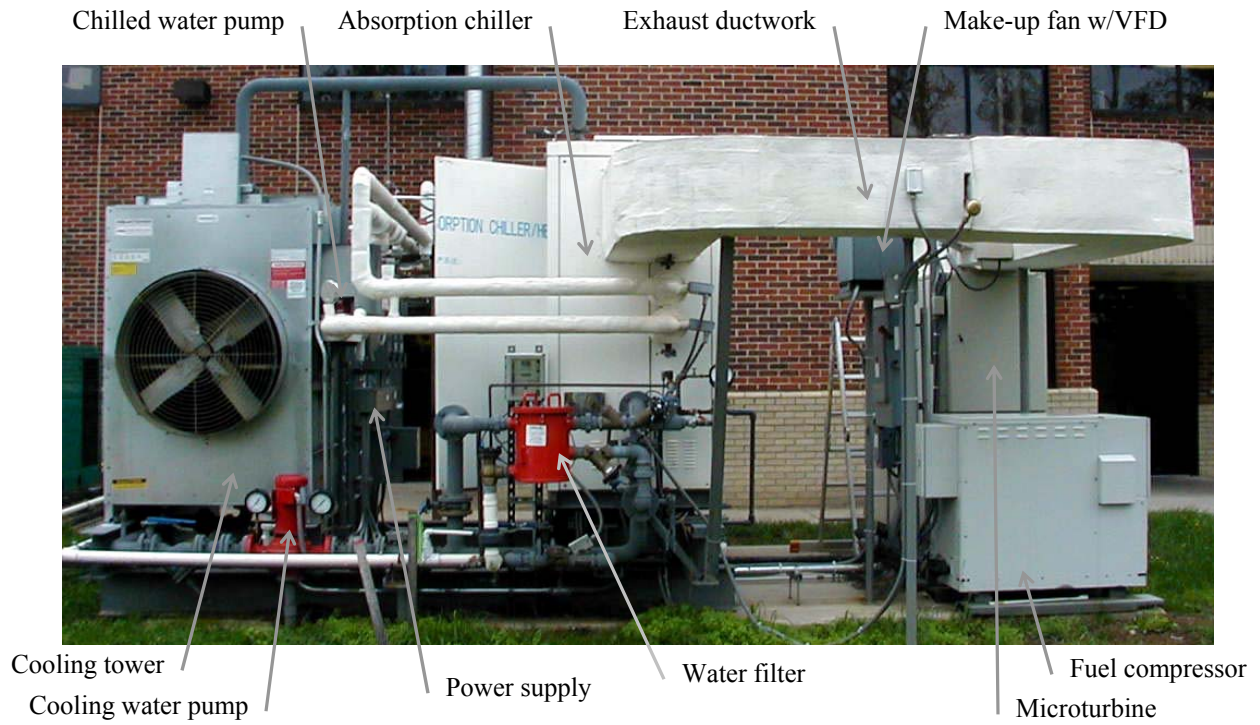


Fig. 79. The complicated second-generation MT-based system



Fig. 80. The simplified third-generation MT-based system

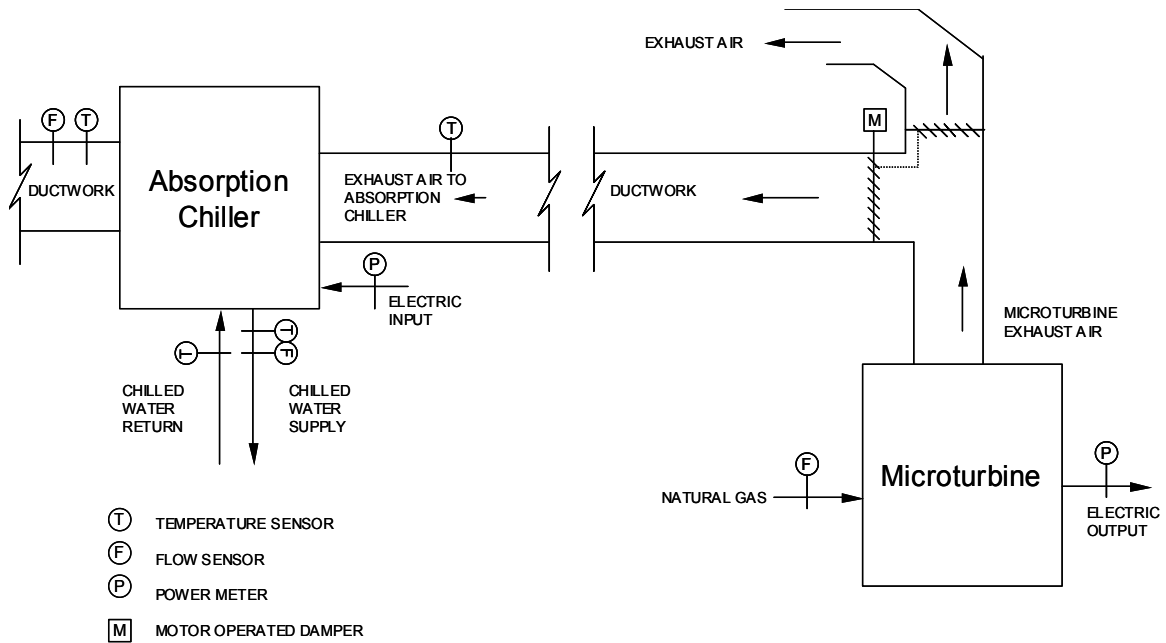


Fig. 81. P&I Diagram for the third-generation microturbine-based system

Exhaust Heat Management

Exhaust heat management is the most important issue in CHP integration. For example, the absorption chiller and the connecting ductwork and/or plenum box will unavoidably apply back pressure to the microturbine, and the exhaust gas is confined in the closed space, which can easily cause heat leak/conduction back to the engine core chamber. All of these issues impair the power generation capacity and efficiency. Although the exhaust heat can be utilized in CHP systems, higher power generation efficiency is still desired because electricity is much more valuable than heat.

Figure 22 shows that the microturbine reduces $\sim 3\text{kW}$ power output due to 2" W.C. back pressure, and Fig. 23 shows that the microturbine compressor inlet temperature is normally higher than the outdoor air temperature, which reduces the air density and consequently reduces the power output.

Figure 82 shows two kinds of plenum box evolved in the CHP Integration Test Center, which are marked with circles; the arrows represent the heat leak/conduction from the plenum box to the engine core chamber. The right design is better than the left design in moderating the heat issue, but the heat leak/conduction still exists.



Fig. 82. Two kinds of plenum box (with circle) installed on the top of MT

A neat damper-actuator combination can simplify the ductwork and controls, minimize the number of dampers and actuators, and reduce the heat loss and pressure drop. The third-generation system adopts a compact damper-actuator combination shown in Appendix E – A Damper-Actuator Assembly, which simplifies the exhaust control and reduces pressure drop. The following Fig. 83 is a full size AutoCAD drawing of the new CHP system.

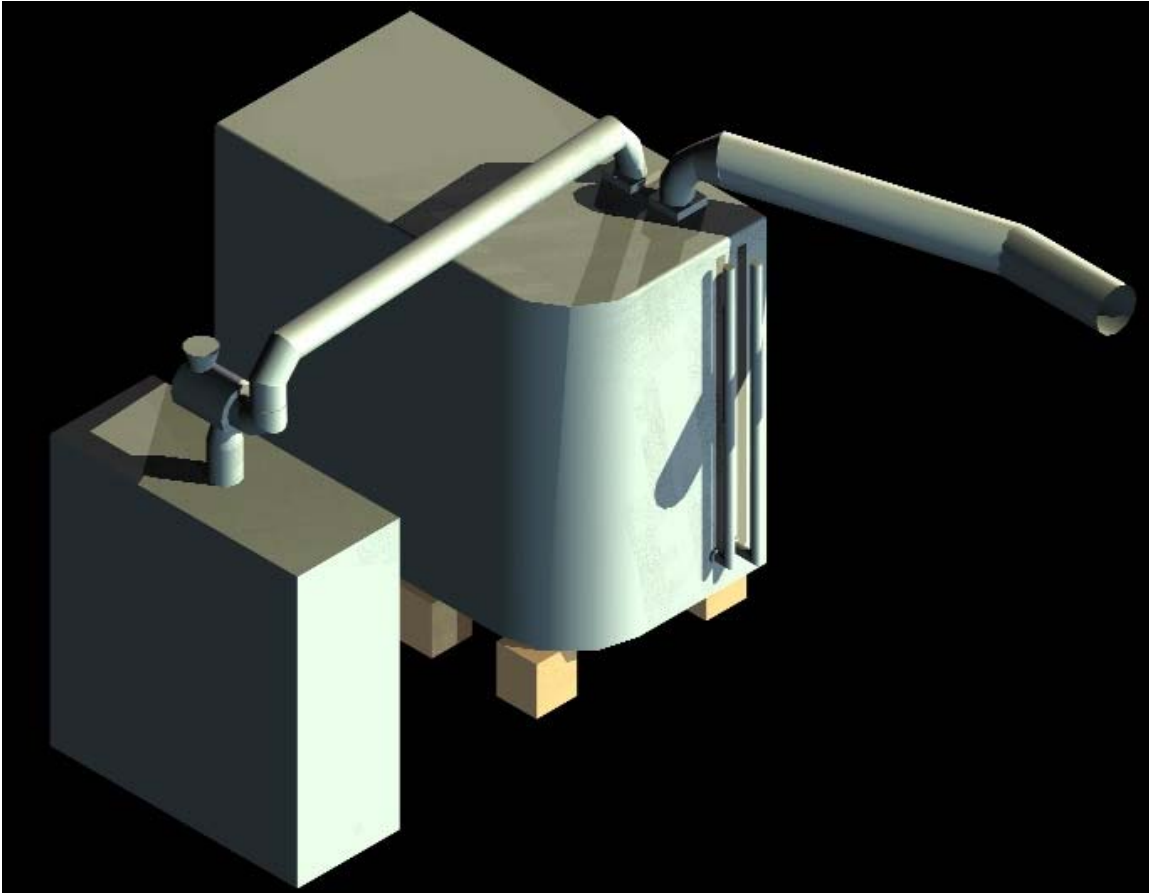


Fig. 83. AutoCAD 3D design of the third-generation MT-based system

Other advice on the integration includes:

- Reduce the length of ductwork and pipework to reduce heat loss and pressure drop, such as the long duct between point ② and point ③ of Fig. 19.
- The chilled water supply temperature should be set as high as possible according to the application.

Simplicity

In aesthetics, simplicity has often been equated with beauty. In CHP applications, one cannot emphasize the importance of simplicity enough. This is because, with so many thermally activated technologies (TAT) available, CHP can easily stray to a

complicated design. As a result of the complicated design, the inescapable capital cost, installation, controls, maintenance and unexpected issues on the CHP equipment and its accessories (such as pumps, fans, valves, dampers, actuators, ducts and pipes) together with the consequent heat loss, back pressure to the prime movers, pressure drop and parasitic power will be enormous, which will impair or even damage the benefits of CHP eventually.

Standardizations

Without the standardized measures of performance, we cannot compare different CHP systems, nor set optimization objectives. The components in CHP systems also need to be standardized, such as fuses, AC/DC voltages, tools, control interfaces and software drivers, to facilitate the commercialization.

Chapter 10 Conclusions

Summary of Accomplishments

On the foundation of the existing CHP Integration Test Center at the Chesapeake Building, located on the campus of the University of Maryland in College Park, major accomplishments and distinguishing contributions of this research carried out by the author are as follows:

1. Comprehensive performance measurements of the second-generation CHP system, which includes a 60 kW microturbine, an 18 ton water-cooled absorption chiller and a 3000 CFM solid desiccant system, were conducted in different operating conditions and wide weather range.
2. A building baseline characterization was conducted. A large amount of year-round data was processed to quantify the power consumption, thermal loads, operation conditions of the HVAC and CHP equipment and the office building.
3. An air-cooled absorption chiller concept and a related computer model that describes the thermodynamic performance in steady state operation were developed. Based on the computer model, a detailed parametric study and crystallization cause analysis were conducted.
4. The computer model of an air-cooled absorption chiller was validated against extensive tests on a water-cooled absorption chiller. The results of the model show good agreement and are within $\pm 8.0\%$ of experimental performance.
5. The application of air-cooled absorption chillers in CHP was proposed, and the most productive and energy efficient configuration of CHP together with the

- HVAC system was developed and described. The primary energy savings can be 40% for the proposed configuration.
6. Design and control guidelines, which highlight all important parameters with special consideration of the crystallization, are proposed. In addition, the application and integration guidelines at both component level and system level are developed. All guidelines are applicable for both air-cooled and water-cooled absorption chillers.
 7. Various and extensive troubleshooting, maintenance and operation of the CHP system running on natural gas and propane were conducted. Valuable lessons and experience from the field operation were gained and summarized for reference of future commercialization of CHP by facility owners, equipment operators or design engineers.
 8. A third-generation, very compact microturbine-absorption chiller-desiccant system was designed and installed for future research. Compared with the previous CHP system, it significantly simplifies the interconnection of ductwork and piping, and greatly reduces the footprint, maintenance, and cost, all of which are very important factors to the commercialization of CHP.

Conclusions

The research presented here investigates the concept of a LiBr-H₂O air-cooled absorption chiller. It focuses on the feasibility, crystallization issues, and the application in a CHP system.

The concept of an air-cooled system is attractive because the cooling tower and the associated installation and maintenance issues can be avoided. However,

crystallization then becomes the main obstacle in the operation of the unit. Five causes may trigger crystallization: one, higher ambient temperature; two, air leak into the machine or non-absorbable gases produced during corrosion; three, too much heat input to the desorber; four, failed dilution after shutdown; five, chilled water supply temperature is set too low when the weather and/or exhaust are too hot.

Novel temperature control strategies are proposed to effectively prevent the occurrence of crystallization, which are applicable for both air-cooled and water-cooled absorption chillers. The methods are to increase the chilled water temperature settings or to reduce the exhaust temperature according to the maps developed in this research.

A steady-state model to accurately reflect the thermodynamic characteristics of single-effect air-cooled LiBr absorption chillers is developed as a part of this research. Extensive simulated field tests on a water-cooled absorption chiller based on steady-state operation conditions validate both the modeling and the crystallization control strategies. The results of the model show good agreement and are within $\pm 8.0\%$ of experimental performance. In summary, the main characteristics of air-cooled absorption chillers are:

- Higher MT exhaust gas temperature or flow rate can result in higher cooling capacity and better heat utilization, while the COP drops slightly.
- Cold weather decreases the condenser pressure and improves the COP and cooling capacity, while hot weather may cause crystallization of the chiller.
- Higher chilled water temperature can improve the chiller performance by increasing the cooling capacity and COP. It is recommended to set chilled water temperatures as high as the application permits.

While CHP provides a good opportunity for the application of air-cooled absorption chillers, detailed investigations about the configurations of CHP together with the conventional HVAC system were conducted. The capital cost of CHP equipment and the load fluctuation of a commercial building restrict the advantage of designing a unit sized at the peak load. Therefore, conventional HVAC is needed to pick up the residual loads, and it should be arranged in series with and after the CHP equipment to ensure obtaining more operating hours out of the CHP system at its full capacity, so that the cost saving achieved through the recovery of waste heat can help to repay its higher initial capital cost. In summary, main conclusions include:

- The series configuration is superior to the parallel configuration in the integration of CHP with conventional HVAC units. CHP is designed to meet the base load of a building.
- A CHP system in series configuration can completely satisfy the whole latent load and part of the sensible load, and no reheat is needed in the entire cooling season.
- The conventional HVAC unit can be much smaller and consume less energy than the baseline design. Since it can use a higher evaporation temperature as it only needs to satisfy the sensible load, the COP can be higher, which consequently brings the benefits of reduced capital cost, compact size, smaller resistance to air due to smaller coils, and smaller fan power required. In addition, since there will be no condensation on the coil the problem of mold growth is eliminated.
- The primary energy consumption of hybrid systems is 60~63% of the baseline for systems with temperature-based economizers or 59~72% of the baseline for systems with enthalpy-based economizers.

- At the locations where the weather conditions are mostly mild, the introduction of enthalpy wheel may not guarantee energy savings, or the savings are insignificant.

As a practical demonstration a fully integrated CHP system has been installed and instrumented at the Chesapeake Building. It is a commercial office building on the University of Maryland campus. The experimental setup, data processing, and experience gained are detailed in this dissertation. Based on the computer simulation, extensive experiments, first hand installation, operation and maintenance experience, valuable guidelines on the integration of an air-cooled absorption chiller in CHP are developed. The guidelines allow facility operators, design engineers, and system integrators to better understand the characteristics of commercial buildings and make better decisions about installing and operating HVAC and CHP systems.

Future Work

The following items are suggested to be addressed in a continuation of the work presented in this research.

- Integrate the commercial capacity control logics into the absorption chiller EES or other software programs. For example, the variable frequency driven (VFD) LiBr solution pump usually is used to adjust cooling capacity.
- Transient modeling of the absorption chiller performance, together with experimental validation.
- EnergyPlus, a building energy simulation program for modeling building heating, cooling, lighting, ventilation, and other energy flows, can be used to assess the overall energy usage of building, HVAC and CHP systems by inputting the local weather data, architecture design data, operation schedules and operation

conditions. Then the simulated results can be validated with year-round experimental data acquired by the DAS in the Chesapeake Building. This methodology provides a new means to assess building energy in different locations. Refer Appendix H – Field Data and EnergyPlus Simulation.

Appendix A – ASHRAE Minimum Ventilation Rate History

Figure 84 shows the long history of ventilation rate research by ASHRAE. The ASHRAE predecessor organization ASHV established a quite "high" rate. The first ASHRAE standard 62-73 used the very low rate established by Yaglou. In the late 1970's, due to the "energy crisis", the rates were halved to 5 CFM while the building envelopes were tightened up, which was a recipe for disaster. The combination of low ventilation rates and tighter buildings was blamed for Sick Building Syndrome (SBS) in the early 1980. In response to SBS, ASHRAE in 1989 increased the recommended ventilation rates from 5 to 20 CFM/person in office spaces. The ventilation rate for smoking lounges is much higher (Janssen, 1999). Later in a revised version of Standard 62, the office ventilation rates were reduced to 15 CFM/person. The current standard ASHRAE 62-2001 adopts the same rates.

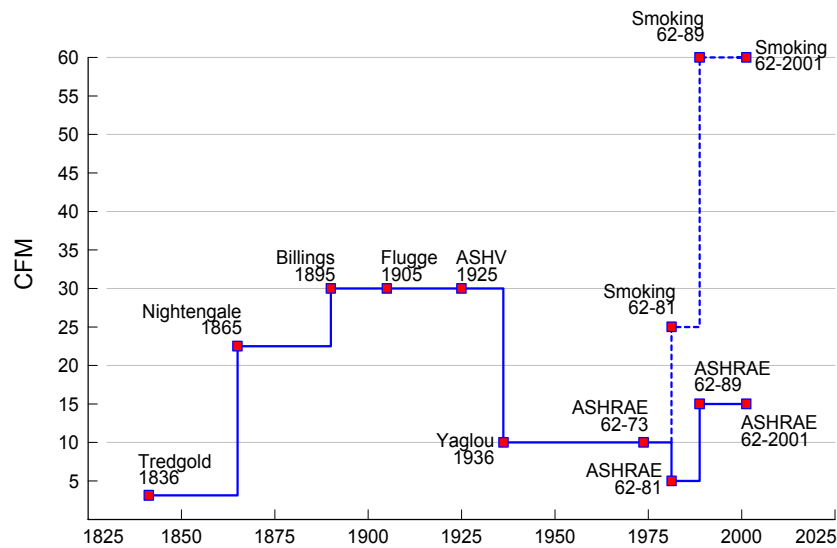


Fig. 84. ASHRAE minimum ventilation rate history (1CFM = 0.47 l/s)

Appendix B – Weather in Three Locations

The data was processed by the author.

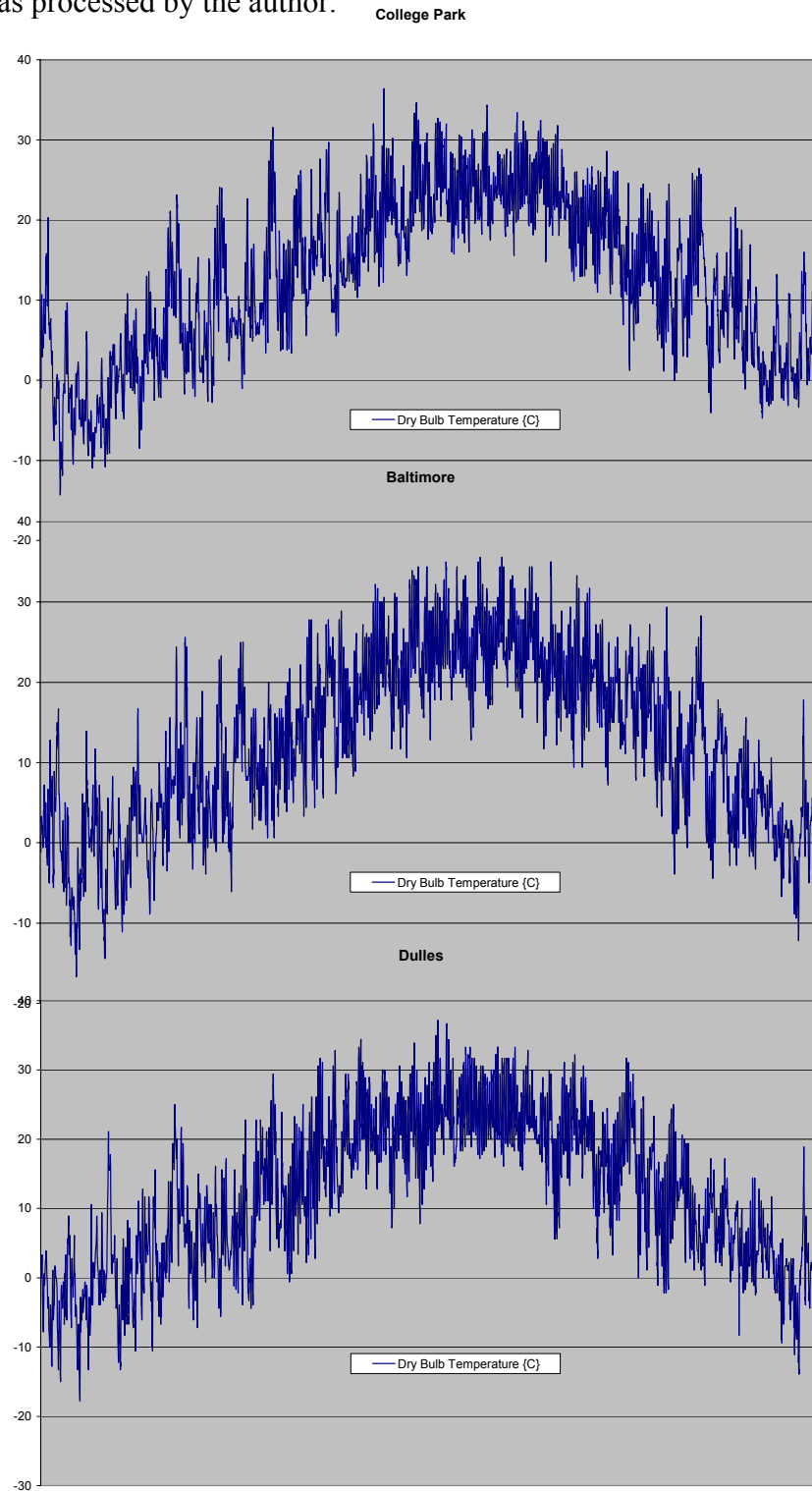


Fig. 85. Year-round dry-bulb temperature ($^{\circ}\text{C}$) comparison (top: College Park, middle: Baltimore, bottom: Dulles)

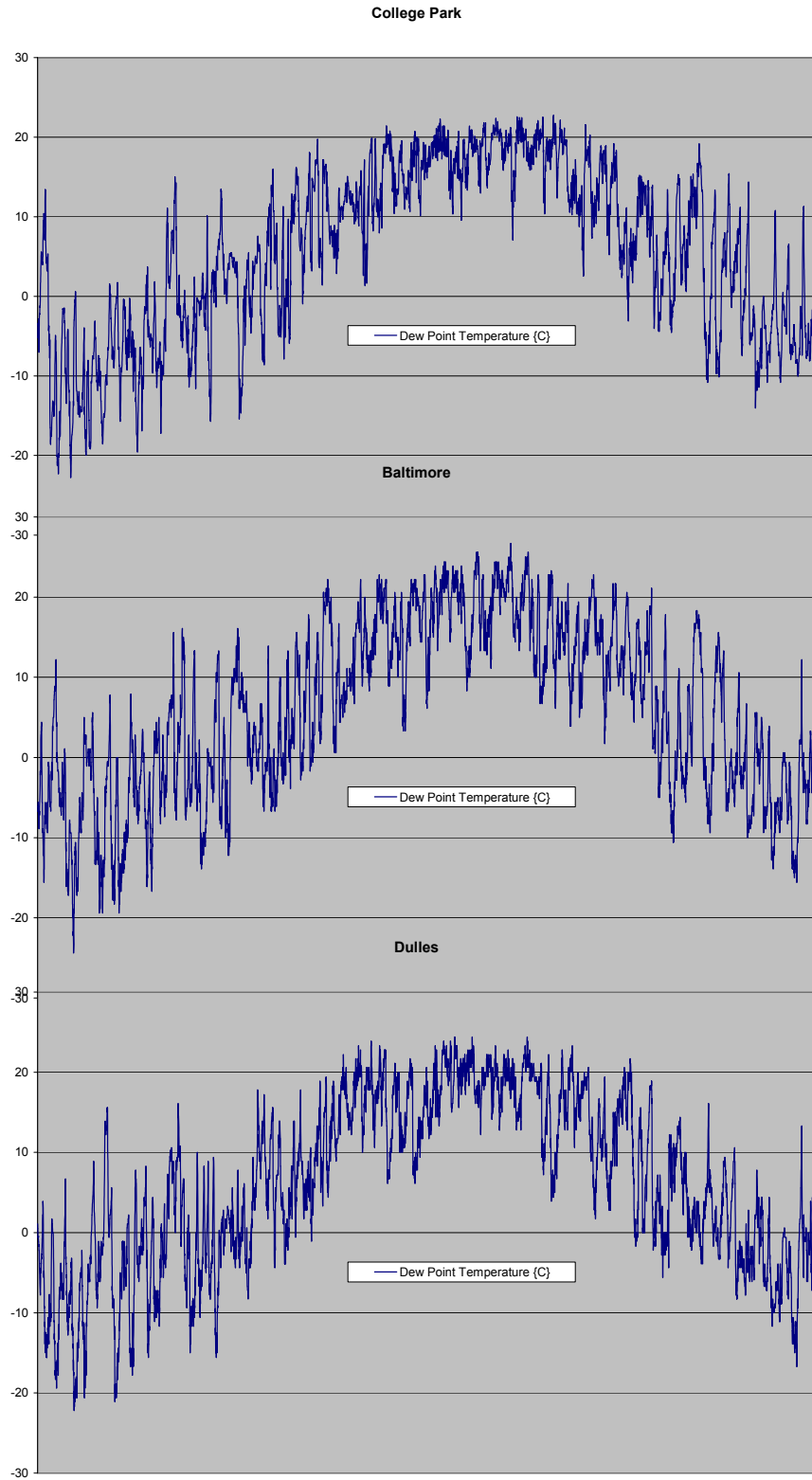


Fig. 86. Year-round dew point ($^{\circ}\text{C}$) comparison (top: College Park, middle: Baltimore, bottom: Dulles)

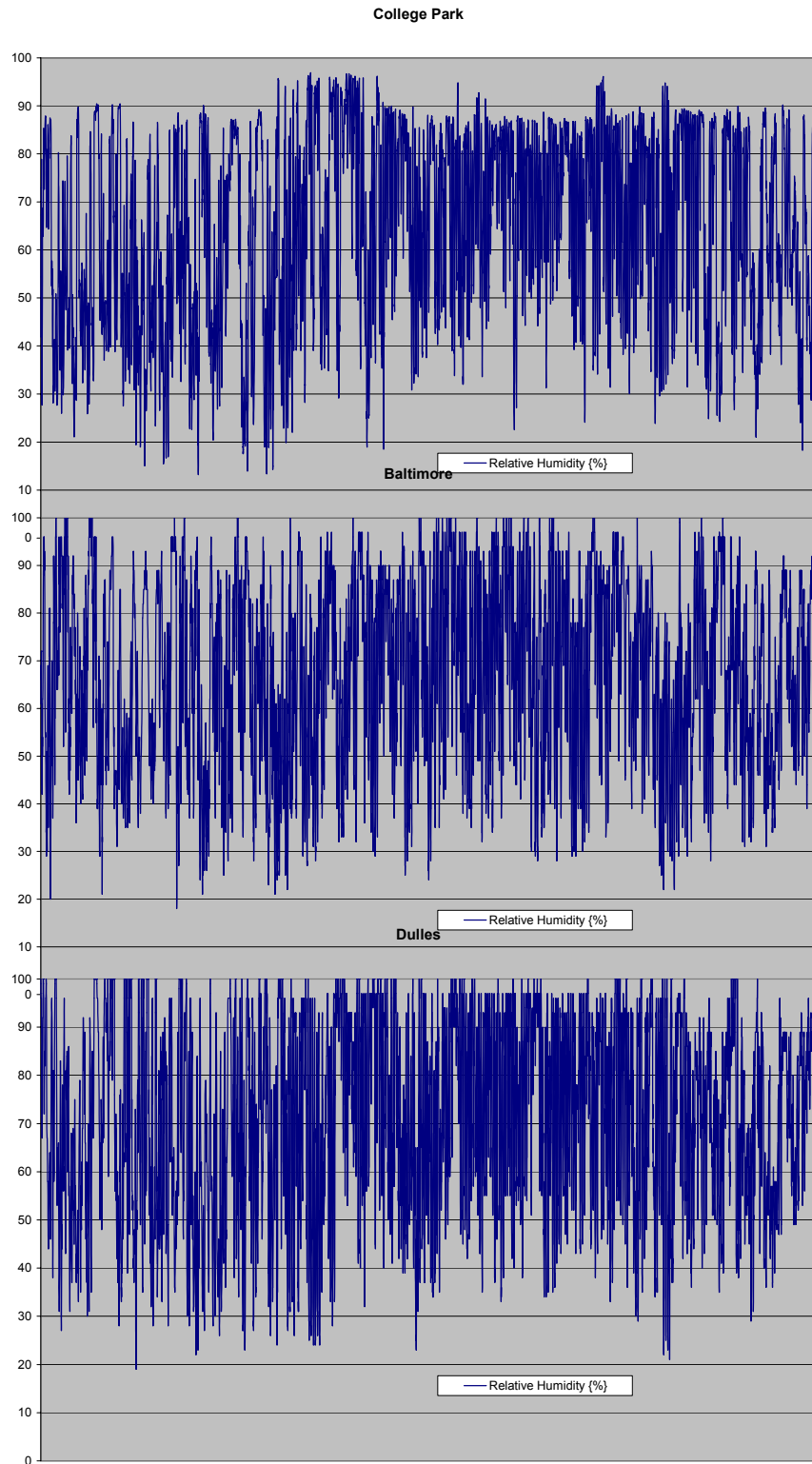


Fig. 87. Year-round relative humidity (%) comparison (top: College Park, middle: Baltimore, bottom: Dulles)

Appendix C – Sensors and Uncertainty Analysis

Marantan, A. (2002 a) calculated the uncertainty of sensors used in the research. Table 10 shows the instrumentation partly marked in Fig. 15 along with the associated error for each sensor.

Table 10: Instrumentation and Sensor Error

Measurement	Sensor	Error
Ambient temperature and humidity	Vaisala humidity and temperature transmitter HMD60Y	$\pm 2\%$ for relative humidity $\pm 0.5^\circ \text{C}$
Exhaust temperature - absorption chiller inlet	Minco High Temp Thermocouple Probe – E Type Thermocouple (Chromel-constantan)	$\pm 1.7^\circ \text{C}$ or $\pm 0.5\%$ (0 to 900°C)
Exhaust temperature - absorption chiller outlet	Minco High Temp Thermocouple Probe – J Type Thermocouple (Iron-constantan)	$\pm 2.2^\circ \text{C}$ or $\pm 0.75\%$ (0 to 750°C)
Chilled water temperature - supply	Minco High Temp Thermocouple Probe – J Type Thermocouple (Iron-constantan)	$\pm 2.2^\circ \text{C}$ or $\pm 0.75\%$ (0 to 750°C)
Chilled water temperature - return	Minco High Temp Thermocouple Probe – J Type Thermocouple (Iron-constantan)	$\pm 2.2^\circ \text{C}$ or $\pm 0.75\%$ (0 to 750°C)
MT exhaust gas flow rate	Davis Stainless Steel Pitot Tube with Modus Differential Pressure Transmitter	$\pm 1\%$ of span
Chilled water flow rate	Signet 515 Flow Sensor – Paddle Wheel Type	$\pm 2\%$ of full scale (14° to 149°F)
Natural gas flow rate	American Meter Company Model AL-425 Dry Gas Meter	$\pm 1\%$
MT power output	Fluke 80i-400 Clamp-On AC Current Probe	$\pm 3\%$
Absorption chiller power consumption	Fluke 80i-400 Clamp-On AC Current Probe	$\pm 3\%$

The total uncertainty of a measurement due to the uncertainty of individual parameters is referred to as the propagation of uncertainty (Beckwith, 1993). Also referred to as precision, the total uncertainty of any function may be calculated using the Pythagorean summation of uncertainties which is defined by Kline (1959) :

$$u_F = \sqrt{\left(\frac{\partial F}{\partial v_1} * u_1\right)^2 + \left(\frac{\partial F}{\partial v_2} * u_2\right)^2 + \left(\frac{\partial F}{\partial v_3} * u_3\right)^2 + \dots + \left(\frac{\partial F}{\partial v_n} * u_n\right)^2}$$

where:

- u_F = uncertainty of the function
- u_n = uncertainty of the parameter
- F = function
- v_n = parameter of interest (measurement)
- n = number of variables

The partial derivatives of each independent measurement in the parameters were calculated using the uncertainty propagation function in the *Engineering Equation Solver* (Klein et al. 2004) and applied within the program to the root mean square outcome. The total uncertainty for characteristic parameters is listed in Table 11. The largest uncertainty is $\pm 7.11\%$ for absorption chiller COP because of the number of sensors required to make this calculated quantity.

Table 11: Uncertainty of Calculated Results

Parameter	Uncertainty
MT Thermal Efficiency	$\pm 3.16\%$
Absorption Chiller Capacity	$\pm 6.15\%$
Absorption Chiller COP	$\pm 7.11\%$

Appendix D – Solid Desiccant Unit Catalogue

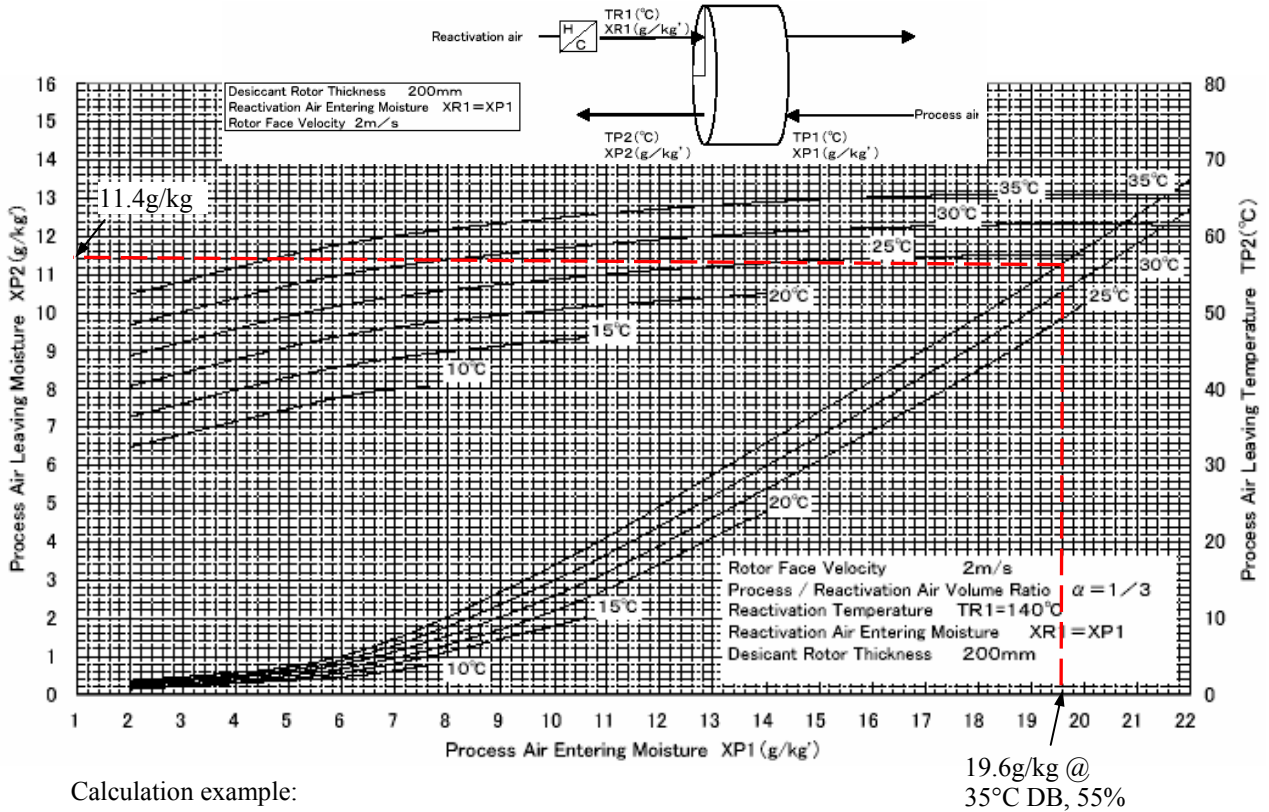
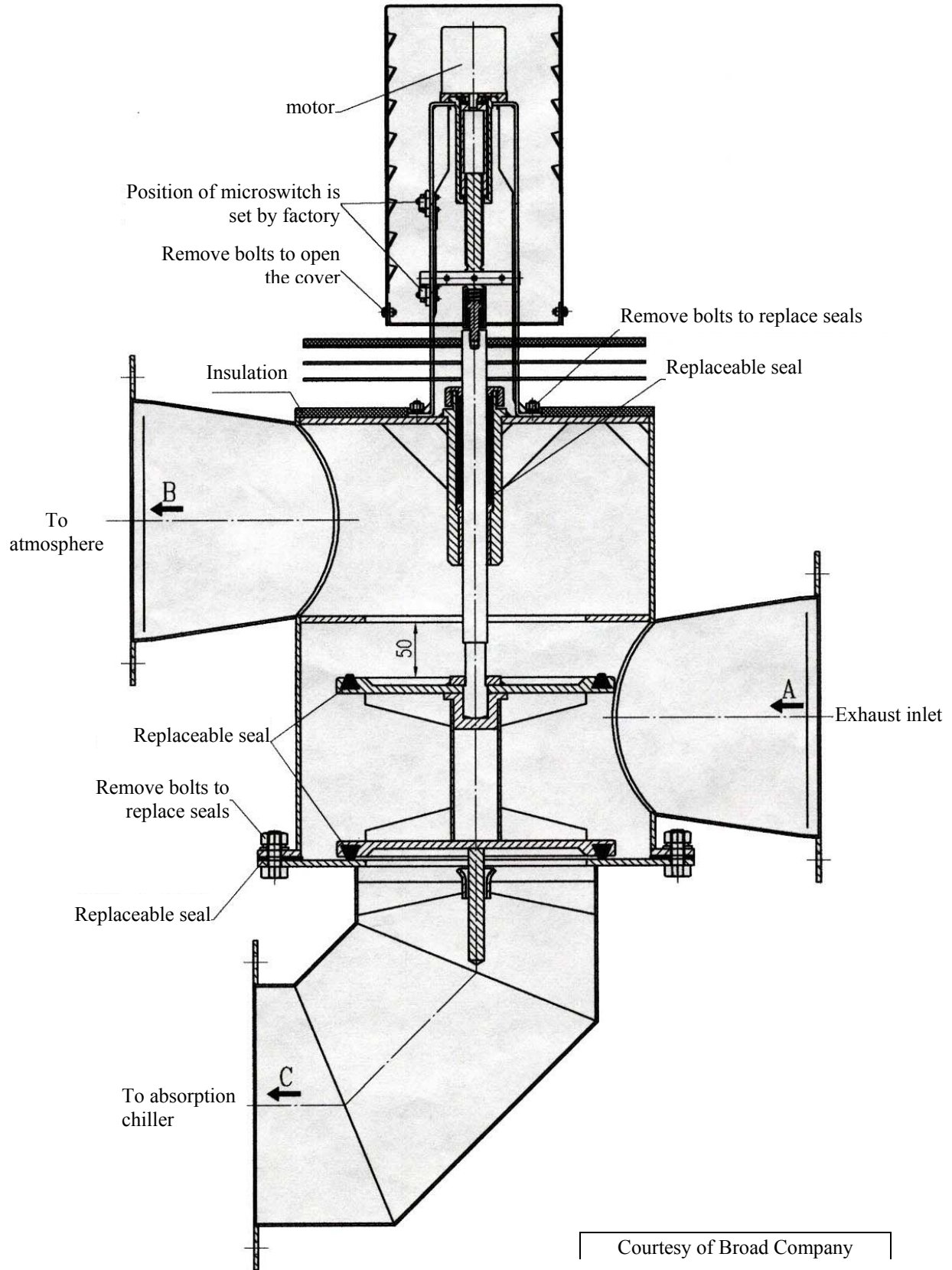


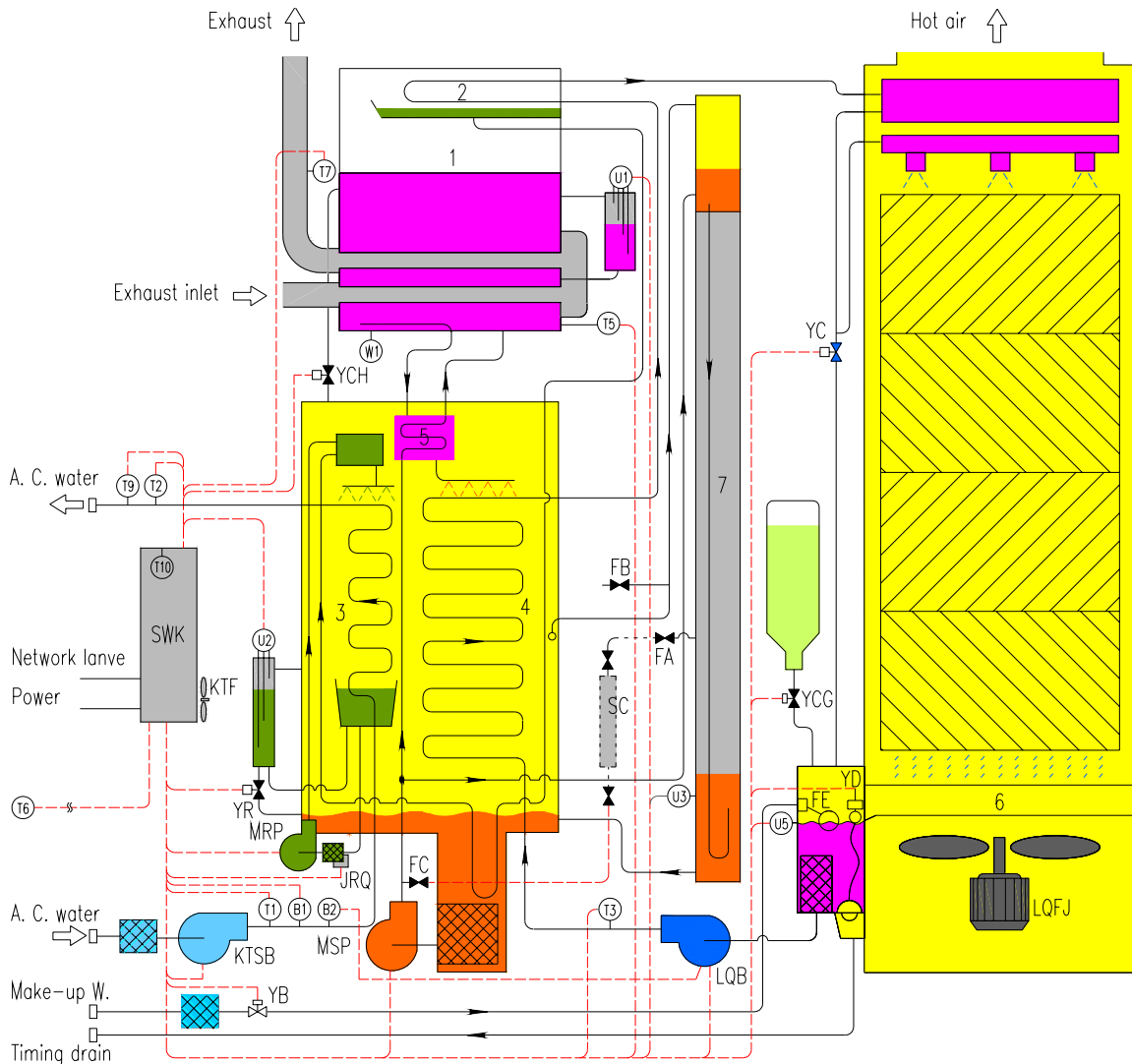
Fig. 88. Performance chart of a commercial solid desiccant dehumidifier

(Courtesy of Seibu Giken America, Inc.)

Appendix E – A Damper-Actuator Assembly



Appendix F – BCTDE P&I Diagram



Legend:

- 1. generator
- 2. condenser
- 3. evaporator
- 4. absorber
- 5. heat exchanger

- 6. cooling tower
- 7. auto purge unit
- MSP: solution pump
- MRP: refrigerant pump
- KTSB: AC water pump
- LQB: cooling w. pump
- LQFJ: cooling fan
- KTF: cooling board draft fan
- JRQ: refrigerant pump heating device

- YCH: cooling/heating valve (close)
- YR: refrigerant valve (close)
- YB: make-up w. valve
- YD: drain device (timing open)
- YC: cooling w. by-pass valve
- FE: floating ball valve
- YCG: water sterilizer valve (timing open)
- FA: air canister valve (manual)
- FB: direct purge valve (manual)
- FC: solution valve (manual)
- SWK: control board
- SC: solution cleaner (used in factory only)

- T1: AC water inlet temp. sensor
- T2: AC water outlet temp. sensor
- T3: cooling w. inlet temp. sensor
- T5: generator temp. sensor
- T6: ambient temp. sensor
- T7: exhaust temp. sensor
- T9: chilled w. outlet temp. sensor 2
- T10: control board temp. sensor
- W1: temp. switch
- B1/B2: AC water flow switch
- U1: generator solution level probe
- U2: refrigerant level probe
- U3: non-condensable probe
- U5: cooling w. level probe

Courtesy of Broad

Appendix G – Test Logs for Summer of 2003

The following tests were conducted by the author.

Settings of chiller since June 23:

chilled water outlet temp	45°F±1.5°F
cooling water in	75 ~ 105°F
HSG	190 ~ 215°F
exhaust	450 ~ 550°F
cooling tower fan start	90°F
cooling tower fan stop	85°F
HSG for high fire	160°F
Cooling water temp for high fire	85°F

Test Date	Time	Components	Note
Monday, June 23, 2003	7:47~ 8:34	MT (60 kW); Chiller (on); ATS (off)	OA: 65~90°F
	8:35~ 17:00	MT (60 kW); Chiller (on); ATS (on exhaust)	
Tuesday, June 24, 2003	7:30~ 10:00	MT (30 kW); Chiller (on); ATS (on exhaust)	OA: 68~92°F The data after 2:00 pm were lost
	10:01~12:36	MT (40 kW); Chiller (on); ATS (on exhaust)	
	12:37~15:00	MT (50 kW); Chiller (on); ATS (on exhaust)	
	15:01~17:30	MT (60 kW); Chiller (on); ATS (on exhaust)	
Wednesday, June 25, 2003	7:00~ 9:30	MT (30 kW); Chiller (on); ATS (on exhaust)	OA: 72~92°F The data before 13:30 were lost
	9:31~ 12:00	MT (40 kW); Chiller (on); ATS (on exhaust)	
	12:01~13:30	MT (50 kW); Chiller (on); ATS (on exhaust)	
	13:31~17:00	MT (60 kW); Chiller (on); ATS (on exhaust)	
Thursday, June 26, 2003	6:15~ 9:00	MT (30 kW); Chiller (on); ATS (on exhaust)	OA: 75~95°F There is no condensate pump data
	9:01~ 12:50	MT (40 kW); Chiller (on); ATS (on exhaust)	
	12:51~15:00	MT (50 kW); Chiller (on); ATS (on exhaust)	
	15:01~18:00	MT (60 kW); Chiller (on); ATS (on exhaust)	
Friday, June 27, 2003	5:20~ 17:00	MT (60 kW); Chiller (on); ATS (on exhaust)	OA: 60~88°F, condensate pump times were set to 0 at 5:20 am
Monday, June 30, 2003	5:20~ 8:20	MT (30 kW); Chiller (on); ATS (off)	OA: 68~88°F
	8:21~ 13:20	MT (40 kW); Chiller (on); ATS (off)	
	13:21~	Shutdown system 2 to compare the condensate pump 1 and 2	

Test Date	Time	Components	Note
Tuesday, July 1, 2003	Whole day	1) No CHP system runs. Manually record the condensate pumps' operation vs. time to compare the baseline of 2 RTUs 2) Blocked the MT exhaust outlet of plenum box, so chiller can have more exhaust.	The DAS can automatically record the pump counter after 5:00pm
Wednesday, July 02, 2003	6:10~ 17:00	MT (60 kW); Chiller (on); ATS (on exhaust) after the exhaust outlet was blocked	OA: 67~74°F
Thursday, July 03, 2003	6:30~ 9:10	MT (60 kW); Chiller (on); ATS (on exhaust)	OA: 65~67°F
	9:40~ 16:03	MT (60 kW); Chiller (on); ATS (on exhaust and burner)	
Monday, July 07, 2003	Whole day	System 2 stops to set the condensate baseline	Hot and humid weather, similar day with July 9
Tuesday, July 08, 2003	8:20~ 16:00	MT (60 kW); Chiller (on); ATS (on exhaust)	OA: 70~90°F
Wednesday, July 09, 2003	9:00~ 17:20	MT (60 kW); Chiller (on); ATS (on exhaust and burner)	OA: 72~88°F
Thursday, July 10, 2003	9:40~ 18:00	MT (60 kW); Chiller (on); ATS (off)	OA: 70~80°F
Friday, July 11, 2003	7:00~ 18:00	MT (60 kW); Chiller (on); ATS (on exhaust)	OA: 65~88°F
Tuesday, July 15, 2003	10:30~13:00	MT (60 kW); Chiller (on); ATS (on exhaust)	OA: 68~85°F (the first day after high T damper installed)
Wednesday, July 16, 2003	7:40~ 12:50	MT (60 kW); Chiller (on); ATS (on exhaust), Test the new high temperature damper	OA: 66~88°F
	12:51~14:30	MT (60 kW); Chiller (on); ATS (off)	
	14:31~17:00	MT (60 kW); Chiller (on); ATS (on, enthalpy wheel is off), test desiccant wheel only	
Thursday, July 17, 2003	7:20~17:10	MT (60 kW); Chiller (on); ATS (on, enthalpy wheel is off).	OA: 68~88°F Vacuum the chiller 10:00~14:00

Test Date	Time	MT (kW)	Chiller	SDU	Note
Friday, July 18, 2003	7:20~10:25	60	On	Off	OA: 65~88°F
	10:27~	40	On	Off	
Monday, July 21, 2003	8:00~17:00	60	On	On, no enthalpy	OA: 72~90°F
Tuesday, July 22, 2003	8:00~17:00	60	On	On, no enthalpy	OA: 70~87°F
Wednesday, July 23, 2003	6:30~17:00	60	On	On, no enthalpy	OA: 67~80°F
Thursday, July 31, 2003	10:30~17:00	60	On	On, new enthalpy wheel	OA: 70~75°F
Friday, August 01, 2003	8:45~16:30	60	On	On, new enthalpy wheel	OA: 70~80°F, humid
Monday, August 04, 2003	9:45~17:30	60	On	On, new enthalpy wheel	OA: 70~85°F, humid
Tuesday, August 05, 2003	9:45~17:30	60	On	On 9:30~ 13:50	OA: 68~80°F, humid
Wednesday, August 06, 2003	8:25~18:15	60	On, exhaust 535°F	Off	OA: 68~85°F
Thursday, August 07, 2003	8:50~17:30	60	On, exhaust 535°F	Off, reverse the new enthalpy wheel	OA: 68~85°F
Friday, August 08, 2003	7:30~824	Off	off	On	OA: 70~80°F
	8:25~16:00	60	On, exhaust 535°F		
Monday, August 11, 2003	9:01~18:00	60	On, exhaust 495°F	on	OA: 70~82°F
Tuesday, August 12, 2003	8:35~15:30	60	On, exhaust 495°F	on	OA: 70~82°F
Wednesday, August 13, 2003	9:05~17:00	60	On, exhaust 483°F	on	OA: 70~88°F
Thursday, August 14, 2003	9:30~16:00	60	On, exhaust 483°F	on	OA: 68~90°F power outage after 16:00
Friday, August 15, 2003	9:15~17:00	60	On, exhaust 528°F	on	OA: 70~95°F, vacuum the chiller
Monday, August 18, 2003	9:15~17:00	60	On, exhaust 528°F	on	OA: 70~85°F
Tuesday, August 19, 2003	13:00~16:30	60	On, exhaust 528°F	on	OA: 70~85°F
Wednesday, August 20, 2003	9:00~17:00	60	On, exhaust 528°F	on	OA: 70~90°F
Thursday, August 21, 2003	9:20~17:00	60	On, exhaust 528°F	on	OA: 70~92°F

Setting of chiller since Aug.25:
 chilled water outlet temp: 50°F±1.5°F
 cooling water: 60 ~ 105°F
 HSG: 190 ~ 215°F
 exhaust 450 ~ 550°F
 cooling tower fan start 95°F
 cooling tower fan stop 90°F
 HSG for high fire 160°F
 Cooling water temp for high fire 85°F

Test Date	Time	MT(kW)	Chiller	SDU	Note
Monday, August 25, 2003	10:00~17:00	60	On, new setting	on	OA: 68~89°F
Tuesday, August 26, 2003	9:00~17:00	60	On	on	OA: 75~88°F
Tuesday, September 02, 2003	9:00~17:00	off	off	On, burner has problem	OA: 70~85°F
Wednesday, September 03, 2003	9:30~17:00	off	off	On, burner has problem	OA: 72~80°F

Setting since Sep.09:
 chilled water outlet temp: 49°F±1.5°F
 cooling water: 60 ~ 105°F
 HSG: 190 ~ 215°F
 exhaust 450 ~ 550°F
 cooling tower fan start 83°F
 cooling tower fan stop 81°F
 HSG for high fire 160°F
 Cooling water temp for high fire 79°F

Test Date	Time	MT (kW)	Chiller	SDU	Note
Wednesday, September 17, 2003	9:30~11:03:30	30	On	Off	OA: 62~78°F
	10:31~11:30	40			
	11:31~12:00	50			
Wednesday, September 24, 2003	9:30~12:00	40	On	On	OA: 55~78°F
Monday, October 27, 2003	8:40~18:00	off	off	on	Rainy
Wednesday, October 29	9:00~12:00	On (stage)	off	off	
Thursday, October 30, 2003	9:20~17:20	On (stage)	off	off	OA: 43~68°F
Monday, November 03, 2003	8:30~16:30	On (stage)	off	off	OA: 55~82°F. the damper of MT exhaust cannot work, so the chiller has no heat input
Tuesday, November 04, 2003	8:00~18:00	On	off	off	OA:60~78°F
Wednesday, November 05, 2003	8:30~14:32	on	off	off	OA: 60~78°F
Thursday, November 06, 2003	8:30~	on	off	off	OA:48~65°F

Appendix H – Field Data and EnergyPlus Simulation

EnergyPlus Overview

Energy simulation has been an important part of building science research, as well as implementation of energy efficiency improvements. EnergyPlus is a building energy simulation program for modeling building heating, cooling, lighting, ventilation, and other energy flows. It merges the best of DOE-2, and BLAST (Building Loads Analysis and System Thermodynamics).

Different from other sequence simulation, EnergyPlus uses integrated and simultaneous simulation to tightly couple the building response and its primary and secondary systems, and thus more accurate energy and thermal performance could be obtained. See Fig. 89.

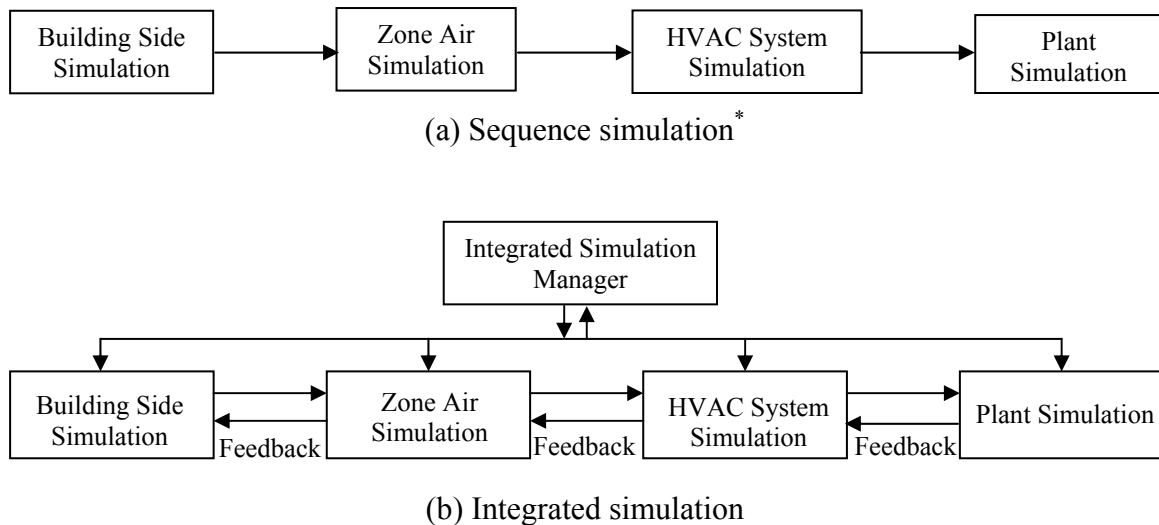


Fig. 89. Comparison of sequence simulation and integrated simulation

* Building side refers the heat transfer through building envelope, internal heat gain and infiltration.

Specifications of the Chesapeake Building

Most specifications of the building, such as the geometry and envelop materials can be obtained from blueprints; some are decided according to typical U.S. construction. In the EnergyPlus modeling, each floor is divided into 5 subzones (Chaoqin Zhai, 2003) as shown in Fig. 90.

The following specifications were sorted out from the building blueprints of the Chesapeake Building.

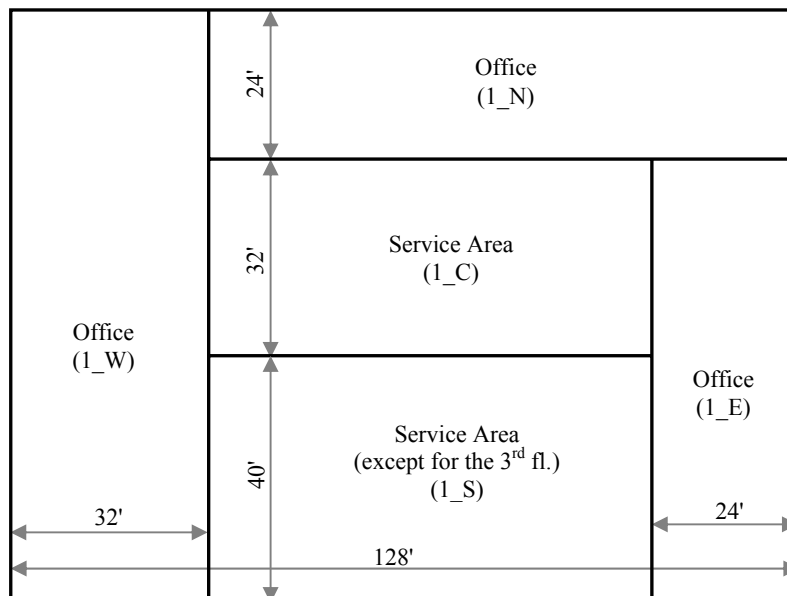


Fig. 90. Floor Plan

▪ Building Envelope

Exterior wall:

4'' face brick
4'' high weight concrete block
2 1/2'' insulation
1/2'' gyp board

Roof:

1'' roof gravel
3'' insulation
8'' low weight concrete block
air space resistance
acoustic tile

Slab-on-ground floor:

4'' gravel
2'' insulation
5'' high weight concrete slab

Window:

6mm tin-oxide coating reflective glass
6mm air space
6mm clear glass
 $U=3.15 \text{ W/m}^2\text{-K}$, $\text{SHGC} = 0.35$, $T_{\text{vis}}=0.18$
with internal blinds
window height: 5ft

Floor:

2.5'' high weight concrete block
carpet

- **Internal Heat Gain of Design Level**

Occupant: 20m²/person for office area, and 40m²/person for service area, about 186 people in the building totally. Lighting: 6.52 W/m². Office equipment: 3.26 W/m².

- **Schedules**

Figures 91 ~ 93 shows some schedules of occupancy, lighting and office equipment. The x-axis is the time (hr) in a day, and the y-axis is the ratio of real load to the maximum design load. The U.S. public holidays are also applied, which have the same schedule as that of the weekend.

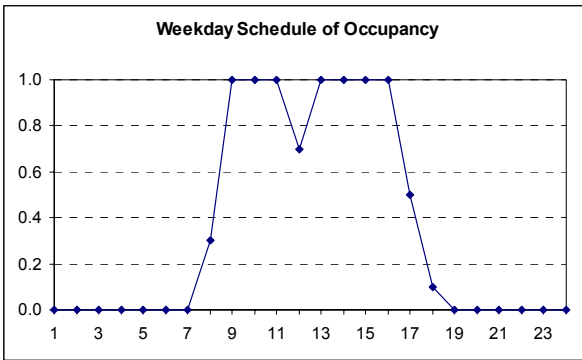


Fig. 91. Weekday schedule of occupancy

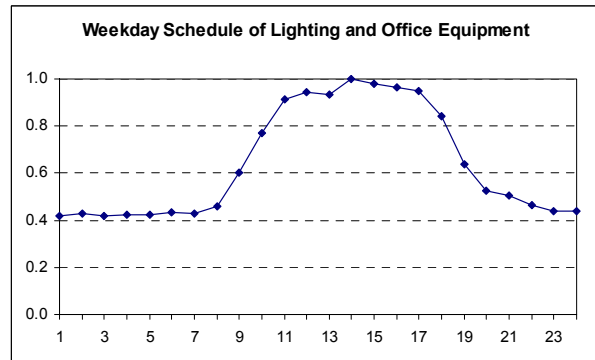


Fig. 92. Weekday schedule of lighting and office equipment

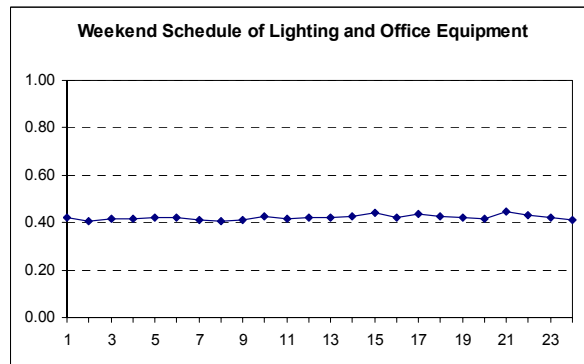


Fig. 93. Weekend schedule of lighting and office equipment

- **Infiltration and Ventilation**

0.2 ACH (Air Changes per Hour) when air-conditioner is off, and no infiltration when air-conditioner is on. Ventilation: 6000 CFM for the whole building, and 32.3 CFM/person.

- **Thermostat Setpoints**

Supply air temperature: 60°F; indoor air temperature: 74°F.

Program Input

An energy simulation that will be useful for commercial buildings with built-up HVAC systems can require tremendous input variables, which are usually based on both the design data and measured data (Liu et al., 2003). The latter can improve the accuracy of modeling prediction. For example, weather data is definitely necessary in the energy simulation, the EnergyPlus supplies the statistic weather data for the Washington D.C. metro area and Baltimore, where the College Park is close to; however, the weather in a specific year of a specific area may differ from the statistic data of a nearby city.

The weather data acquired by the weather station that was mounted on the roof of the Chesapeake Building is used as the weather input, and the psychrometric chart is shown in Fig. 57. In addition to the dry bulb temperature and relative humidity, the weather station also records the solar intensity, barometric pressure, wind speed, and wind direction. The weather data base of other locations in the world can be downloaded from the EnergyPlus Website.

Simulation Examples

Low Voltage Power

The low voltage power includes the power that appliances (such as computer, desk lights, telephone, microwave, and Xerox.) take from the outlets in kitchens and offices. Figure 94 shows the measured and simulated year-round low voltage power consumed by the whole Building. The simulation assumed a regular usage pattern of low voltage power over the whole year, however, in the real building there are more factors effect the low voltage power consumption and measurement, e.g. some people use portable electric heaters in winter, more people travel in summer, random visitors and training groups in the building which are hard to quantify and predict in the simulation program. Figure 95 zooms in the data of few days in the summer to elaborate the detailed patterns of workday and weekend.

High Voltage Power

The high voltage power consumers include the VAV boxes and ceiling lights. Figure 96 is the year-round high voltage power consumed by the 1st and 2nd floors; the simulation shows a good trend match with the experimental data. In the simulation, the designed weekday/weekend schedules (such as Figures 91 ~ 93) and U.S. holidays are applied, however, in the actual building operation the schedules cannot be followed exactly, for example some lights will not be turned off after hours because some employees are still working. If we zoom in to one week, see Fig. 97, it obviously shows that the actual high voltage power consumption is higher than the design-based simulation, particularly in the after hours.

Summary

A validated energy simulation of commercial building will be very helpful to predict the energy consumption in different location, weather and operation conditions, and it will also be helpful to the optimization of HVAC design. EnergyPlus provides a new means to assess building energy. However, the program itself is still in the process of developing, and extensive empirical correlations of HVAC equipment are needed to obtain an accurate simulation.

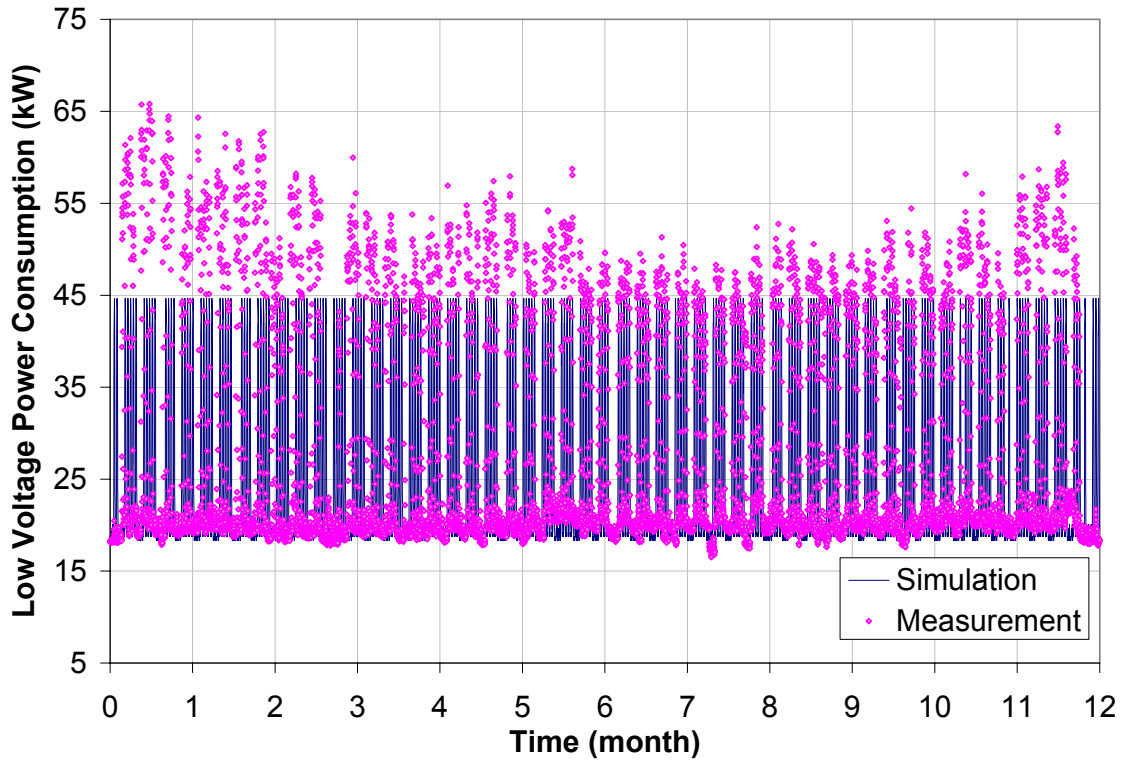


Fig. 94. The Year-round low voltage power in the Chesapeake Building

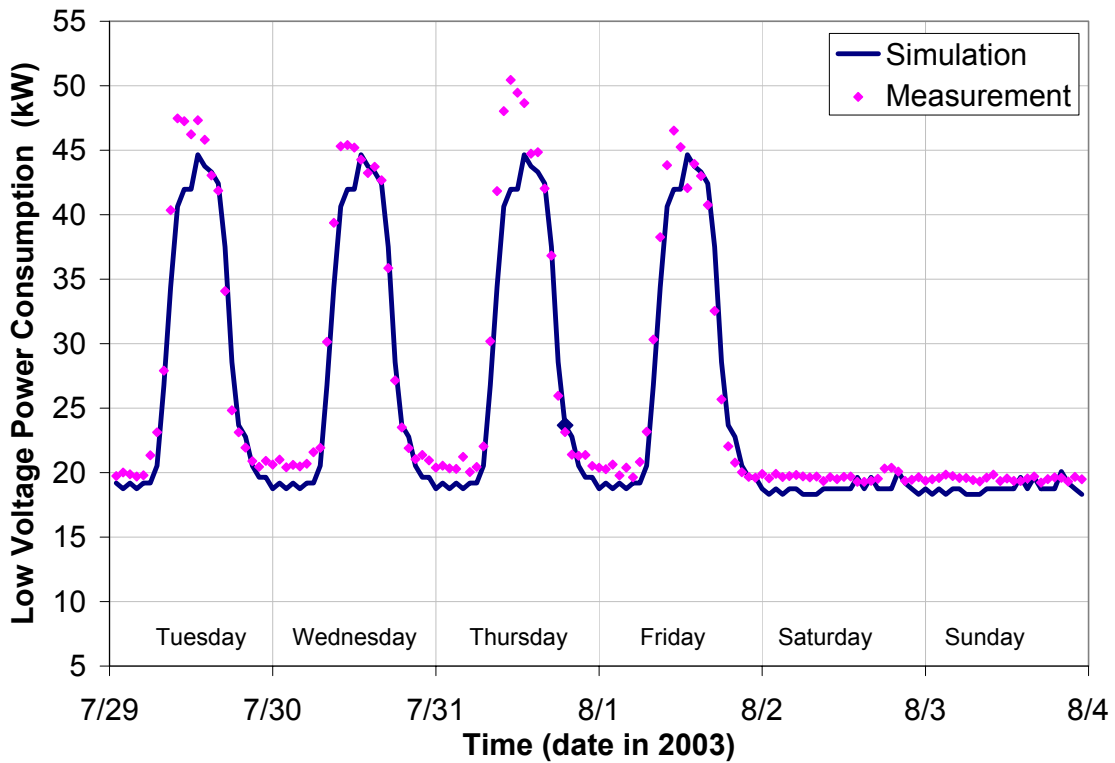


Fig. 95. Weekly low voltage power in the Chesapeake Building

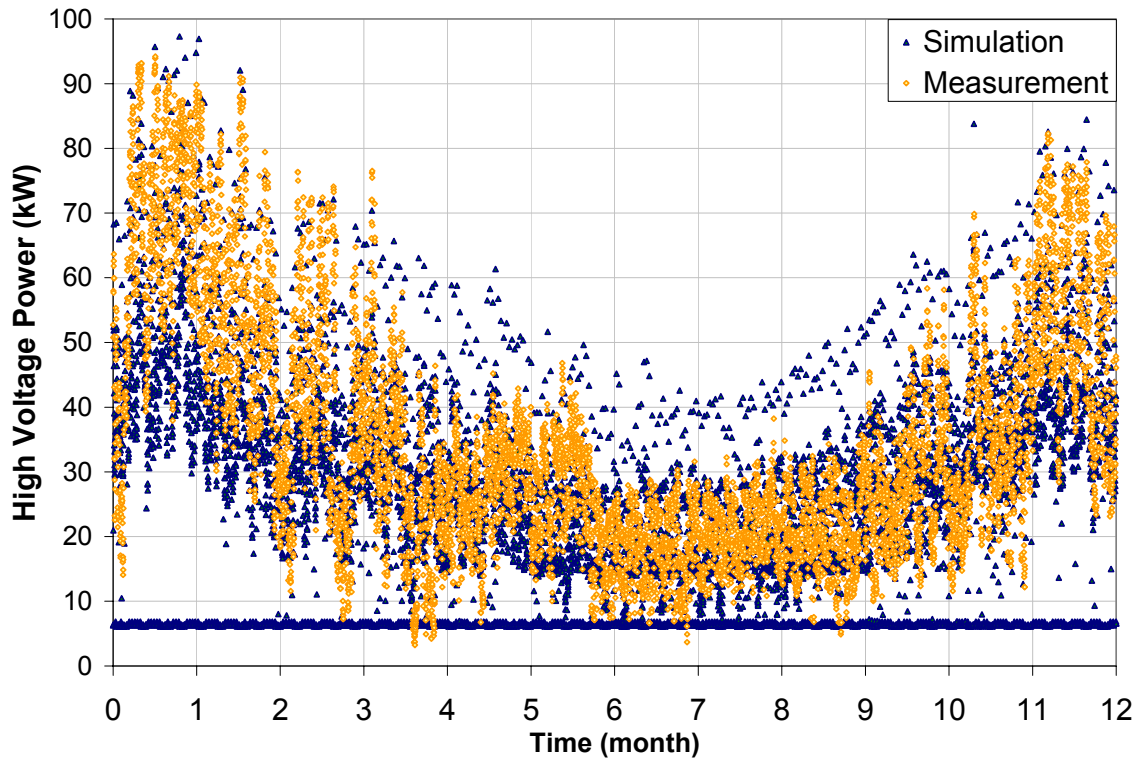


Fig. 96. Year-round high voltage power for the 1st and 2nd floors

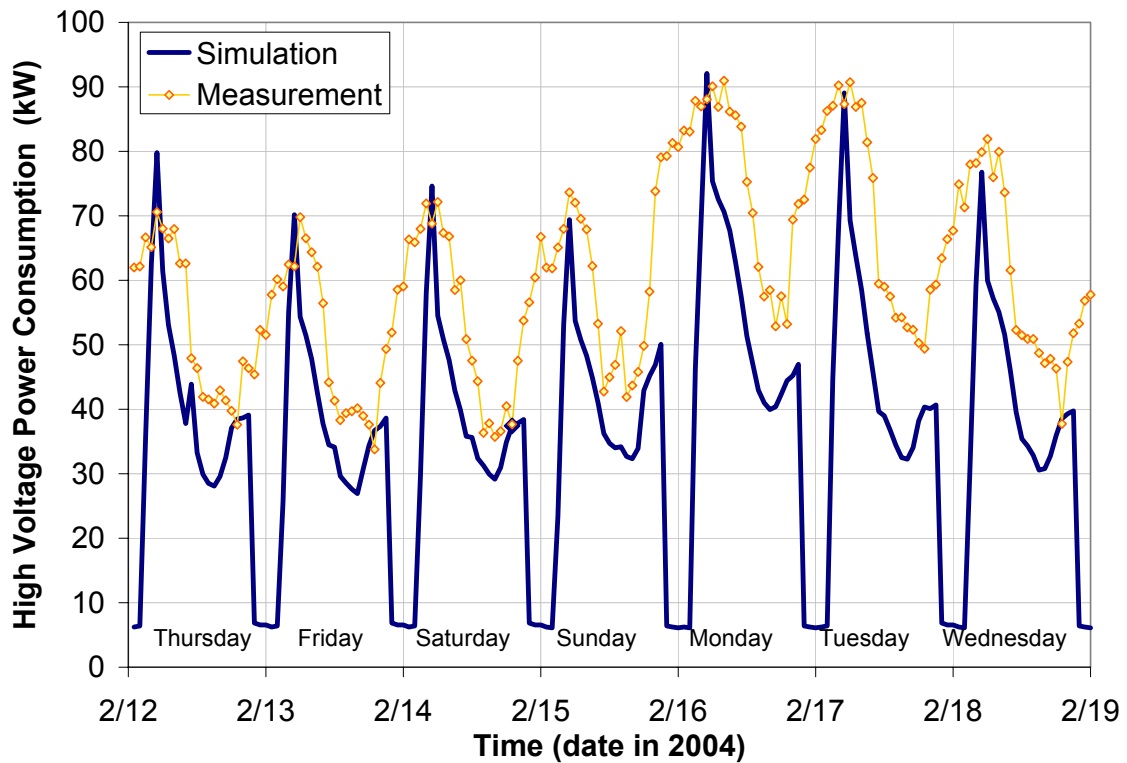


Fig. 97. Weekly high voltage power for the 1st and 2nd floors

Bibliography

1. Abrahamsson, K. and Jernqvist, A. *Modelling and Simulation of Absorption Heat Cycles*. ASME IAHP conference proceedings, AES-Vol.31. 1994.
2. Abrahamsson, K., Aly, G., et al. *Applications of Absorption Heat Cycles in the Pulp and Paper Industry*. ASME IAHP conference proceedings, AES-Vol.31. 1994.
3. Abrahamsson, K., Jernqvist, A. and Aly, G. *Thermodynamic Analysis of Absorption Heat Cycles*. ASME IAHP conference proceedings, AES-Vol.31. 1994.
4. Ahachad, M. and Charia, M. *Absorption Heat Transformer Applications to Absorption Refrigerating Machine*. ASME IAHP conference proceedings, AES-Vol.31. 1994.
5. Alefeld, G., Radermacher, R. *Heat Conversion Systems*. CRC Press, Boca Raton, Florida, 1994.
6. Alva, L., González, J. *Simulation of an Air-cooled Solar-assisted Absorption Air Conditioning System*. ASHRAE Transactions, V. 124, 2002.
7. ANSI/ASHRAE Standard 62-1999, *Ventilation for acceptable indoor air quality*. Atlanta: American Society of Heating, Refrigerating and Air-Conditioning Engineers, Inc.
8. Arh, S. *Absorption Heat Pump/Transformer cycle for Simultaneous Heating and Cooling*. ASME IAHP conference proceedings, AES-Vol.31. 1994.
9. ARI standard 940. *Standard for Desiccant Dehumidification Components*. Air-Conditioning and Refrigeration Institute, 4301 North Fairfax Drive, Suite 425, Arlington, VA 22203, U.S.A. 1998.
10. *ASHRAE Handbook - Fundamentals*, Atlanta: American Society of Heating, Refrigerating and Air-Conditioning Engineers, Inc. 2001.
11. *ASHRAE Handbook - HVAC Systems and Equipment*, Atlanta: American Society of Heating, Refrigerating and Air-Conditioning Engineers, Inc. 2000.
12. Ataer, A. and Kilgis B. *An Analysis of the Solar Absorption Cycle When Coupled with in-slab Radiant Cooling Panels*. ASME IAHP conference proceedings, AES-Vol.31. 1994.

13. Bassols, J., Schneider, R. et al. *First Operation Results of a Gas-fired 250kW Absorption Heat Pump with Plate-Fin Heat Exchangers*. ASME IAHP conference proceedings, AES-Vol.31. 1994.
14. Beckwith, T. Marangoni, R., Lienhard, J. *Mechanical Measurements*. Fifth Edition. Addison-Wesley Publishing Company, New York. 1993.
15. Bedard, G. *Varied Flow Rate Applications for Commercial Absorption Liquid Chillers*. ASME IAHP conference proceedings, AES-Vol.31. 1994.
16. *BinMaker[®] Weather Data for Engineering*. InterEnergy Software/Gas Technology Institute, Des Plaines, IL. 2004.
17. Boer, D., Huor, M., Prevost, M. and Coronas, A. *Combined Vapor Compression-Double Effect Absorption Cycle for Air Conditioning: A New High Performance Cycle*. ASME IAHP conference proceedings, AES-Vol.31. 1994.
18. Bougard, J., Jadot, R. and Poulain, V. *Solid-gas Reactions Applied to Thermotransformer Design*. ASME IAHP conference proceedings, AES-Vol.31. 1994.
19. Bowman, R., Freeman, B., Ryba, E. and Phillips, J. *Design and Evaluation of Hydrogen Joule-Thomson Sorption Cryocoolers*. ASME IAHP conference proceedings, AES-Vol.31. 1994.
20. Carmody, S. and Shelton, S. *Direct Second Law Analysis of Advanced Absorption Cycles Utilizing an Ideal Solution Model*. ASME IAHP conference proceedings, AES-Vol.31. 1994.
21. Castro, J., Leal, L., et al. *Development and Performance of an Air-cooled Water-LiBr Absorption Cooling Machine*. International Forum on Renewable Energies FIER'2002 Proceedings. 2002.
22. Conlisk, A. *The Use of Boundary Layer Techniques in the Design of Falling Film Absorber*. ASME IAHP conference proceedings, AES-Vol.31. 1994.
23. Cowie, M. *Characterizing Combined Heating, Cooling and Power Systems for Buildings through Theory and Testing*. M.S. thesis. Mechanical Engineering, University of Maryland, College Park. 2002.
24. Cowie, M., and Liao, X., and Radermacher, R. *Second Generation Integrated Microturbine, Absorption Chiller and Solid Desiccant System*. The 21st IIR International Congress of Refrigeration. 2003.
25. Cowie, M., Liao, X., Radermacher, R. *Applying CHP to the Ventilation Air of buildings*. ASME IMECE 2003-43920. 2003.

26. Cowie, M., Liao, X., Radermacher, R., *Performance Comparison of Waste-Heat Driven Desiccant Systems*. ASHRAE Summer Meeting and ASHRAE microturbine seminar in Kansas City, MO. 2003.
27. Cowie, M., Marantan, A. Garland, P., Radermacher, R. *CHP for Buildings - the Challenge of Delivering value to the commercial sector*. Proceedings of the International Mechanical Engineering Congress and Exposition Emerging and New Technologies for Heat Pump and Refrigeration Cycles and CHP. 2002.
28. Daltrophe, N., Jelinek, M. and Borde, I. *Heat and Mass Transfer in a Jet Ejector for Absorption Systems*. ASME IAHP conference proceedings, AES-Vol.31. 1994.
29. *EnergyPlus Documentation*. University of Illinois, University of California, Lawrence Berkeley National Laboratory. 2004.
30. Feuerecker, G., Scharfe, J., Greiter, I., et al. *Measurement of Thermophysical Properties of Aqueous LiBr-Solutions at High Temperatures and Concentrations*. ASME IAHP conference proceedings, AES-Vol.31. 1994.
31. Fineblum, S. *Economics of Absorption Chillers Powered by Low-Grade Heat with, and without, Vortex-Induced Pressure Reduction in the Generator*. ASHRAE Transactions V107. 2001.
32. Florides, G.A., Kalogirou, S.A., Tassou, S.A. and Wrobel, L.C. *Design and construction of a LiBr–water absorption machine*. Energy Conversion and Management 44 (2003) 2483–2508. 2003.
33. *Forum on ARI Standard 550/590-98*. HPAC Engineering 1999, May.
34. Fujimaki, S., Kawakami, R., et al. *Analysis of Technical Tasks for Improving the Safety of Ammonia Absorption Heat Pumps*. ASME IAHP conference proceedings, AES-Vol.31. 1994.
35. Gansler, R., Reindl, D. and Jekel, T. *Simulation of Source Energy Utilization and Emissions for HVAC Systems*. ASHRAE Transactions V107. 2001.
36. Garimella, S. and Christensen, R. *Gas-fired Absorption Systems for Space Conditioning in Recreational Vehicles*. ASME IAHP conference proceedings, AES-Vol.31. 1994.
37. Garimella, S. and Coleman, J. *Design of Cross-Flow Condensers for Ammonia-Water Absorption Heat Pumps*. ASHRAE Transactions V104. 1998.
38. Garimella, S. *Microchannel Components for Absorption Space-Conditioning Systems*. ASHRAE Transactions V106. 2000.

39. Gee, T.A., Cao, J., Mathias, J.A., Christensen, R. N. *Experimental Testing and Modeling of a Dual-Fired LiBr-H₂O Absorption Chiller*, ASHRAE Transactions, V. 107, 2001.
40. Ghosh, K., Zhou, X. and Herold, K. *Circulation of 2-Ethyl-Hexanol in an Absorption Chiller*. ASHRAE Transactions V108. 2002
41. Gierow, M. and Jernqvist, A. *Selection of Working Pair for Sorption Heat Pumps: A Computer Simulation Study*. ASME IAHP conference proceedings, AES-Vol.31. 1994.
42. Gommed, K., Grossman, G. and Koenig, M. *Numerical Study of Absorption in a Laminar Falling Film of Ammonia-Water*. ASHRAE Transactions V107. 2001.
43. Goodheart, K.A. *Low firing temperature absorption chiller system*, M.S. thesis, Mechanical Engineering, University of Wisconsin, Madison. 2000.
44. Goodheart, K.A., Klein S.A., and Schultz K. *Economic Assessment of Low Firing Temperature Absorption Chiller Systems*. ASHRAE Transactions, V108. 2002.
45. Greiter, I., Schweigler, C., Alefeld, G. and Scharfe, J. *A 500 kW Absorption Heat Pump for Heating at Two Temperature Levels*. ASME IAHP conference proceedings, AES-Vol.31. 1994.
46. Greiter, I., Wagner, A., Weiss, V. and Alefeld, G. *Experimental Investigation of Heat and Mass Transfer in a Horizontal-tube Falling-film Absorber with Aqueous Solutions*. ASME IAHP conference proceedings, AES-Vol.31. 1994.
47. Groll, E. and Radermacher, R. *Vapor Compression Heat Pump with Solution Circuit and Desorber/Absorber Heat Exchanger*. ASME IAHP conference proceedings, AES-Vol.31. 1994.
48. Grossman, G. *Advanced modular simulation of open absorption systems*. Keynote Lecture, Proceedings, the 7th International Sorption Heat Pump Conference. 2002.
49. Grossman, G. and Zaltash, A. *ABSIM - modular simulation of advanced absorption systems*. International Journal of Refrigeration, vol.24. 2001.
50. Grossman, G. *Modular and Flexible Simulation of Advanced Absorption Systems*. ASME IAHP conference proceedings, AES-Vol.31. 1994.
51. Guilleminot, J., Chalfen, J. and Choisier, A. *Heat and Mass Transfer Characteristics of Composites for Adsorption Heat Pumps*. ASME IAHP conference proceedings, AES-Vol.31. 1994.
52. Hellmann, H. and Ziegler, F. *Simple Absorption Heat Pump Modules for System Simulation Programs*. ASHRAE Transactions V105. 1999.

53. Herold, K. and Moran, M. *Thermodynamic Properties of LiBr/H₂O Solutions*, ASHRAE Transactions, 1, 35-48. 1987.
54. Herold, K., Radermacher R. and S. Klein. *Absorption Chillers and Heat Pumps*, CRC Press, Boca Raton, Florida. 1996.
55. Hisaki, H., Kobayashi, N. Yonezawa, Y. and Morikawa, A. *Development of Ice-thermal Storage System Using an adsorption Chiller*. ASME IAHP conference proceedings, AES-Vol.31. 1994.
56. Homma, R., Nishiyama, N. and Wakimizu, H. *Simulation and Experimental Research of Single-effect Absorption Refrigerators Driven by Waster Hot Water*. ASME IAHP conference proceedings, AES-Vol.31. 1994.
57. Inoue, N., Lizuka, H., et al. *COP Evaluation for Advanced Ammonia-Based Absorption Cycles*. ASME IAHP conference proceedings, AES-Vol.31. 1994.
58. Itard, L. and Machielsen, C. *Parameters Study for the Optimization of a Wet Compression Hybrid Cycle for the Working Pair NH₃/H₂O*. ASME IAHP conference proceedings, AES-Vol.31. 1994.
59. Ivester, D. and Shelton, S. *Varying Heat Exchanger Parameters in the Triple-effect Absorption Cycle*. ASME IAHP conference proceedings, AES-Vol.31. 1994.
60. Iyoki, S., Inoue, Y. and Uemura, T. *Performance Comparison of Various Absorption Heat Transformers Using Nitrate-Based Absorbent Systems*. ASHRAE Transactions V105. 1999.
61. Izquierdo, M., Venegas, M., et al. *Crystallization as a limit to develop solar air-cooled LiBr-H₂O absorption systems using low-grade heat*. Solar Energy Materials and Solar Cells 81. 2004.
62. Janssen, J. *The History of Ventilation and Temperature Control*. ASHRAE Journal. 47-52. Sept. 1999.
63. Jeong, S., Kang, B., Lee, C. and Karng, S. *Computer Simulation on Dynamic Behavior of a Hot Water Driven Absorption Chiller*. ASME IAHP conference proceedings, AES-Vol.31. 1994.
64. Jeong, S., Lee, S. and Koo, K. *Heat Transfer Performance of a Coiled Tube Absorber with Working Fluid of Ammonia/Water*. ASHRAE Transactions V104. 1998.
65. Ji, W. and Setterwall, F. *Effects of Surfactant on the Stability of Falling Liquid Films*. ASME IAHP conference proceedings, AES-Vol.31. 1994.

66. Jones, J. *Carbon/Ammonia Regenerative Adsorption Heat Pump*. ASME IAHP conference proceedings, AES-Vol.31. 1994.
67. Jung, S., Sgamboti, C. *An Experimental Study of the Effect of some Additives on Falling Film Absorption*. ASME IAHP conference proceedings, AES-Vol.31. 1994.
68. Jurinak, J., Mitchell, J. and Bechman, W. *Open-Cycle Desiccant Air Conditioning as an Alternative to Vapor Compression Cooling in Residential Applications*. ASME Transactions V106. 1984.
69. Kahn, R., Alefeld, G., Hammerer, S. et al. *An Ammonia-water Absorption Cycle with High Temperature Lift*. ASME IAHP conference proceedings, AES-Vol.31. 1994.
70. Kang, Y. and Christensen, R. *Development of a Counter-Current Model for a Vertical Fluted Tube GAX Absorber*. ASME IAHP conference proceedings, AES-Vol.31. 1994.
71. Kawada, A., Furutera, M., Hoshida, T., et al. *NG₃/H₂O system Absorption-Compression Hybrid Heat Pump COP Evaluation of Temperature Amplifier Type Heat Pumps*. ASME IAHP conference proceedings, AES-Vol.31. 1994.
72. Kim, K., Berman, N. and Wood, B. *Experimental Investigation of Enhanced Heat and Mass Transfer Mechanisms Using Additives for Vertical Falling Film Absorber*. ASME IAHP conference proceedings, AES-Vol.31. 1994.
73. Klein, S., Alvarado, F. *Engineering Equation Solver software*. 1992-2004.
74. Kline, S., McClintock, F. *Describing Uncertainties in Single-Sample Experiments*. *Mechanical Engineering*. 1959.
75. Klingenberger, U. *Modeling and Analysis of Solid and Liquid Desiccant Systems in CHP for Buildings Applications*. M.S. thesis. University of Applied Sciences Offenburg. 2002.
76. Koepfel, E.A. *The Modeling, Performance and Optimal Control of Commercial Absorption Chillers*. M.S. thesis, Mechanical Engineering, University of Wisconsin, Madison. 1994.
77. Kouider, M., Nadi, M. and Kourtiche, D. *Sensors Auto-calibration Method - Using Programmable Interface Circuit Front-end*. *Sensors* ISSN 1424-8220, 3. 2003.
78. Kulankara, S. and Herold, K. *Theory of Heat/Mass Transfer Additives in Absorption Chillers*. ASHRAE Transactions V107. 2001.

79. Labidi, J., Schwarzer, B. and LeGoff, P. *Absorption Heat Pumps Composed of Multiple Stages Either Independent or Belonging to a Unique Column*. ASME IAHP conference proceedings, AES-Vol.31. 1994.
80. Labinov, S., Zaltash, A. et al. *Predictive Algorithms for Microturbine Performance for BCHP Systems*. ASHRAE Transactions, V. 108. 2002.
81. Lee, S. and Sherif, S. *Second-Law Analysis of Multi-Effect Lithium Bromide/Water Absorption Chillers*. ASHRAE Transactions V105. 1999.
82. Lee, S. and Sherif, S. *Second Law Analysis of Multi-Stage Lithium Bromide/Water Absorption Heat Transformers*. ASHRAE Transactions V106. 2000.
83. Lee, S. and Sherif, S. *Second Law Analysis of Various Double-Effect Lithium Bromide/Water Absorption Chillers*. ASHRAE Transactions V107. 2001.
84. Lee, S. and Sherif, S. *Thermoeconomic Analysis of Absorption Heat Transformers*. ASHRAE Transactions V107. 2001.
85. Lee, S. and Sherif, S. *Thermoeconomic Analysis of Absorption Systems for Cooling*. ASHRAE Transactions V107. 2001.
86. Liao, X., Cowie, M., Radermacher, R. *CHP Dedicated Outdoor Air Systems for Buildings*. International Conference on Improving Energy Efficiency in Commercial Buildings "IEECB'04", Frankfurt, Germany. 2004.
87. Liao, X., Garland, P., Radermacher, R. *The Modeling of Air-cooled Absorption Chiller Integration in CHP System*. ASME IMECE 2004-60308 2004.
88. Liu, m., Claridge, D. et al. *Manual of Procedures for Calibrating Simulations of Building Systems*. California Energy Commission, Public Interest Energy Research Program HPCBS # E5P23T2b. 2003.
89. Lohr, S. *Sampling: Design and Analysis*. 1st edition, Duxbury Press, ISBN 0-534-35361-4. 1999.
90. Mannschott, D. *Report on the 2nd Practical Semester*. Hochschule für Technik und Gestaltung. 2003.
91. Marantan, A. *Optimization of Integrated Microturbine and Absorption Chiller Systems in CHP for Buildings Applications*, Ph.D. dissertation, Mechanical Engineering, University of Maryland, College Park. 2002.
92. Marantan, A., Popovic, P. and Radermacher, R. *The Potential of CHP Technology in Commercial Buildings - Characterizing the CHP Demonstration Building*. ASHRAE Symposium on CHP Technologies for the New Century, ASHRAE Transactions, V. 108, Pt. 1. 2002.

93. Mardorf, L. *Controllable Cycle Investigation of Direct Fired Absorption Heat Pump for Residential Heating Systems*. ASME IAHP conference proceedings, AES-Vol.31. 1994.
94. Mazet, N., Meyer, P., Neveu, P. and Spinner, B. *Concept and Study of a Double Effect Refrigeration Machine Based on the Sorption of Solid and Ammonia Gas and Controlled by Heat Pipes*. ASME IAHP conference proceedings, AES-Vol.31. 1994.
95. McGahey, K., Garimella, S., Cook, F. and Christensen, R. *Enhancement of the ORNL Absorption Model and Simulation of Double-effect Absorption Heat Pump*. ASME IAHP conference proceedings, AES-Vol.31. 1994.
96. McNeely, L.A. *Thermodynamic Properties of Aqueous Solutions of Lithium Bromide*, ASHRAE Transactions, 85, 413-434. 1979.
97. Merrill, T., Setoguchi, T. and Perez-Blanco, H. *Compact Bubble Absorber Design and Analysis*. ASME IAHP conference proceedings, AES-Vol.31. 1994.
98. Miller, W. and Perez-Blanco, H. *Vertical-tube Aqueous LiBr Falling Film Absorption Using Advanced Surfaces*. ASME IAHP conference proceedings, AES-Vol.31. 1994.
99. Mumma, S. A. *Overview of Integrating Dedicated Outdoor Air Systems with Parallel Terminal Systems*. ASHRAE Transactions, V107. 2001.
100. Mumma, S. A., and Shank K. M. *Achieving Dry Outside Air in an Energy-Efficient Manner*, ASHRAE Transactions, V107. 2001.
101. Mumma, S. *Designing Dedicated Outdoor Air Systems*. ASHRAE Journal 43(5). 2001.
102. Murakami, K., Sato, H. and Watanabe, K. *Boiling Heating Transfer in High Temperature Generator of absorption Chiller/Heater*. ASME IAHP conference proceedings, AES-Vol.31. 1994.
103. Ng, K. Chua, H., Han, Q., Kashiwagi, T., Akisawa, A. and Tsurusawa, T. *Thermodynamic Modeling of Absorption Chiller and Comparison with Experiments*. Heat Transfer Engineering, Vol. 20, No.2. 1999.
104. Nomura, T., Nishimura, et al. *Heat and Mass Transfer Mechanism in the Absorber of Water/LiBr Convective Absorption Refrigerator: Experimental Examination by Visualized Model*. ASME IAHP conference proceedings, AES-Vol.31. 1994.
105. Oh, M., Kim, S. and Kim, Y. *Cycle Analysis of Air-cooled Double-effect Absorption Heat Pump with Parallel Flow Type*. ASME IAHP conference proceedings, AES-Vol.31. 1994.

106. Okano, T., Asawa, Y. Fujimoto, M., Nishiyama, N. and Sanai, Y. *Development of an Air-cooled Absorption Refrigerating Machine Using a New Working Fluid*. ASME IAHP conference proceedings, AES-Vol.31. 1994.
107. ORNL. ABSIM version 5. *Modular Simulation of Absorption Systems*, Oak Ridge National Laboratory. 1998.
108. Ouimette, M. and Herold, K. *Performance Modeling of a Triple Effect Absorption Chiller*. ASME IAHP conference proceedings, AES-Vol.31. 1994.
109. Patnaik, V. and Perez-Blanco, H. *A Counter-flow Heat-exchanger Analysis for the Design of Falling-film Absorbers*. ASME IAHP conference proceedings, AES-Vol.31. 1994.
110. Persson, L. and Holmberg, P. *Heat Transfer by Falling Film Desorption of concentrated LiBr Aqueous Solutions with Surfactant Octanol Addition*. ASME IAHP conference proceedings, AES-Vol.31. 1994.
111. Petrov, A., Labinov, S., Rizy, T., Liao, X., Radermacher, R. *Evaluation of Different Efficiency Concepts of an IES*. ASME IMECE 2004-60285. 2004.
112. Petrov, A., Zaltash, A., Vineyard, E. et al. *Baseline and IES Performance of a Direct-Fired Desiccant Dehumidification Unit under Various Environmental Conditions*. ASHRAE Transactions, V109. 2003.
113. Popovic, P., Marantan, A., Radermacher, R. and Garland, P. *Integration of a Microturbine with a Single Effect Exhaust Driven Absorption Chiller and a Solid Wheel Desiccant System*, ASHRAE Transactions. 2002.
114. Priedeman, D. and Christensen, R. *GAX Absorption Cycle Design Process*. ASHRAE Transactions V105. 1999.
115. Radermacher, R., Liao, X. *The Impact of Waste Heat Activated Desiccant Systems on Buildings*. International conference on Building Systems and Facilities Management in Singapore, Keynote speech, 2003.
116. Rahman, M., Gui, F. and Scaringe, R. *Design and Experimental Performance Evaluation of a Hybrid Chemical/Mechanical Heat Pump*. ASME IAHP conference proceedings, AES-Vol.31. 1994.
117. Rane, M. and Erickson, D. *Advanced Absorption Cycle: Vapor Exchange Gax*. ASME IAHP conference proceedings, AES-Vol.31. 1994.
118. Rizy D.T., Zaltash A., Labinov S.D., Petrov A.Yu, Vineyard E.A., and Linkous R.L. *CHP Integration (or IES): Maximizing the Efficiency of Distributed Generation with Waste Heat Recovery*. Proceedings of the Power System 2003 Conference "Distributed Generation and Advance Metering", Clemson, SC, USA. March 12-14, 2003.

119. Rockenfeller, U. and Kirol, L. *HVAC and Heat Pump Development Employing Complex Compound Working Media*. ASME IAHP conference proceedings, AES-Vol.31. 1994.
120. Rose, D., Zuritz, C. and Perez-Blanco, H. *Thermodynamic Analysis and Pilot Plant Design for a Solar Assisted Double-effect Refrigeration Absorption Cycle*. ASME IAHP conference proceedings, AES-Vol.31. 1994.
121. Ryan, W. *Water Absorption in an Adiabatic Spray of Aqueous LiBr Solution*. ASME IAHP conference proceedings, AES-Vol.31. 1994.
122. Salim, M. *Simulation of Automotive LiBr/H₂O Absorption A/C Machine*, ASME IMECE2001/AES-23620. 2001.
123. Savada, N., Minato, K., et al. *Cycle Simulation and COP Evaluation of Absorption-compression Hybrid Heat Pumps: Heat Amplifier Type*. ASME IAHP conference proceedings, AES-Vol.31. 1994.
124. Sawada, N., Tanaka, T and Mashimo, K. *Development of Organic Working Fluids and Application to Absorption Systems*. ASME IAHP conference proceedings, AES-Vol.31. 1994.
125. Schaefer, L. A. *Single Pressure Absorption Heat Pump Analysis*, Ph.D. Dissertation, Georgia Institute of Technology, Department of Mechanical Engineering. May 2000.
126. Schinner, E. and Radermacher, R. *Performance Analysis of a Combined Desiccant/Absorption Air-Conditioning System*. Vol. 5, No. 1, HVAC&R Research. 1999.
127. Schwarzer, B., Rahbar, M. and Legoff, P. *A Spiral Fin Tube: A Novel Type of Falling Film Heat and Mass Exchanger*. ASME IAHP conference proceedings, AES-Vol.31. 1994.
128. Schweigler, C., Hellmann, H., et al. *Operation and Performance of a 350 kW (100 RT) Single-Effect/Double-Lift Absorption Chiller in a District Heating Network*. ASHRAE Transactions V104. 1998.
129. Serpente, C., Kernén, M., et al. *A 2kW LiBr absorption Machine with Heat Recovery and Recirculation for Novel Fluid Testing*. ASME IAHP conference proceedings, AES-Vol.31. 1994.
130. Shank, K., S.A. Mumma. *Selecting the supply air conditions for a dedicated outdoor air system working in parallel with distributed sensible cooling terminal equipment*. ASHRAE Transactions 107 (1). 2001.
131. Shelton, S. and Stewart, S. *Bubble Pump Design for Single Pressure Absorption Refrigeration Cycles*. ASHRAE Transactions V108. 2002.

132. Shelton, S., Jacob, D. and Schaefer, L. Modeling and Analysis of the Air Cooled Ammonia-water Triple Effect Cycle. Advanced Energy Systems Division, Mechanical Engineering Congress and Exposition, Nashville, TN. 1999.
133. Shelton, S., Schaefer, L. *The Economic Payoff for Global Warming Emissions Reduction*. Elsevier Science. 1999.
134. Strenger, U. and Setterwall, F. *Investigations on Lammellas in an Absorption Heat Pump*. ASME IAHP conference proceedings, AES-Vol.31. 1994.
135. Sweetser, R. et al. *Absorption Technologies for Buildings: Cooling, Heating, and Power (BCHP) Systems*. HPAC Heating/Piping/Air Conditioning Engineering. 51-56, July 2000.
136. Tongu, S., Makino, Y., Ohnishi, K. and Nakatsugawa, S. *Practical Operating of Small-sized Air-cooled Double-effect Absorption Chiller-heater by using LiBr and Aqueous*. ASME IAHP conference proceedings, AES-Vol.31. 1994.
137. Tozer, R. and James, R. *Thermodynamics of Absorption Refrigeration: Ideal Cycles*. ASME IAHP conference proceedings, AES-Vol.31. 1994.
138. Tozer, R. Sorption Thermodynamics. ASHRAE Transactions V108. 2002.
139. Tozer, R., Valero, A. and Lozano, M. *Thermoeconomics Applied to HVAC Systems*. ASHRAE Transactions V105. 1999.
140. Trane Company. *Application Guide - Designing Dedicated Outdoor-Air Systems*. SYS-APG001-EN, American Standard Inc. 2003.
141. Treffinger, P. and Peter, T., *Test Results for an Absorption Heat Pump with Adjustable Composition*. ASHRAE Transactions V105. 1999.
142. U.S. Department of Energy, Energy Efficiency and Renewable Energy. *Thermally Activated Technologies Basics*,
http://www.eere.energy.gov/de/technologies/det_thermal_tech_basics.shtml. 2004.
143. U.S. Department of Energy, Energy Efficiency and Renewable Energy. *EnergyPlus Energy Simulation Software*.
<http://www.eere.energy.gov/buildings/energyplus/> 2004.
144. Vineyard, E., Sand, J., Durfee, D. *Parametric Analysis of Variables That Affect the Performance of a Desiccant Dehumidification System*. ASHRAE Transactions, V. 106. 2000.
145. Vineyard, E., Sand, J., Durfee, D. *Performance Characteristics for a Desiccant System at Two Extreme Ambient Conditions*. ASHRAE Transactions, V. 108. 2002.

146. Vliet, G. and Chen, W. *Location of Non-absorbable Gases in a Simplified Absorber Geometry*. ASME IAHP conference proceedings, AES-Vol.31. 1994.
147. Wongsosaputro, W., Marantan, A., Popovic, P., Garland, P. and Radermacher, R. *Environmental Analysis of Two Cooling, Heating and Power Systems for Commercial Buildings*, Building Energy Journal. 2001.
148. Zhai, C. *Energy Simulation of the Chesapeake Building*. Internship internal report. University of Maryland. July. 2003.
149. Zhou, C. and Machielsen, C. *Experimental Measurements of an Absorption Heat Transformer with the Working Pair TFE-Pyr*. ASME IAHP conference proceedings, AES-Vol.31. 1994.
150. Ziegler, F. and Alefeld, G. *Comparison of Multi-effect Absorption Cycles*. ASME IAHP conference proceedings, AES-Vol.31. 1994.

Publications and Reports

1. Cowie, M., Liao, X. and Radermacher, R. *Applying CHP to the Ventilation Air of buildings*. American Society of Mechanical Engineers (ASME) - International Mechanical Engineering Congress and Exposition, Washington, DC. November 16-21, 2003.
2. Cowie, M., Liao, X. and Radermacher, R. *Performance Comparison of Waste-Heat Driven Desiccant Systems*. ASHRAE Summer Meeting and ASHRAE microturbine seminar in Kansas City, MO. June 28- July 2, 2003.
3. Cowie, M., Liao, X., Radermacher, R., *Second Generation Integrated Microturbine, Absorption Chiller and Solid Desiccant System*. The 21st IIR International Congress of Refrigeration in DC. August 17-22, 2003.
4. Liao, X., Cowie, M., Radermacher, R., *CHP Dedicated Outdoor Air Systems for Buildings*. International Conference on Improving Energy Efficiency in Commercial Buildings "IEECB'04", Frankfurt, Germany. 19-20 April 2004.
5. Liao, X., Garland, P., Radermacher, R. *The Modeling of Air-cooled Absorption Chiller Integration in CHP System*. ASME IMECE 2004-60308 2004.
6. Liao, X., Radermacher, R. *Annual reports "Operation of CHP Systems, Measurement and Data Evaluation and Technology Transfer"*. FY2002, FY2003.
7. Liao, X., Radermacher, R. *Microturbine in CHP at University of Maryland*. DOE Microturbine Applications Workshop. Poster session. January 20-22, 2004.
8. Petrov, A., Labinov, S., Rizy, T., Liao, X., Radermacher, R., et al. *Evaluation of Different Efficiency Concepts of an IES*. ASME IMECE 2004-60285 2004.
9. Radermacher, R., Liao, X. *The Impact of Waste Heat Activated Desiccant Systems on Buildings*. International conference on Building Systems and Facilities Management in Singapore, October 8-10, 2003.

